Supraspinal Control of Unilateral Locomotor Performance: An FMRI Study Using a Custom Pedaling Device

Brett Arand
Marquette University

SUPRASPINAL CONTROL OF UNILATERAL LOCOMOTOR PERFORMANCE: AN FMRI STUDY USING A CUSTOM PEDALING DEVICE

by

Brett Arand, B.S.

A Thesis submitted to the Faculty of the Graduate School,
Marquette University,
in Partial Fulfillment of the Requirements for
the Degree of Master of Science

Milwaukee, Wisconsin

December 2013

ABSTRACT

SUPRASPINAL CONTROL OF UNILATERAL LOCOMOTOR PERFORMANCE: AN FMRI STUDY USING A CUSTOM PEDALING DEVICE

Brett Arand, B.S.

Marquette University, 2013

This study aimed to develop a novel unilateral pedaling device, validate its function, and use it in an fMRI study of bilateral vs. unilateral locomotor control. The new device is MRI compatible and allows for conventional coupled bilateral pedaling, along with decoupled unilateral pedaling. It was designed with an assistance mechanism to simulate the presence of the non-contributing leg while pedaling unilaterally. During coupled bilateral pedaling, the two legs work in unison: while one leg is extending in the downstroke, it provides support to lift the other leg back up as it is flexing in the upstroke. The device uses an eccentric pulley to stretch elastic bands during the downstroke, storing energy that is released back during the upstroke to assist the leg as the bands relax.

A phantom scan in the MRI machine was performed, which confirmed that the device did not interfere with signal detection. Experiments were performed to test the function of the device, showing that the assistance mechanism was able to adequately simulate the presence of the non-contributing leg during unilateral pedaling. The velocity and EMG profiles matched between unilateral and bilateral pedaling, with consistent results across days.

An fMRI study was performed to compare brain activation associated with coupled bilateral, right unilateral, and left unilateral pedaling in able-bodied individuals with a healthy nervous system. Task related brain activity was seen in the primary sensorimotor cortex (M1S1), Brodmann's area 6 (BA6), and the cerebellum (Cb). The laterality of activation was shifted to the contralateral M1S1 and ipsilateral Cb during unilateral pedaling, but some bilateral activation remained. BA6 showed no lateralization in activity. Additionally, there was no difference in the magnitudes of the laterality shift in right and left pedaling, and bilateral pedaling was not shifted to either hemisphere. Volume during unilateral pedaling showed no significant change in any brain area across conditions. These observations of laterality and volume suggest the existence of common regions of brain activation for bilateral and unilateral pedaling. Mean intensity in the common area of activation was lower in M1S1, BA6, and Cb for right and left unilateral compared to bilateral pedaling.

ACKNOWLEDGMENTS

Brett Arand, B.S.

I would like to start my thanking my adviser, Dr. Sheila Schindler-Ivens for the opportunity, knowledge, and guidance throughout working on my thesis. Also, thank you to my committee members, Dr. Brian Schmit and Dr. Taly Gilat-Schmidt, for their support and education during my time at Marquette. For teaching me how to collect and analyze MRI data, and for guidance and encouragement while working on my project, a special thanks goes to Dr. Nutta-on Promjunyakul. Thanks to David Seck for proofreading, and my other fellow lab members, Shancheng Bao, Ruth Swedler, Taylor Derr, Cara Lewellyn, and Jan Struhar for their help and support throughout my time here. Lastly, I would like to extend my gratitude to the funding sources for my thesis, the National Center for Medical and Rehabilitation Research at the National Institute of Child Health and Human Development (NICHD-NCMRR #K01HD00600693) and the Ralph and Marion Falk Medical Research Trust.

TABLE OF CONTENTS

LIST OF TABLES

LIST OF FIGURES

LIST OF ABBREVIATIONS

AFNI: Analysis of Functional NeuroImages

ANOVA: analysis of variance

AT: anterior transition

BA6: Brodmann's Area 6

BF: biceps femoris

BOLD: blood-oxygen level dependent

Cb: cerebellum

COV: coefficient of variance

CPGS: central pattern generators

DICOM: Digital Imaging and Communication in Medicine

EEG: electroencephalography

EX: extension

FL: flexion

FMRI: Functional Magnetic Resonance Imaging

FOV: field of view

FWHM: full width half maximum

HDR: hemodynamic response

HRF: hemodynamic response function

LBF: left biceps femoris

LI: laterality index

LRF: left rectus femoris

LTA: left tibialis anterior

M1: primary motor cortex

M1S1: primary motor and primary sensory areas

MEG: magnetoencephalography

NIRS: Near-infrared Spectroscopy

OXYHB: oxygenated hemoglobin

PC: polycarbonate

PET: positron emission tomography

PMA: premotor area

POM: polyoxymethylene

PT: posterior transition

RBF: right biceps femoris

RF: radio frequency

RF: rectus femoris

RL: right or left pedaling

RMS: root mean square

ROI: Regions of interest

RPM: revolutions per minute

RRF: right rectus femoris

RTA: right tibialis anterior

S1: primary somatosensory cortex

SE: standard error of the mean

SMA: supplementary motor area

SNR: signal to noise ratio

SPECT: single photon emission computed tomography

TA: tibialis anterior

TDC: top-dead-center

TE: echo time

TMS: transcranial magnetic stimulation

TR: repetition time

VM: vastus medialis

CHAPTER 1 –LITERATURE REVIEW

1.1 Introduction

In people post-stroke, previous work has outlined evidence of a change in brain control of locomotion (Miyai et al. 2002, Miyai et al. 2003, Suzuki et al. 2004, Miyai et al. 2006, Promjunyakul et al. *in prep*). The results from Miyai and colleagues demonstrated that lateral activation of the sensorimotor cortices occurs during walking in people post-stroke (Miyai et al. 2002, Miyai et al. 2003, Suzuki et al. 2004, Miyai et al. 2006). However, the previous study in our laboratory demonstrated different results, in which activation is bilateral between the two hemispheres during pedaling by people post-stroke, but volume is reduced (Promjunyakul et al. *in prep*). These different results suggest that more studies in brain control of locomotion in people post-stroke are needed. Moreover, these results have raised the question of what are the contributions of each hemisphere (damaged and undamaged) in controlling locomotion involving the two legs.

Further studies in our laboratory are planned to examine whether reduced pedaling related brain activation volume post-stroke is due to enhanced spinal control of this task or behavioral compensation. To this end, people with stroke will pedal with the non-paretic limb only and with the paretic limb only. Comparison will be made between brain activation observed during these movements and during conventional bilateral pedaling. However, prior to beginning these studies, we thought it prudent to understand normal control of unilateral pedaling. To complete these aims, a new pedaling device needed to be made that allows for both conventional coupled bilateral pedaling and decoupled unilateral pedaling.

` This study aimed to develop a novel pedaling device, validate its function, and use it in an fMRI study of unilateral pedaling. The new device allows for conventional coupled bilateral pedaling, along with decoupled unilateral pedaling. During unilateral pedaling, the device is designed with an assistance mechanism to simulate the presence of the non-contributing leg. The first chapter of this thesis describes the relevant literature that justifies the development and use of the new pedaling device. The second chapter covers the design of the device and validation experiments performed to ensure the assistance mechanism functions accurately. The third chapter describes the use of the device in an fMRI study comparing bilateral to unilateral pedaling in neurologically intact, able-bodied individuals.

1.2 Neural Control of Locomotion

Human locomotion, such as walking, running, or pedaling, requires precise coordination between the legs, involving extension and flexion at the hip, knee, and ankle in an alternating, reciprocal pattern, resulting in a kinematically complex task despite its simple appearance and frequent use. Likewise, the neurological control systems for locomotion are complex, requiring precise scaling and timing of motor movements while maintaining balance and body weight support, and immediately adapting to any unexpected situations that would require a change in movement pattern. Spinal neuronal circuits, sensory feedback signals, and descending supraspinal commands are all integrated to control locomotion.

Our understanding of neural control of locomotion in humans started with animal models, which have been more extensively studied. It was previously thought that

locomotion in animals is simply a less complex version of human locomotion, but we know now that is not the case. However, they do share several similarities that make animal studies relevant to our understanding of human motor control.

1.2.1 Spinal Cord

While serving primarily as a pathway from the brain to motor neurons, it is now known that the spinal cord contains neural networks called central pattern generators (CPGs) which are able to generate basic rhythmic locomotor movement (Sherrinton et al. 1910, Brown et al. 1911, Whelan et al. 1996). After stroke, it is possible that the CPGs have an increased role in locomotion due to a decrease in the brain's motor control abilities resulting from the lesion. The greatest evidence of the existence of CPGs is seen in non-human animals, and it is likely that the amount the CPGs contribute to locomotion varies based on how neurologically complex the species is.

Experiments on cats showed the CPG can be a complete system able to generate automatic locomotor movement (Forssberg and Grillner 1973, Barbeau and Rossignol 1987). Cats were given spinal cord transections, referred to as spinal cats, and placed over a motorized treadmill. They were given body weight support so that their hind limbs touched the treadmill surface but did not need to hold their body up. When the treadmill is on, the hind limbs show an alternating stepping pattern that is well coordinated and adapted to various treadmill speeds. With time and training, the spinal cat's movement on the treadmill continues to improve to the point that it closely resembled healthy, functioning cats. However, the locomotor pattern is not perfect; step

length and step cycle duration are reduced and the EMG amplitude of flexor muscles are increased (Belanger et al. 1987).

In humans, there is also evidence of the CPG, however it does not produce locomotor movements that are as robust as seen in other species. Infants less than two months old were supported under the arms and moved over a horizontal surface (Forssberg 1985). This elicits locomotor leg movements that lacks specific components unique to mature human plantigrade locomotion, including no heel strike in front of the body and no propulsive force. The same movement patterns are seen in anencephalic infants (Yang et al. 1998), supporting CPG control. Evidence of a non-robust CPG also exists in people with incomplete spinal cord injuries. One study involving a patient with this injury at the cervical level found that when experimenters extend the hip while lying supine, involuntary rhythmic, alternating, and forceful movements involving all muscles of the legs occurs (Calancie et al. 1994). When the external perturbation is removed, these movements continued spontaneously. With body weight support over a treadmill, patterned EMG activity is seen in people with spinal cord injury when coordinated stepping movements are induced (Dietz et al. 1994, Dobkin et al. 1995). When only a hip extension movement is imposed in people with spinal cord injury, EMG indicates coactivation of the knee and ankle joints (Schmit et al. 2002).

Despite evidence of a non-robust CPG in humans, it is unable to elicit movements without supraspinal input. The need for supraspinal control is demonstrated by paraplegic patients with complete spinal cord injury. In this group, locomotor movement cannot be stimulated by moving the limbs as in cats, but patterned step-like movement is

elicited by non-patterned electrical stimulation in the posterior structures of the lumbar spinal cord, simulating a supraspinal input (Dimitrijevic et al. 1998).

1.2.2 Peripheral Sensory Feedback

Peripheral afferents form a sensory network that is involved in the timing of transitions in locomotion and the magnitude of ongoing activity based on proprioceptive feedback (Pearson 1995). To accomplish these functions, peripheral afferents are thought to regulate the rhythmic locomotor pattern produced by spinal central pattern generators. They can also react to input by producing reflexes directly without the signal traveling all the way up to the brain. Sensory feedback is also needed to make corrective adjustments of stepping patterns when perturbations arise (Nielsen 2003). Since some corrections based on sensory input can be made without input from the brain, this network may become more important after stroke if sensory connections to the brain are disrupted.

Studies using spinal cats were used to investigate the affects of peripheral afferents on gait without supraspinal input. With body weight supported and hind limbs on a treadmill, one leg was held and slowly pulled backwards causing it to react and flex forward when the hip position reached an angle very close to that seen during swing initiation of normal locomotion (Grillner and Rossignol 1978). Unloading the ankle extensors at the end of stance also allows for swing to begin, whereas an additional load prevents the initiation of swing phase (Duysens et al. 1980), indicating that sensory regulation of the pattern of locomotion exists based on proprioception of limb position.

Similar results are found when infants are held over a treadmill (Pang 2000). Manipulating the hip position and load on one limb results in prolonged stance and

delayed swing when the hip was flexed and the limb load was high, and short stance with advanced swing when the hip was extended and the load was low. Finding these reactions in infants suggests that stepping adaptations are in humans from birth. In healthy adults, loading does not affect the step cycle duration (Stephens and Yang 1999). Loading does increase hip extension moments in both SCI and able-bodied people, and if the load is applied early or late in the gait cycle, there is a significant phase shift in the hip moment profile (Gordon et al. 2009). In adult humans with spinal cord injury, timing of muscle activity during walking is not affected by electrical stimulation over hip flexors, which is also similar to animal studies (Wu et al. 2011).

1.2.3 Supraspinal Input

The third major component to motor control is supraspinal input. Roles of the cortex in locomotion are some of the most difficult to study due to technical limitations, and therefore least understood. Again, much of the understanding of supraspinal motor control of locomotion started with animal studies. Although cats are able to produce locomotor movements without cortical input, the brain is involved in initiation and regulation of movement (Shik et al. 1966). Locomotion can be initiated in decerebrate cats by applying electrical stimulation to the mid-brain, and walking speed does not increase with increasing stimulation intensity. Although walking can be elicited without this supraspinal input, it is needed to respond to obstacles in a complicated environment. With obstacles fixed to a moving treadmill, healthy cats negotiate them by making large adjustments in limb trajectory with large changes in forelimb flexor activity, and an increase in peak discharge of some pyramidal tract neurons was recorded (Drew 1988).

Supraspinal input is required for initiating and maintaining walking in humans, as people with complete spinal cord injuries are never able to functionally walk again (Dietz et al.1994, Dietz et al. 1995). Not only does it initiate movement, cortical input continues to have an effect during locomotion. Transcranial magnetic stimulation (TMS) can be used to externally excite projections from the motor cortex to corticospinal pathways. TMS applied to different areas in the motor cortex can be excitatory and increase muscle activity during walking (Schubert et al. 1997, Peterson et al. 1998, Capaday et al. 1999) or inhibitory and suppress muscle activity (Petersen et al. 2001). Corticospinal input was also shown to play a role in modulating muscle activity during different phases of pedaling (Pyndt and Nielson 2003) and walking (Petersen et al. 1998, Capaday et al. 1999, Petersen et al. 2001, Schubert 1999). TMS during various phases of the step cycle did not affect the cycle pattern, meaning that the motor cortex may not be involved in timing of motor bursts (Capaday et al. 1999).

Using functional imaging and electrophysiological techniques, it is possible to examine human brain activity during locomotor activities such as walking, running, or pedaling. Techniques include functional magnetic resonance imaging (fMRI) (Mehta et al. 2012, Promjunyakul et al. *in prep*), near infrared spectroscopy (NIRS) (Miyai et al. 2001, Suzuki et al. 2004, Suzuki et al. 2008), positron emission tomography (PET) (Christensen et al. 2001), electroencephalography (EEG) (Gwin et al. 2010, Peterson et al. 2012, Jain et al. 2013), and transcranial magnetic stimulation (TMS) (Petersen, et al. 1998, Capaday et al. 1999, Schubert et al. 1999, Petersen et al. 2001, Pyndt and Nielsen 2003). The primary motor (M1) and primary somatosensory (S1) cortices, supplemental motor area (SMA), premotor area (PMA), and cerebellum (Cb) have consistently been

shown to be active during locomotion (Fukuyama et al. 1997, Williamson et al. 1997, Christensen et al. 2000, Miyai et al. 2001, Suzuki et al. 2004, Mihara et al. 2007, Suzuki et al. 2008, Harada et al. 2009, Mehta et al. 2012).

M1 is connected to the spinal cord through corticospinal pathways, and S1 is connected to the spinal cord through the posterior column-menial lemniscus pathway, with some synapses in the thalamus and reticular formation. Both areas play a role in controlling locomotion. Electrodes have directly measured neuronal discharging in M1 during walking in cats (Armstrong and Drew 1984). S1 is involved in integrating sensory inputs from visual, vestibular, and somatosensory systems, and subsequently uses this information to modify locomotion. Passive pedaling studies have shown essentially equivalent activity in M1 and S1 compared to active pedaling, suggesting that these areas are involved with sensory feedback of locomotion rather than initiation (Christensen et al. 2000, Mehta et al. 2012).

The supplementary motor area (SMA) has been connected to postural control (Massion 1992), predicting movements from memory, motor planning, and execution of gait in humans (Deiber et al. 1999, Jenkins et al. 2000, Miyai et al. 2001, Sahyoun et al. 2004). SMA activity has also been related to the rate of locomotion in a pedaling study (Mehta et al. 2012). The pre-motor area (PMA) is related to planning of movements guided by sensory cues (Elsinger et al. 2006). SMA and PMA both showed increased activity during preparation for gait with verbal cues compared to without cues (Suzuki et al. 2008).

For locomotion, the cerebellum is thought to be involved in the generation and coordination of appropriate limb movement, regulation of balance, and adaptation of

posture and locomotion through practice (Morton and Bastian 2004, Jayaram et al. 2011). The cerebellum may also play a role in acquisition and discrimination of sensory data relating to motor control, and can be active in response to sensory stimuli in the absence of movement (Fox et al. 1985, Gao et al. 1996, Naito et al. 2002, Mehta et al. 2012).

1.3 Functional Magnetic Resonance Imaging (fMRI)

This study used magnetic resonance imaging (MRI) to study brain control of locomotion. MRI is a medical imaging technique that visualizes both anatomical structures of the brain and locations of neural activity related to tasks. Anatomical images are created based on molecular differences between types of brain tissue. Functional images are most commonly developed using the blood-oxygen level dependent (BOLD) signal. The bold signal is sensitive to the changes in blood oxygenation, which is related to active neural tissue (Boynton et al. 1996).

MRI works by exploiting the electrical properties of the nuclei of hydrogen atoms in the brain (Huettel et al. 2008). Due to the high concentration of water in the brain, hydrogen is the most abundant element. Hydrogen atoms have one proton, possessing a positive charge, which is constantly spinning about an axis. This axis of spin also rotates around another axis, like a wobbling top or gyroscope, known as precession. Normally, the axis of precession is randomly aligned compared to all other hydrogen molecules; however, in the presence of a strong magnetic field these axes all align parallel with the field. The majority is aligned in the direction of the field, the low energy state, and a fraction is in the opposite direction to the field, the high energy state. This results in a magnetic vector created by the hydrogen protons in the direction of the external magnetic

field created by the MRI scanner. Even though the direction of the precession axis is aligned in one direction, the phases of all the protons' precession are different. The differing phases cancel each other out, so there is no net magnetic vector in any direction perpendicular to the external magnetic field.

To produce an MRI signal, a radio frequency (RF) pulse is first emitted to excite a portion of the protons and temporarily change their alignment from the low to high energy state. The RF pulse also causes the phase of all the protons precessing to become aligned. The protons possess a positive charge, so when their phases are aligned they create a magnetic vector in the transverse direction. When the protons are not in phase their positions cancel each other out, therefore the net magnetism is zero. Once the RF pulse is removed, the protons move back to equilibrium from the high energy state back to the low energy state, which is known as longitudinal, or spin-lattice relaxation. When moving to the low energy state, electromagnetic energy is released and detected by the scanner. The time it takes for longitudinal relaxation to occur is called the T1 recovery time. The precession of the protons will also become out of phase, causing the transverse magnetic vector to dissipate, which is caused by two phenomena. Intrinsically, the protons have an effect on each other, a spin-spin interaction. The positive charges of neighboring protons repel each other causing a loss of coherence in the phase of precession, referred to as transverse relaxation or T2 decay. Extrinsically, the external magnetic field has slight inhomogeneities along the length of the bore caused by both technological imperfections and variances in human body physiology that affect the field local to the variance. Because the proton's precession is dependent on the external magnetic field, changes along the bore will affect the precession phase. Also, any

magnetic or RF interference that is present in the scanner room will further affect the transverse relaxation. True spin-spin interactions cannot be measured because it is impossible to completely prevent these extrinsic factors, so the combined relaxation is measured in T2* decay, with an associated T2* relaxation time. T1 and T2* times vary for different materials, such as bone or brain matter, based on the hydrogen proton density. Since the amount of change of the longitudinal and transverse magnetic vector over time is related to the proton density, the signals can be displayed as a varying grayscale gradient representing the range of material densities.

Images based on T1 recovery (T1-weighted) are commonly used for anatomical data because they are able to achieve high contrast between white and gray matter, but not blood or cerebrospinal fluid. Functional images are created by measuring the hemodynamic changes in blood flow to active areas of the brain. When increased neural activity occurs, blood flow to that area of the brain increases. The body oversupplies the area with blood, so the ratio of oxygenated to deoxygenated blood actually increases, even though oxygen uptake by the neural tissue increases. These changes in blood flow are termed the hemodynamic response (HDR) function. While oxygenated hemoglobin is only weakly diamagnetic, deoxygenated hemoglobin is paramagnetic and introduces inhomogeneity to the nearby magnetic field. T2*-weighting is sensitive to the changes in homogeneity of the magnetic field so it is used for functional imaging. The change in signal due to these changes in the blood is known as the blood-oxygen level dependent (BOLD) response.

Spatial resolution of fMRI is a few millimeters. The cubic area created by the width in each of the three spatial dimensions is called a voxel. To determine which

voxels are active during the experimental task, the MRI signal in each voxel is correlated to a model of the hemodynamic response and the timing of the experimental task. The signal change is delayed a few seconds from the onset of neural activity due to the physiological lag of the change in blood flow, and the signal lasts for seconds after activity ceases for the same reason. Because of this, the best temporal resolution fMRI can achieve is a few seconds (Huettel et al. 2008).

1.4 Locomotor Performance and Brain Activation after Stroke

In people post stroke, hemiparesis causes a change in locomotor symmetry between the two legs, with reduction in work output or a change in gait pattern of the paretic leg. The associated changes in brain control, however, are unclear.

In healthy individuals, performance during walking varies by only a small percentage in both the vertical and anterior-posterior components of gait between the two legs, showing that neither leg exhibits preference over the other and the bilateral locomotion was symmetric (Herzog et al. 1989). Individuals with hemiparetic locomotion after a stroke show asymmetric performance between the left and right lower extremities during walking (Dettmann et al. 1987, Balasubramanian et al. 2007). Specifically, the paretic leg was shown to have a decrease in propulsive impulse, measured as ground reaction force that produces propulsion, and an increase in braking impulse, resulting in a net negative impulse for that leg. The non-paretic leg compensated with an increase in propulsion impulse (Bowden et al. 2008).

Pedaling can be used as a model of locomotion, because as with walking, it involves coordinated extension and flexion of the hip, knee, and ankle of both legs in an

alternating, reciprocal pattern. During conventional bilateral pedaling, it is well documented that work output of each leg is similar in healthy, able-bodied individuals, whereas the non-paretic leg of people post-stroke contributes more than half the mechanical work required to accelerate the crank (Brown et al. 1998, Brown et al. 1999, Kautz et al. 2005, Schindler-Ivens et al. 2008, Liang et al. 2013). This stroke related behavioral adaptation is effective for successful task performance because, during conventional bilateral pedaling, the left and right pedals are mechanically coupled, making it possible for the non-paretic limb to accelerate both pedals.

Using functional imaging techniques, researchers have been able to observe brain activity related to locomotor tasks and compare the findings to performance with respect to laterality. Brain imaging has shown that in healthy individuals, activity is seen bilaterally in the medial primary sensorimotor cortices and the supplementary motor areas during treadmill walking and pedaling (Miyai et al. 2001, Promjunyakul et al. *in prep*).

Prior work in our laboratory has used fMRI to examine human brain activity during pedaling in individuals with chronic post stroke hemiparesis, in an effort to understand supraspinal contributions to the control and recovery of locomotor like movements of the lower extremities. Our results demonstrated that the volume of pedaling related brain activity was reduced in people post-stroke compared to age-matched controls. (Promjunyakul et al. *in prep*). While it is possible that reduced brain activation volume during pedaling post-stroke reflects enhanced reliance on spinal pattern generating circuits for the production and maintenance of locomotor-like movements of the legs, it is also possible that this observation was caused by stroke related changes in

task performance. The reduced brain activation volume observed during pedaling post stroke may simply reflect the reduced contribution from the paretic limb. However, the results found in our laboratory differ from studies of stroke-related brain activation during treadmill walking in people post-stroke using NIRS. They found that subjects with hemiparetic gait resulting from a stroke have lateralized activation in the SMC, PMC, and pre-SMA, with the shift towards the unaffected hemisphere (Miyai et al. 2002, Miyai et al. 2003, Suzuki et al. 2004, Miyai et al. 2006).

These different results suggest that more studies in brain control of locomotion in people post-stroke are needed. Additionally, the shortcoming of these studies of brain control of locomotion is that the locomotor tasks performed were only bilateral, and isolation of brain activity during unilateral locomotion can examine the contributions of each hemisphere (damaged and undamaged) in controlling the locomotion involving the two legs. To date, all lower extremity motor control studies using functional imaging involve only single joint flexion and extension. Motor control strategies in the brain for these movements may not extend to locomotor control, which involves continuous, reciprocal, multi-joint extension and flexion.

1.5 Unilateral Lower Extremity Motor Control

Comparisons of brain activity during unilateral and bilateral locomotor tasks have not been previously looked at directly, but we can draw hypotheses from other lower extremity motor studies. During bilateral locomotor tasks, brain activation has been shown to be bilaterally activated between left and right hemispheres in the regions M1S1, BA6, and Cb for healthy, able-bodied individuals (Christensen et al. 2000, Miyai et al.

2001, Suzuki et al. 2004, Mihara et al. 2007, Suzuki et al. 2008, Mehta et al. 2009, Mehta et al. 2012, Promjunyakul *in prep*).

One might assume that unilateral pedaling would produce brain activation that is distributed contralateral to the moving limb with approximately half the volume of that seen during bilateral pedaling. However, prior work examining brain activity during unilateral knee, ankle, and toe movements suggest that these assumptions may be inaccurate. These studies have found that activation is lateralized to the contralateral M1S1 and ipsilateral Cb, but the extent of lateralization differs between these studies. For example, studies of ankle and toe movement produced low group average laterality indices (LI of 1 is completely lateral, LI of 0 is completely bilateral) in M1S1 of 0.23 – 0.25 toward the contralateral side (Luft et al. 2002, Sahyoun et al. 2004). Another found knee, ankle, and toe activation laterality to be 0.28 – 0.59 (Kapreli et al. 2006). One study found average lateralization related to ankle movement to be much higher at 0.81 – 0.85 (Kim et al. 2006). Cerebellar activity has shown laterality indices of 0.27 – 0.59 (Luft et al. 2002, Kapreli et al. 2006). Laterality of SMA activity during lower extremity movement is also inconsistent across studies, reported as completely contralateral, low laterality to the contralateral side, and bilaterally activated (Luft et al. 2002, Sahyoun et al. 2004, Kim et al. 2006, Kapreli et al. 2006). These data provide no clear framework explaining supraspinal control of unilateral movements, particularly during a continuous, multi-joint task like pedaling. However, they do suggest that unilateral movements are not under complete contralateral control. Hence, there may be brain regions that are activated during both unilateral left and right, and bilateral movements of the lower extremities.

1.6 Existing Unilateral Locomotor Solutions

Walking studies have previously been performed using NIRS while bilaterally walking on a treadmill (Miyai et al. 2001, Suzuki et al. 2004, Mihara et al. 2007, Harada et al. 2009). This method, or a similar one using EEG, could be used to study unilateral walking by keeping one leg in place off the treadmill and walking with the other, or by providing body weight support and suspending the idle leg, however it has not yet been done. FMRI offers a distinct advantage over NIRS and EEG with much higher spatial resolution. Temporal resolution is lower in fMRI, but this is not as significant when studying locomotion as it is a continuous action.

Pedaling tasks are well suited for studying locomotion using fMRI, as it can be done while lying supine on a scanner bed (Mehta et al. 2009). During conventional bilateral pedaling, the two legs are working in unison. While one leg is extending in the downstroke, it provides support to lift the other leg back up as it is flexing in the upstroke. Mechanically, torque applied by one leg is positive during the downstroke and negative during the upstroke. The negative torque is compensated for by the greater positive torque of the other leg, and the net torque on the crankshaft remains positive. Pedaling with only one leg causes a change in the mechanics of the task. During the upstroke, the torque must be positive to keep the crank moving. Since the other leg is not contributing the positive torque to cancel out the negative work during flexion, the single leg must use different muscle activity to produce positive work and complete the pedaling cycle (Ting et al. 1998). To properly study unilateral locomotion using pedaling, the work of the non-contributing leg must be simulated.

One simple method for simulating the missing leg's contribution is with a human motor. This has been done previously by coupling two ergometers together where a trained experimenter can pedal to match the missing crank torque for the subject (Ting 1998). This coupled pedaling device would be difficult to use in MRI experiments because there is not a practical way to set up a dual bike system on a scanner bed. The experimenter could also produce the missing crank torque by hand pedaling one side of the MRI pedaling device, however this requires an additional person to perform experiments that is well trained, and the hand pedaling may be inconsistent in performance over the course of the experiment.

A better method is to design a device to accurately simulate the contribution of the missing leg. One such device uses servo motors controlled by a computer to deliver torque at any point in the cycle, which can be set up for unilateral pedaling simulation (Van der Loos et al. 2002). While this design is very effective, it is not suited for use in an MRI environment because of the metals required to construct it, namely the electromagnets in the motors. This device could be used with NIRS or EEG studies, but it would lack the spatial resolution of fMRI.

One robotic stepping device that is MRI compatible has been developed (Hollnagel et al. 2011). It allows for a movement pattern similar to walking and uses pneumatic cylinders to provide forces at the knee and foot at any time. It can be used for active movements with the pneumatic actuation providing resistance, or programmed to move the leg passively. It is currently being used for studying adaptation related to robotic therapy (Marchal-Crespo et al. 2011). This design could also be programmed to

work for unilateral locomotor fMRI experiments, but it is more complex than is necessary.

Our laboratory has previously used pedaling as a model to study brain activation during locomotion. By using this model again for unilateral studies, we can build on the knowledge base that we already have for conventional bilateral pedaling in neurologically intact, able-bodied individuals, and those with hemiparesis resulting from stroke. The new unilateral pedaling device has been designed to simulate the presence of the non-contributing leg to eliminate the need of another person acted as a human motor during the experiments. It has also been designed without the use of motors, so it can be used in an MRI environment.

1.7 Study Overview

To better understand how each leg is controlled during locomotion, my study aimed to develop a new method of performing unilateral locomotor tasks during functional imaging by developing a novel, unilateral pedaling device. The new pedaling device will be similar to one used previously (Mehta et al. 2009), however it will incorporate new features to allow for unilateral pedaling. The device was be designed, tested, and validated for proper task performance, and then used to compare brain activation associated with unilateral and bilateral pedaling in individuals with a healthy nervous system.

1.7.1 Hypotheses

For the second chapter of the thesis, we hypothesized that the phantom experiment would show that the device does not interfere with signal detection during fMRI scanning, and that validation experiments will show that the device is able to simulate the presence of the non-contributing leg during unilateral pedaling. For the third chapter, we hypothesize that if unilateral pedaling was similarly controlled as unilateral single joint movements of the lower extremities, then activation will show laterality towards contralateral M1S1and BA6 and ipsilateral Cb, but laterality indices will be less than 1 indicating that some activity exists in ipsilateral M1S1and BA6 and contralateral Cb. Along with the laterality change, the volume of activation during unilateral pedaling will decrease due to the decreased muscle activity needed to move one leg compared to two. Also, because there will be brain activation in both hemispheres during unilateral pedaling, we also hypothesize that there will be a common area in the brain that will be active during right and left unilateral and bilateral pedaling. This area could be involved in coordination and the underlying control of the alternating, flexion and extension motor movements used in locomotion. Intensity of activation in this common area will be decreased in unilateral compared to bilateral pedaling for both right and left conditions, due to decreased muscle activity of the task.

CHAPTER 2 – DEVICE DESIGN AND VALIDATION

2.1 Introduction

Neural imaging technologies, including functional magnetic resonance imaging (fMRI), make it possible to obtain high resolution images of human brain activity during motor tasks. Research using fMRI has lead to a greater understanding of motor control at the supraspinal level for both healthy individuals and those with disease or injury affecting the brain (Luft et al. 2002, Sahyoun et al. 2004, Ciccarelli et al. 2005, Kapreli et al. 2006, Mehta et al. 2012).

Locomotion is an important motor function, which quality of life after disease such as stroke is dependent on (Ahlsio et al. 1984, Go et. al. 2013). Technical and practical limitations have made it difficult to study locomotion with functional imaging. Walking cannot be done during fMRI due to the physical setup of the scanner, since the subject is required to lie supine on the bed. An appropriate model for locomotion must be selected that can be done while supine in the scanner, with the head kept still to prevent movement artifacts in the images.

Pedaling is similar to walking as it involves repetitive, reciprocal flexion and extension of both legs. This model has been used for studying normal and impaired locomotor control (Brown et al. 1997, Raasch et al. 1997, Kautz et al. 1998). Our laboratory has previously built a pedaling device for use in an MRI scanner, and used it to study brain activation during conventional bilateral pedaling in able-bodied individuals and those with stroke (Mehta et al. 2009, Mehta et al. 2012, Promjunyakul et al. *in prep).*

In people post-stroke, previous work has outlined evidence of a change in brain control of locomotion (Miyai et al. 2002, Miyai et al. 2003, Suzuki et al. 2004, Miyai et al. 2006, Promjunyakul et al. *in prep*). The results from Miyai and colleagues demonstrated that asymmetrical activation of the sensorimotor cortices occurs during walking in people post-stroke (Miyai et al. 2002, Miyai et al. 2003, Suzuki et al. 2004, Miyai et al. 2006). However, the previous study in our laboratory demonstrated different results, in which the activation was symmetric between the two hemispheres during pedaling by people post-stroke, but volume was reduced (Promjunyakul et al. *in prep*). These different results suggest that more studies in brain control of locomotion in people post-stroke are needed. Moreover, these results have raised the question of what the contributions of each hemisphere (damaged and undamaged) are in controlling the locomotion involving the two legs. In order to shed light on this issue, studying unilateral movement of a locomotor task is required. In order to study unilateral locomotion, a new pedaling device was needed.

For the first aim of this study, a novel MRI compatible pedaling device was developed to allow for both bilateral and unilateral pedaling in an MRI scanner. It is similar to the existing pedaling device used in our laboratory (Mehta et al. 2009), but has been redesigned by adding an innovative assistance mechanism to simulate the presence of the non-contributing leg during unilateral pedaling.

This chapter will discuss the development of the new pedaling device. The first part will elaborate on the fabrication of the device, including the requirements, design specifications, and materials used. The second part will cover the experiment done with a phantom in the MRI scanner to ensure the device did not interfere with the signals the

scanner is detecting. The next part covers the experiments that test the function of the device to show that the assistance mechanism is able to adequately simulate the presence of the non-contributing leg during unilateral pedaling. we hypothesized that the phantom experiment would show that the device does not interfere with signal detection during fMRI scanning, and that validation experiments will show that the device is able to simulate the presence of the non-contributing leg during unilateral pedaling.

2.2 Development of MRI Compatible Unilateral Pedaling Device

The new unilateral pedaling device was based on a design previously built and used in our laboratory (Mehta et al. 2009). In short, the previous devise is a direct-drive pedaling apparatus fabricated of nonmetallic materials designed for use in a supine position. The device is mounted on a backboard that the subject lies on to stabilize the device during use. The subject's feet are strapped to two pedals, which are coupled by a single crankshaft that only allows for coupled bilateral pedaling.

2.2.1 Design Requirements

To be used in the MRI environment, the device must be made completely of non-magnetic and non-conductive materials. Magnetic materials can be pulled into the scanner bore, which poses a safety hazard and could damage the scanner. Furthermore, magnetic or electrically conductive materials can distort the magnetic field of the scanner, or disrupt the radio frequency pulses, which would lead to artifacts in the images. In light of these constraints, materials used for the device were plastics, wood, glass, and brass.

To meet the aims of this and future studies, several new features have been added to the design of the existing device. The first major addition was the split crankshaft and coupler. This gives the device the ability to pedal coupled bilaterally, bilaterally uncoupled, or unilaterally. The crankshaft that connects the two pedals together is split in the middle, with a coupler that allows for quick changes. Furthermore, when coupling the crankshaft, the pedals can be oriented 180° out of phase as in conventional pedaling, 0° so the legs are in phase with each other, or with one leg leading or lagging the other by 90°.

The second major addition is a system of pulleys. The first set of pulleys is for a novel assistance mechanism that is to be used during unilateral pedaling. The new device has been designed to simulate the presence of the non-contributing leg during unilateral pedaling. During coupled bilateral pedaling, the two legs are working in unison 180° out of phase. While one leg is extending in the downstroke, it provides support to lift the other leg back up as it is flexing in the upstroke. Mechanically, torque applied by one leg is positive during the downstroke and negative during the upstroke. The negative torque is compensated for by the greater positive torque of the other leg, and the net torque on the crankshaft remains positive. Pedaling with only one leg causes changes in the mechanics of the task. During the upstroke, the torque must be positive to keep the crank moving. Since the other leg is not contributing the positive torque to cancel out the negative work during flexion, the single leg must use different muscle activity to produce positive work and complete the pedaling cycle (Ting et al. 1998). To compensate during one legged pedaling, the assistance mechanism provides the missing torque during the upstroke that the noncontributing leg would otherwise be providing. The torque that the

mechanism adds during the flexion phase of unilateral pedaling will be defined as "assistance."

A second set of pulleys is used to change the workload during pedaling through use of a frictional resistance. Modifying the workload is needed in coupled bilateral pedaling to match the workload created by the assistance mechanism. Stretching the elastic bands during extension requires increased work that would not be seen during coupled bilateral pedaling. Changing the workload can also be used for other experiments that desire an increased workload in any pedaling condition.

Since the two pedals can now move independently, each side must have its own position encoder. The previous device used a bearing free design for the crankshaft, but it had instances of seizing caused by thermal expansion when pedaling at too high of a rate. Therefore, bearings were incorporated into the new device.

2.2.2 Design Description

Figure 2.1 shows the structural components of the pedaling device. The device is attached to a base board [polyvinyl chloride – (PVC)] that the subject lies on, which provides stabilization so the device does not move when it is in use. Four uprights [polycarbonate (PC)] are used to rigidly support the crankshaft [polyoxymethylene (POM), commonly sold as Delrin®] at 10 inches above the base. Connecting the crankshaft to the uprights are four ball bearings [POM shells and glass balls]. In the middle of the crankshaft there is a coupler [POM] with a removable pin [nylon] used to couple or decouple the two sides. On the end of each side of the crankshaft, the crank arms [POM] extend perpendicularly to attach the pedals. The width between the two

crank arms is 9 inches. The pedals are made of wooden blocks with Velcro strap sandals glued on. The pedals rotate freely on the pedal shaft [POM] that is affixed to the crank arms. The distance between the crankshaft and pedal shafts is 3 inches, making this the effective crank arm length. Two optical position encoders (model: TD 5207, Micronor Inc., Newbury Park, CA) are attached near the base of the device, with a timing belt connecting them each to one half of the crankshaft with one-to-one ratio timing pulleys.

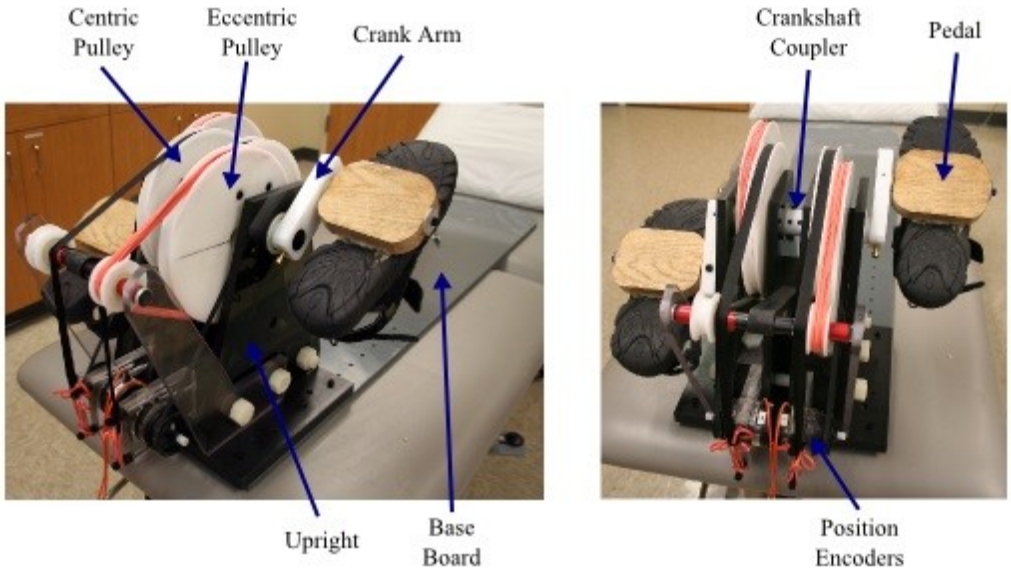

Figure 2.1 Pictures of the novel, custom designed pedaling device. The centric pulley is used for adjusting the workload and the eccentric pulley is the assistance mechanism. The crankshaft coupler is able to couple both legs for in-phase or out-of-phase bilateral pedaling, or decouple for unilateral pedaling.

A system of pulleys is used to adjust the workload and for the assistance mechanism, with an identical setup on each half of the crankshaft. To adjust the workload, a centric pulley [POM] is used. It is an 8 x 0.75 inch cylinder with a groove in the circular face and a hole through the center of the flat faces for the crankshaft. A nylon strap surrounds this pulley, creating frictional resistance as the device is pedaled

which affects the workload. The workload is adjusted by increasing or decreasing the tension on the nylon strap, and each side of the device can be adjusted independently.

Two more pulleys on each side are used for the assistance mechanism to assist the unilateral pedaling leg during the flexion phase. The first is an eccentric pulley [POM] next to the workload pulley on the crankshaft. This pulley is also an 8 x 0.75 inch cylinder, except the grove in the circular face is concave and the hole for the crankshaft is 2 inches offset from the center. The second is a small centric, 2 x 0.75 inch cylinder with a concave groove in the circular face and hole through the center of the flat faces. This pulley is mounted 8.5 inches posterior to, and at the same height as the crankshaft. They contain ball bearings [POM shells and glass balls] and spin freely on a shaft [PC] that is held up with supports [PC] extending from the uprights. Elastic bands are around the eccentric and small centric pulley. During the downstroke, the eccentric pulley stretched these elastic bands, storing potential energy that was released back during the upstroke as the bands relaxed. The eccentric pulley was positioned at an angle with respect to the crank arm in such a way that the onset of stretching the elastic bands from their most relaxed state lags the start of the pedaling cycle from top-dead-center (TDC) by 45° (45° from anti-parallel to the crank arm). This position was chosen through a process of trial and error, in which we tested the effect of the pulley on pedaling in 8 positions beginning at -90° through 90° in increments of 22.5°. The position needed to take into account the effect of gravity on pedaling given the user's supine position, and ensure the elastic bands are being stretched during the appropriate part of the cycle. The final angle of 45° felt right for all subjects during testing, and no one failed to be able to pedal unilaterally with the assistance mechanism in a way that matched bilateral pedaling.

The assistance mechanism in four stages of stretching and relaxing is shown in Figure 2.2. Adjustments can be made to tune the device for each individual. For a constant workload of the device and constant pedaling rate, the amount of assistance required varies based on muscle tone and the weight of the subject's leg. Therefore, a varying number of elastic bands can be used on the eccentric pulley so the assistance mechanism provides the matching amount of torque to simulate presence of the non-contributing leg for different subjects. Detailed components diagrams and materials used for the device can be found in Appendix (A).

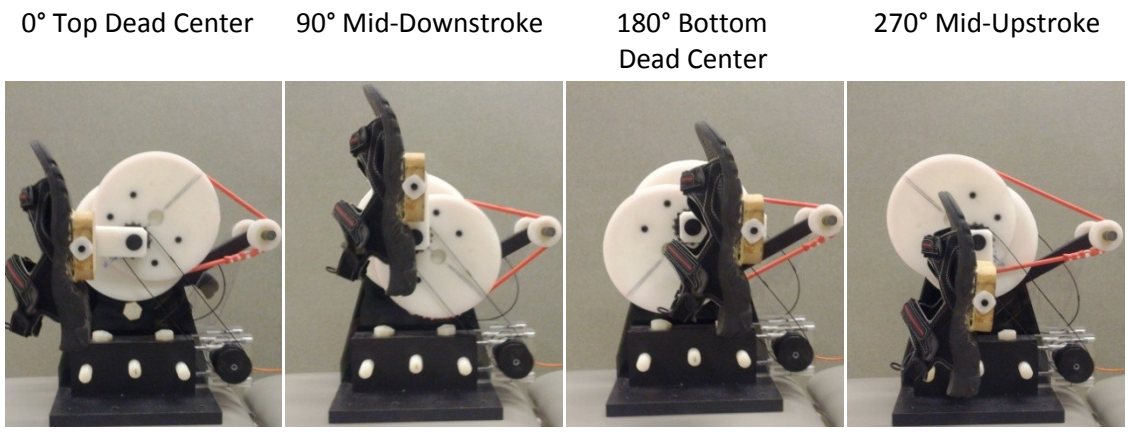

Figure 2.2 The assistance mechanism works by stretching the band during pedaling between 45° where it is most relaxed and 225° where it is maximally stretched, which stores energy. The band releases that energy back to help the user after 225°, when non-contributing leg would be doing most of the work.

2.3 Phantom Scan Experiment

The first experiment was performed to ensure that the new device did not interfere with the MRI signals. A phantom is an anthropogenic object used to test the performance of an MRI and any equipment used during scanning. The phantom is scanned alone and

then under various conditions with the pedaling device to see if it results in images different than the phantom alone.

2.3.1 Methods

Instrumentation and Data Recording

For the phantom experiment, a 3T short bore scanner (Discovery MR750 3T, General Electric Healthcare) was used with a single channel transmit/receive split head coil assembly (Model 2376114, General Electric Healthcare). The scan sequence used to acquire the phantom data was T2* weighted echo-planar imaging, collecting thirty-six slices along the sagittal plane (repetition time (TR): 2000 ms, echo time (TE): 25 ms, flip angle: 77º, 64 x 64 matrix, 4 mm slice thickness, and field of view (FOV): 24 cm, 3.75 x 3.75 x 4.00 mm slice thickness). Each run consisted of 60 TR repetitions.

Data Analysis

The phantom data were processed using Analysis of Functional NeuroImages (AFNI) software (Cox 1996). MRI files obtained from the scanner were in Digital Imaging and Communication in Medicine (DICOM) format, and were first converted to 3D images using to3d [time: zt, number of points (slices) in the z-direction: 36, number of points in the t-direction (time): 60 TRs, TR time: 2000ms, alt+z]. A time series of each individual voxel was aligned to the same temporal origin within each TR using 3dTshift to perform a 7th order Lagrange polynomial interpolation [align each slice to tzero (time offset): 0, ignore the first 4 TRs, heptic]. Multiple runs of the same condition were concatenated together, and the first 4 TR's were removed for each run to eliminate

non-steady state magnetization artifacts using 3dTcat. The concatenated functional data for each condition were registered to the first run to account for any movement of the setup using iterative linearized weighted least squares technique with 3dvolreg [heptic, base: 0].

To test the hypothesis that the device would not interfere with signal detection during MRI scanning, the phantom and several conditions were tested to determine if anything caused signal intensity change, a degradation of the signal to noise ratio (SNR), or artifacts. The SNR was found by comparing the mean signal intensity of a 36000 μL (4x4x4 voxels) volume at the center of the phantom to a 36000 μL region of empty space outside of the phantom. Any signal seen in the empty space would be caused by noise. The calculation used for SNR was:

$$SNR = S / (0.655*SD_{noise})$$

where S is the mean signal of a region of interest at the center of the phantom, SD_{noise} is the standard deviation of the noise in a region outside of the phantom, and 0.655 is the scaling factor used to correct for changes in the distribution of Gaussian noise present on the raw dataset caused by calculation of the magnitude image from original complex MRI data (Haacke et al. 1999). Change in signal intensity was determined by finding the percent difference between conditions in the 3600 μL volume in the center of the phantom. The 3D datasets of signal intensity for the three conditions were also subtracted from the phantom alone to visually show any changes in signal intensity, noise, or artifacts caused by use of the device.

Procedure

The phantom was scanned under four different conditions: the phantom alone, phantom + device, phantom + device + electronics, and phantom + device + electronics + movement. A wooden stick was connected to a pedal of the device that reached outside the 10 gauss line of the scanner. An experimenter moved the stick in a pedaling fashion to simulate the operation of the device. Two runs were performed for each condition.

2.3.2 Results

Signal to noise ratios from the phantom experiment are shown in Table 2.1, and the subtraction images between the phantom and the phantom+condition(s) are shown in Figure 2.3. The results suggest that the pedaling device, electronics, and movement did not produce signal changes that would be consistent with task related activity while in the MRI environment. With the device, electronics, and movement, the SNR decreased 1.8%, and the mean intensity changed 0.78%. The images show that the intensity differences were not visually distinguishable when the conditions subtracted from the phantom, but the very small differences can be seen when the intensity scale was reduced to 1% of the original. These results support our hypothesis that the device would not interfere with MRI signal detection.

Also seen are two forms of artifacts. The first is Gibbs ringing, which are lines that run parallel to the circumference of the phantom, created during the numerical evaluation of the Fourier series at the sharp transition of the phantom's edge. The second is the Nyquist ghost, seen as faint mirror images above and below the phantom, is created by the EPI pulse sequence technique (Haacke et al. 1999). These artifacts are only seen

because the image is amplified to 1% of the original scale, and will not be misinterpreted as task-related activity.

Table 2.1 Signal to noise ratio (SNR) and signal intensity comparing the phantom to the phantom with each condition added to the scan.

Condition	SNR	SNR Difference	Intensity Difference
Phantom	2279		
Phantom + Device	2265	0.6%	0.31%
Phantom + Device + Electronics	2281	0.1%	0.63%
Phantom + Device + Electronics + Movement	2238	1.8%	0.78%

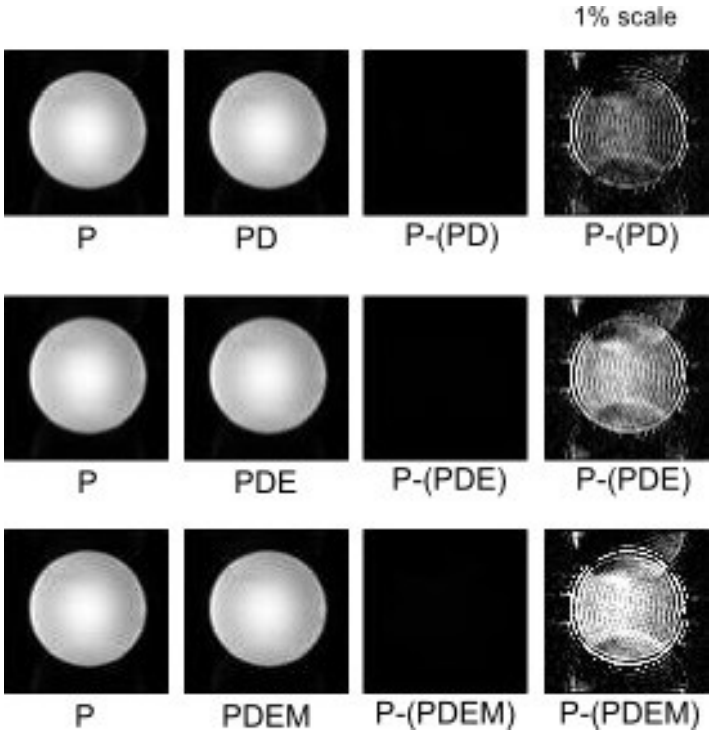

Figure 2.3 Scan results showing the phantom alone and with each condition added in, and the subtraction of the conditions from the phantom alone. P: Phantom, D: Device, E: Electronics, M: Movement

2.4 Validation Experiments

The second set of experiments was performed to verify the function of the device. The new device incorporates a novel assistance mechanism that is used during unilateral pedaling. Since this is a new design, we needed to verify that pedaling unilaterally with the assistance mechanism is able to adequately simulate the presence of the non-contributing leg by comparing it to coupled bilateral pedaling.

2.4.1 Methods

Instrumentation and Data Recording

For the validation experiments, muscle activity was recorded using an 8-channel EMG amplifier system (Delsys Bangoli-8) along with a 16-bit analog to digital converter board (Micro 1401mkII, Cambridge Electronic Design). EMG, crank velocity, and crank position data were recorded using Spike2 software on a Windows XP computer at a sampling rate of 2000 Hz.

Data Analysis

For the purpose of validating the device, velocity and EMG data were analyzed to test our hypothesis that the leg's performance during unilateral assisted pedaling accurately replicated how it performs during bilateral pedaling. Before the data were processed, each run was visually checked to see if the subject stopped pedaling at any point. Any cycle that contained a pause was removed and the good data were concatenated.

Instantaneous velocity was recorded continuously over the duration of each run, which captured multiple complete revolutions, or cycles, of pedaling. For the purpose of analysis, the data were condensed down to a single velocity profile, which showed how the velocity varied over one cycle of the crank. The velocity profile consisted of 360 points representing the average velocity at each degree of the crank cycle. To create this profile, the data were binned, so that all the data points of velocity throughout an entire run that occur within a one degree bin (centered at whole degrees) were averaged together into one point. The velocity profiles from the two runs taken on the same day were averaged together and smoothed using a 5° averaging kernel (h = [1/5 1/5 1/5 1/5 1/5]).

For comparing between conditions, the crank cycle was broken into four quadrants based on the kinematic movement of the leg, an analysis method that has been previously used for pedaling (Kautz et al. 2002). The quadrants consist of the 90 degrees around the anterior and posterior transitions (AT and PT), the extension (Ex), and the flexion (Fl) phases of pedaling. The downstroke of pedaling consists of the second half of AT, all of Ex, and the first half of PT. The upstroke consists of the second half of PT, Fl, and the first half of AT. These quadrants and phases are shown in Figure 2.4. Within each quadrant, the mean and peak velocities were compared between the conditions tested using repeated measures ANOVAs and Bonferroni post-hoc tests. The effect size was calculated for peak and mean velocity individually in each quadrant as bilateral pedaling minus unilateral assisted or unassisted pedaling.

Figure 2.4 Quadrants of the pedaling cycle, anterior transition (AT), extension (EX), posterior transition (PT), and flexion (FL).

EMG data from the experiment were reduced down to a profile that represented activity during one pedaling cycle for each muscle. First, the gain from the amplifier system and any mean offset were removed. A second order Butterworth band-pass zero-lag filter was then applied with the frequency band of 10 to 500 Hz. Rectification and a 10 ms root mean square (RMS) smoothing filter were then applied. The net effect of the filtering is frequency components between 10 and 100 Hz. The EMG data were then binned into a single profile in the same process as the velocity. A physiologically probable EMG signal was not successfully recorded for each muscle on every subject. Based on the physiology of individual subjects, including muscle tone and subcutaneous fat, the task may not have been demanding enough to produce an EMG signal that would reach the skin. Runs of muscles with no signal were removed so they did not affect the statistical analysis. For EMG recordings to be considered to have no physiological signal, the EMG profile would appear flat-lined with no modulation or peaks. The coefficient of variance (COV) of the EMG signal across the pedaling cycle is reported for all data that is kept and thrown out. Since EMG data were analyzed as a set of 3 conditions (bilateral vs. unilateral assisted and unassisted), data were thrown out as a set.

All three conditions in the set had to show no signal for it to be thrown out. If one condition had a signal it was left in for analysis.

Peak EMG and area under the curve (sum) were calculated to compare EMG profiles between conditions and tested with repeated measures ANOVAs. To compare the phasing and peak location of EMG, the data were further processed. For each individual EMG profile, the minimum value was removed and the profile was then normalized to the maximum value, and the individual profiles were averaged across the group for both days. The effect size was calculated for EMG in each muscle for the peak and sum individually as bilateral pedaling minus unilateral assisted or unassisted pedaling.

For both velocity and EMG data, bilateral pedaling was considered the nominal condition that all others were compared against during post-hoc tests.

Procedure

To validate that the pedaling device could simulate the presence of the non-contributing leg while pedaling unilaterally, we conducted a unilateral pedaling experiment outside of the MRI environment. We recruited 11 able-bodied individuals (5 female, 6 male) 21 years of age or older (mean age 25), all right-side dominant with no known neurological or physical disorders. Subjects were consented for the experiment according to Marquette University and the Medical College of Wisconsin guidelines for human subject research.

The subject lay on an examination table with feet strapped to the pedals. Padding was placed on the backboard to provide comfort. EMG electrodes were placed on the

tibialis anterior (TA), vastus medialis (VM), rectus femoris (RF), and biceps femoris (BF) on each leg along with one ground electrode on the medial aspect of the leg, proximal to the medial malleolus.

Five pedaling conditions were performed for validation of the device's function: bilateral, assisted unilateral right, assisted unilateral left, unassisted unilateral right, and unassisted unilateral left. The run for each condition was 60 seconds, and each condition was performed twice. The order that the conditions were performed was counterbalanced between sessions and subjects. The experimental data collection sheet can be found in Appendix B.

In the unilateral assisted conditions, only one leg pedaled during each run with the assistance mechanism engaged. The non-contributing leg was removed from the pedal and supported by a large, curved cushion. The amount of assistance required for each subject varied based on muscle tone and the weight of the subject's leg. The assistance mechanism was adjusted by adding or removing rubber bands from around the eccentric pulley. The experimenter estimated how many elastic bands the subject may need based on body type, and tested a range of three amounts. The number of elastic bands used ranged between 5 and 10. Unilateral pedaling was also tested with the assistance mechanism disengaged, meaning no elastic bands were used. This was done to show that unassisted unilateral pedaling varies too much from assisted.

Coupled bilateral pedaling was the nominal condition. Both legs pedaled together 180° out of phase, as on a conventional bicycle. During this condition, three different workloads were tested. The assistance mechanism adds a workload during unilateral

pedaling, so increasing the workload using the centric pulley is needed to match it during bilateral coupled pedaling.

An auditory timing cue was used to keep pedaling rate constant at 45 revolutions per minute (RPM) across conditions and subjects. During each run, subjects were asked to begin pedaling with the timing cue. After a few seconds when a constant pedaling rate was reached, data recording began. Recording lasted for 60 seconds, after which the subject was told to stop. Between each run, the subject was asked if a break to rest would be needed, or if the next run could begin. Also following each run, the average pedaling rate was calculated to check if it was between 42 and 48 RPM. If it was not within that range, the run was repeated. Runs were repeated until two were collected for each condition within the accepted pedaling rate range.

Velocity across the pedaling cycle and EMG data recorded during these trials were used to select the number of elastic bands and work load that provided the best match between unilateral and bilateral pedaling for the each subject. The criteria for selecting the best match of elastic bands and resistive load was based on finding the least amount of difference between the bilateral and unilateral condition's velocity and EMG profiles. Visual inspection usually revealed the best match. If it was not visually apparent which bands and load resulted in least difference, the absolute value of the difference was calculated between each combination of bilateral loads and unilateral assisted bands for velocity and EMG, and the combination with the lowest total difference was the best match. Typically, velocity profiles were used to select the number of elastic bands for the assistance mechanism, as velocity varied more based on the number of bands than on the bilateral work load. Likewise, EMG profiles were

typically used to select the bilateral workload since it caused more EMG variance than the number of bands in unilateral pedaling. In some cases, however, all combinations of the number of elastic bands and workload were considered using both velocity and EMG profiles. Figure 2.5 shows the velocity profiles for bilateral pedaling and unilateral pedaling with the different numbers of elastic bands. The dotted lines show the absolute difference between bilateral and each amount of bands, which can help in selection. In Figure 2.6, EMG profiles are shown for bilateral pedaling at the different load levels and one unilateral assisted pedaling. After the first session, the data were analyzed to select the optimum number of elastic bands and amount of load for the subject.

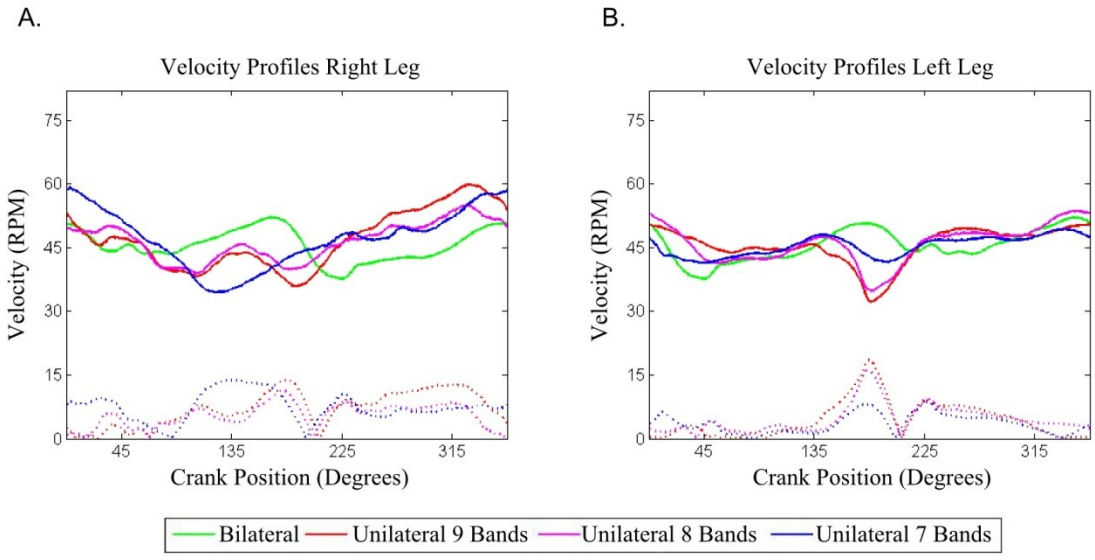

Figure 2.5 Representative example of crank velocity profiles for elastic band selection during bilateral pedaling (green), unilateral assisted pedaling with 9 bands (red), 8 bands (magenta), and 7 bands (blue). The data shown are from the same subject performing right (A) and left (B) pedaling. Dotted lines show the absolute difference.

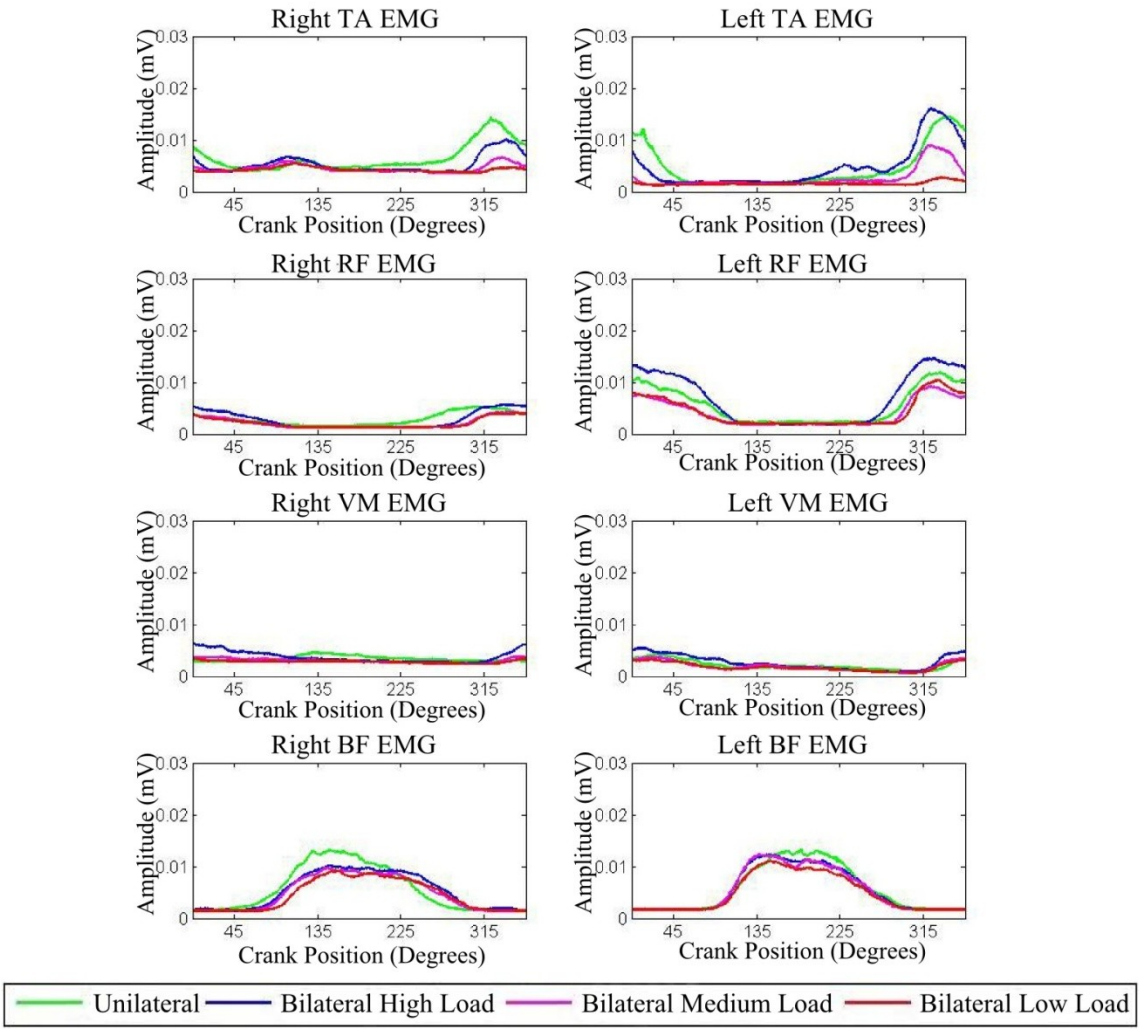

Figure 2.6 Representative example of EMG profiles for load selection during unilateral assisted pedaling (green), bilateral pedaling at high load (blue), medium load (magenta), and low load (red). The data shown for EMG activity of the tibialis anterior (TA), rectus femoris (RF), vastus medialus (VM), biceps femoris (BF).

To establish repeatability, the same subjects returned on a different day to repeat the experiment with only the selected number of elastic bands and resistive load used. The setup and procedure for the second session was the same as the first aside from not varying the number of elastic bands or resistive load. The results from the second session were compared to the first to show that the subjects perform the same each time they use the device.

2.4.2 Results

The assistance device used during unilateral pedaling successfully mimicked the role of the non-contributing lower limb, supporting our hypothesis. The effectiveness of the assistance device was evident in the spatiotemporal profile of the crank velocity and the pattern of lower extremity muscle activity observed during pedaling. Eleven subjects completed the two sessions of the study (6 males, 5 females, mean age 25). All velocity data recorded were used. Nineteen out of 176 total sets of EMG profiles had to be thrown out due to no signal. The average coefficient of variance (COV) for EMG data that was considered to be no signal and thrown out was 0.117, and the average COV of the remaining data was 0.494.

Figure 2.7 provides a representative example of the crank velocity recorded across the pedaling cycle during bilateral coupled, unilateral assisted pedaling, and unilateral unassisted pedaling performed by the right and left leg on two different days. One can see that without the assistance device in the unilateral unassisted task, the spatiotemporal profile of crank velocity was not well matched to the bilateral coupled condition. Also during the unilateral unassisted condition, the crank velocity varied considerably from the

desired 45 RPM, particularly at about 180° where the limb transitioned from the extension to flexion phase of the pedaling cycle. When the assistance was added to the unilateral pedaling, the velocity profile was much more similar to the the velocity profile during coupled bilateral pedaling. These observations are maintained in the group data, shown in Figure 2.8, which also depicts a poor match in the velocity profile between the unilateral unassisted and bilateral coupled pedaling conditions. Velocity was much better matched for unilateral pedaling when the assistance mechanism was added. These observations were consistent for both right and left legs, and could be reproduced across days.

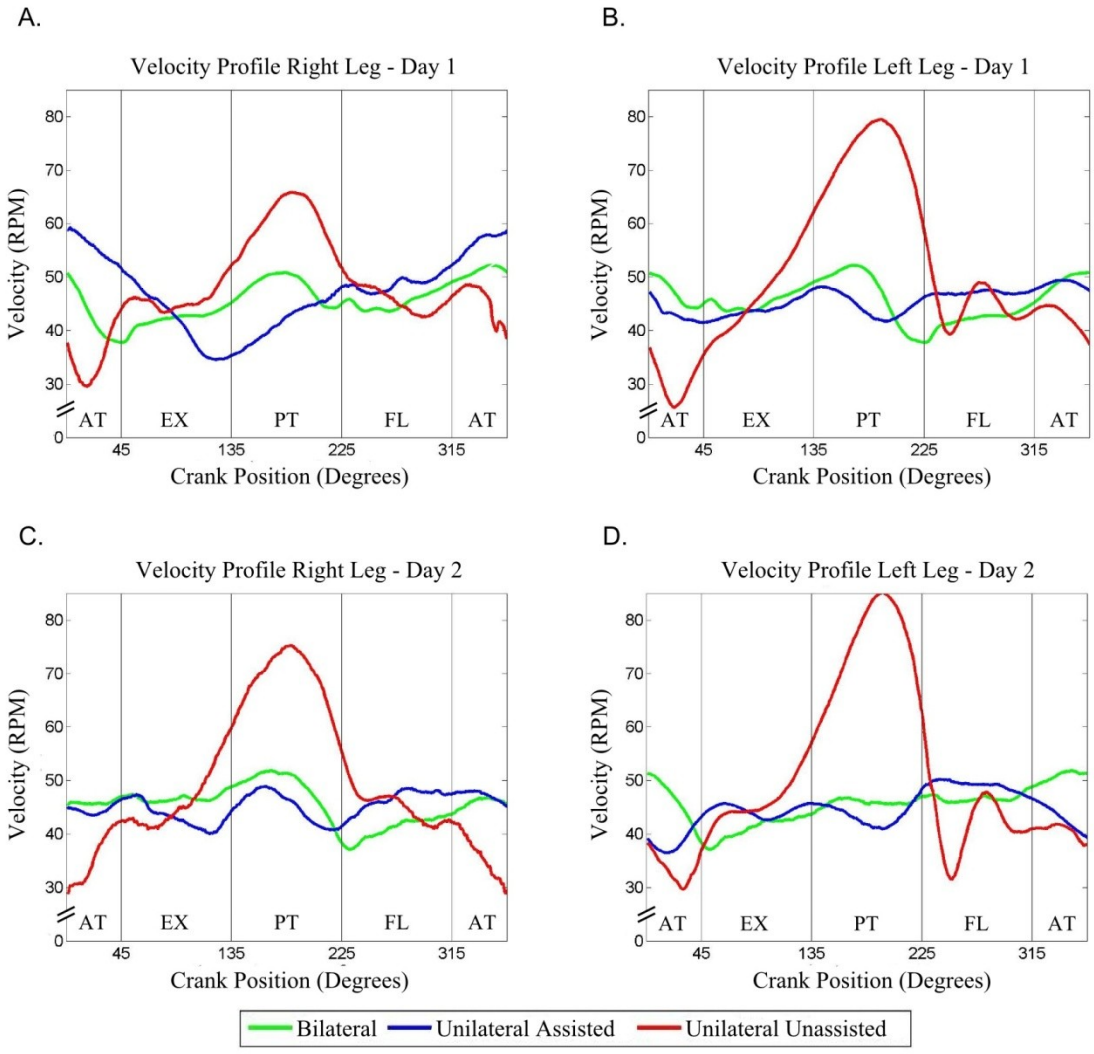

Figure 2.7 Representative example of crank velocity profiles during bilateral pedaling (green), unilateral assisted pedaling (blue), and unilateral unassisted (red). The data shown are from the same subject performing right (A) and left (B) pedaling on day 1, and right (C) and left (D) on day 2. Zero degrees represents the top-dead-center with respect to the unilateral pedaling leg, left or right. Vertical black lines indicate the four quadrants of the pedaling cycle, which are the anterior transition (AT), extension (EX), posterior transition (PT), and flexion (FL).

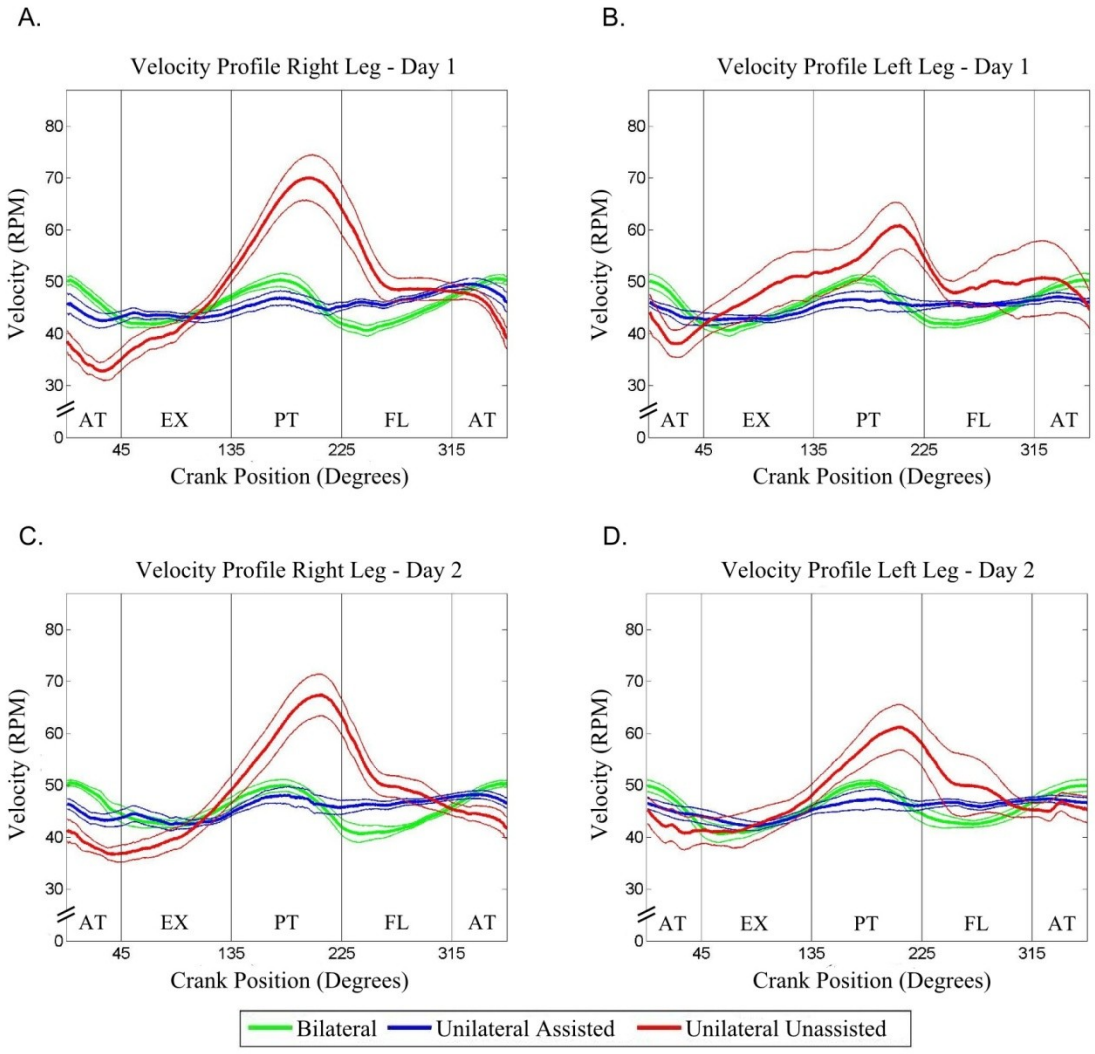

Figure 2.8 Group average crank velocity profiles during bilateral pedaling (green), unilateral assisted pedaling (blue), and unilateral unassisted (red). Heavier lines are the mean and lighter lines are the standard error. The data shown are group averages of right (A) and left (B) pedaling on day 1, and right (C) and left (D) on day 2. Zero degrees represents the top-dead-center with respect to the unilateral pedaling leg, left or right. Vertical black lines indicate the four quadrants of the pedaling cycle, which are the anterior transition (AT), extension (EX), posterior transition (PT), and flexion (FL).

Quantitative examination of the peak and mean crank velocity in each of the four quadrants of the pedaling cycle provided further support that unilateral assisted pedaling provided a good match to coupled bilateral pedaling. The peak velocity was matched between coupled bilateral pedaling and unilateral assisted pedaling in all four quadrants on day 1 (Figure 2.9A and B, Table 2.2A) and day 2 (Figure 2.10A and B, Table 2.3A). Without the assistance mechanism, the peak velocity was significantly different during PT and FL for right leg and PT for left leg on day 1. On day 2, it was also different during AT, PT, and FL for right leg and PT for left leg. The mean velocity was the same between bilateral coupled and unilateral assisted pedaling in all quadrants except FL for right leg on day 1 (Figure 2.9C and D, Table 2.2B) and day 2 (Figure 2.10C and D, Table 2.3B), during which it was slightly greater. The effect size across quadrants for bilateral pedaling compared to unilateral assisted pedaling ranged from 0.12 – 3.14 RPM for peak velocity and 0.11 – 4.39 RPM for mean velocity. The effect size for bilateral pedaling compared to unilateral unassisted pedaling across quadrants ranged from 0.98 – 23.34 RPM for peak velocity and 0.86 – 16.28 RPM for mean velocity (Table 2.4). Without the assistance mechanism, the mean velocity was significantly different during PT and FL for right leg on day 1. On day 2, it was also different during AT, PT, and FL for right leg. The difference between velocity profiles of each condition, calculated as bilateral minus unilateral assisted and bilateral minus unilateral unassisted, is shown in Figure 2.11A for day 1 and Figure 2.11B for day 2.

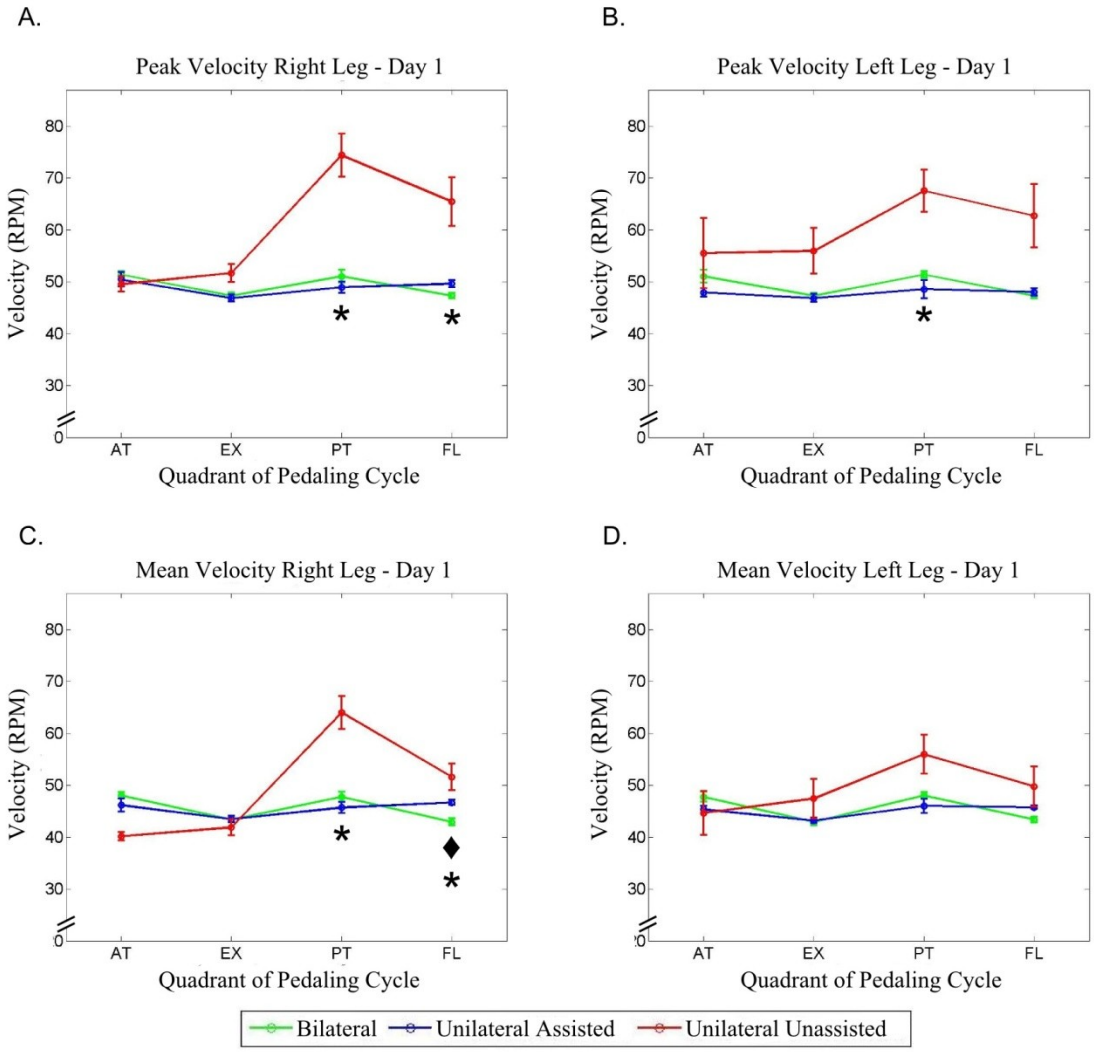

Figure 2.9 Mean (±SE) values on day 1 for the peak velocity in each quadrant for right (A) and left (B) pedaling, and mean velocity of each quadrant for right (C) and left (D) pedaling. The four pedaling quadrants are anterior transition (AT), extension (EX), posterior transition (PT), and flexion (FL). Statistical results are also shown for each quadrant, with * indicating a significant difference between bilateral and unilateral unassisted pedaling, and ♦ indicating a significant difference between bilateral and unilateral assisted pedaling.

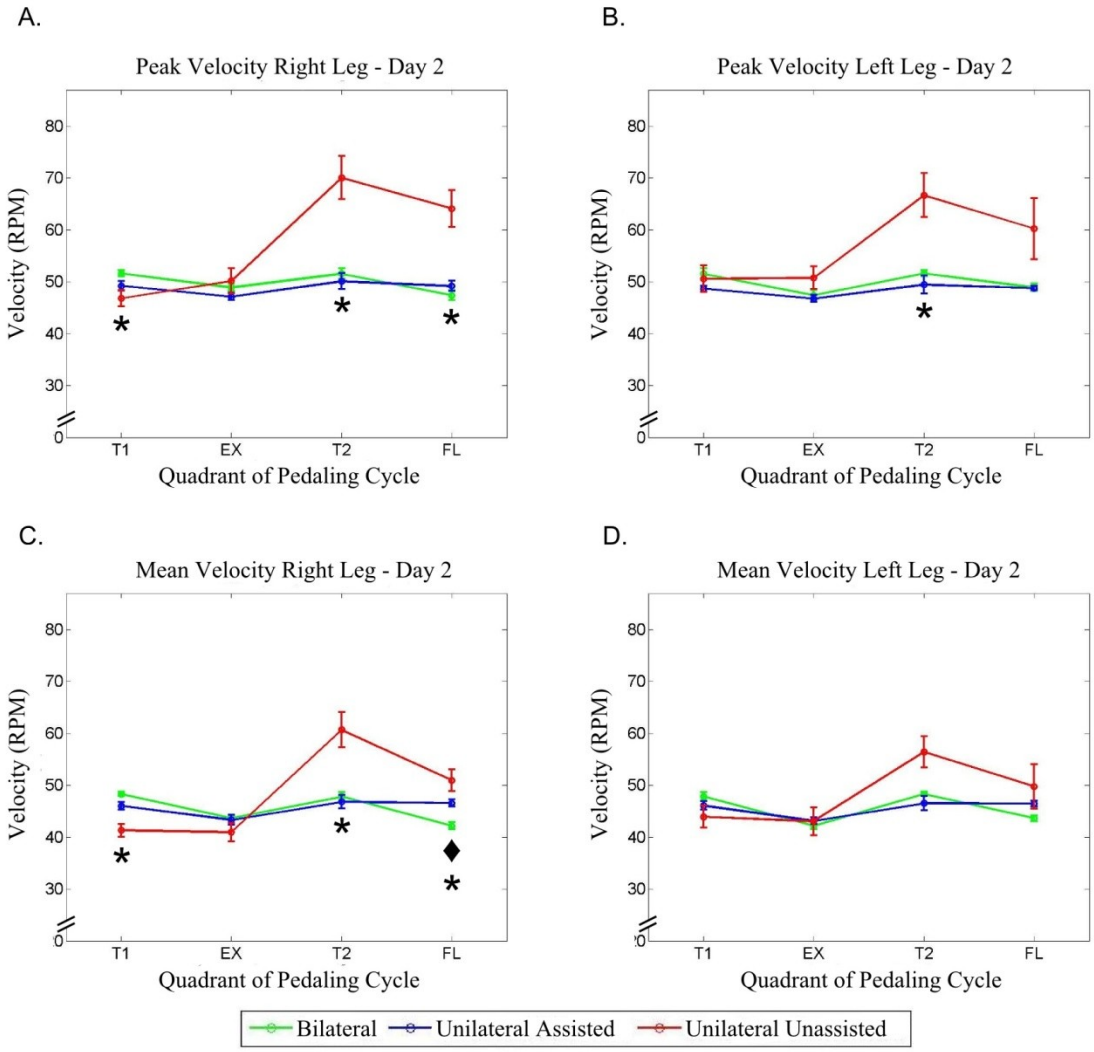

Figure 2.10 Mean (±SE) values on day 2 for the peak velocity in each quadrant for right (A) and left (B) pedaling, and mean velocity of each quadrant for right (C) and left (D) pedaling. The four pedaling quadrants are anterior transition (AT), extension (EX), posterior transition (PT), and flexion (FL). Statistical results are also shown for each quadrant, with * indicating a significant difference between bilateral and unilateral unassisted pedaling, and ♦ indicating a significant difference between bilateral and unilateral assisted pedaling.

Table 2.2 Group mean (±SE) values for peak crank velocity and mean crank velocity in each quadrant of the pedaling cycle recorded on Day 1, and statistical results of the repeated measures ANOVA. AT = anterior transition, EX = extension, PT = posterior transition, FL = flexion, Bilat = bilateral coupled pedaling, Unilat A = unilateral assisted, Unilat Un = unilateral unassisted, '…' indications no post hoc due to non-significant global effect of condition

A. Day 1 Peak Crank Velocity

		Mean ± SE (RPM)			P-Value		
		Bilat	Unilat A	Unilat Un	Global Effect	Bilat vs Unilat A	Bilat vs Unilat Un
AT	Right	51.4±0.66	50.5±1.34	49.5±1.48	0.438	…	…
	Left	51.1±1.23	47.9±0.81	55.5±6.77	0.329	…	…
EX	Right	47.4±0.53	46.9±0.67	51.7±1.74	0.010	1.00	0.087
	Left	47.4±0.50	46.9±0.75	55.9±4.39	0.069	…	…
PT	Right	51.1±1.23	48.9±1.13	74.4±4.15	<0.001	0.214	0.001
	Left	51.4±0.66	48.6±1.77	67.6±4.07	<0.001	0.591	0.005
FL	Right	47.4±0.50	49.6±0.69	65.5±4.72	0.004	0.063	0.010
	Left	47.4±0.53	48.0±0.72	62.7±6.15	0.032	1.000	0.078

B. Day 1 Mean Crank Velocity

		Mean ± SE (RPM)			P-Value		
		Bilat	Unilat A	Unilat UN	Global Effect	Bilat vs Unilat A	Bilat vs Unilat Un
AT	Right	48.0±0.59	46.2±1.25	40.2±0.84	<0.001	0.658	<0.001
	Left	47.8±0.95	45.3±0.69	44.7±4.20	0.528	…	…
EX	Right	43.4±0.55	43.5±0.59	41.9±1.58	0.332	…	…
	Left	42.9±0.68	43.2±0.48	47.4±3.78	0.261	…	…
PT	Right	47.8±0.95	45.7±1.04	64.0±3.21	<0.001	0.283	0.002
	Left	48.0±0.59	46.0±1.35	56.0±3.74	0.027	0.673	0.167
FL	Right	42.9±0.68	46.7±0.50	51.6±2.57	0.017	0.010	0.037
	Left	43.4±0.55	45.8±0.33	49.7±2.86	0.178	…	…

Table 2.3 Group mean (±SE) values for peak crank velocity and mean crank velocity in each quadrant of the pedaling cycle recorded on Day 2, and statistical results of the repeated measures ANOVA. AT = anterior transition, EX = extension, PT = posterior transition, FL = flexion, Bilat = bilateral coupled pedaling, Unilat A = unilateral assisted, Unilat Un = unilateral unassisted, '…' indications no post hoc due to non-significant global effect of condition

A. Day 2 Peak Crank Velocity

		Mean ± SE (RPM)			P-Value		
		Bilat	Unilat A	Unilat Un	Global Effect	Bilat vs Unilat A	Bilat vs Unilat Un
AT	Right	51.6±0.61	49.2±0.91	46.8±1.51	0.001	0.102	0.019
	Left	51.6±0.99	48.7±0.55	50.6±2.58	0.400	…	…
EX	Right	48.9±0.74	47.1±0.69	50.2±2.45	0.378	…	…
	Left	47.4±0.94	46.8±0.70	50.7±2.21	0.189	…	…
PT	Right	51.6±0.99	50.1±1.52	60.1±4.14	0.004	0.444	0.004
	Left	51.6±0.61	49.5±1.72	66.7±4.23	0.002	0.809	0.018
FL	Right	47.4±0.94	49.2±1.01	64.1±3.60	<0.001	0.368	0.001
	Left	48.9±0.74	48.8±0.40	60.2±5.90	0.067	…	…

B. Day 2 Mean Crank Velocity

		Mean ± SE (RPM)			P-Value		
		Bilat	Unilat A	Unilat UN	Global Effect	Bilat vs Unilat A	Bilat vs Unilat Un
AT	Right	48.3±0.41	46.0±0.71	41.3±1.21	<0.001	0.070	<0.001
	Left	47.8±0.82	46.1±0.82	43.9±2.16	0.186	…	…
EX	Right	43.6±0.56	43.3±0.97	41.0±1.80	0.131	…	…
	Left	42.2±0.68	43.2±0.16	43.1±2.70	0.784	…	…
PT	Right	47.8±0.82	46.8±1.25	60.7±3.39	0.003	1.000	0.020
	Left	48.3±0.41	46.5±1.40	56.4±2.99	0.003	0.884	0.084
FL	Right	42.2±0.68	46.6±0.68	51.0±2.10	0.004	0.002	0.004
	Left	43.6±0.56	46.5±0.52	49.8±4.33	0.254	…	…

Table 2.4 Effect size values for peak crank velocity and mean crank velocity in each quadrant of the pedaling cycle recorded on Day 1 and 2. AT = anterior transition, EX = extension, PT = posterior transition, FL = flexion, Bilat = bilateral coupled pedaling, Unilat A = unilateral assisted, Unilat Un = unilateral unassisted.

A. Effect Size for Peak Crank Velocity (RPM)

		Day 1		Day 2	
		Bilat - Unilat A	Bilat - Unilat Un	Bilat - Unilat A	Bilat - Unilat Un
AT	Right	0.93	1.85	2.36	4.77
	Left	3.14	-4.46	2.90	0.98
EX	Right	0.51	-4.35	1.77	-1.28
	Left	0.52	-8.58	0.63	-3.33
PT	Right	2.15	-23.34	1.46	-18.51
	Left	2.82	-16.16	2.12	-15.11
FL	Right	-2.27	-18.09	-1.78	-16.69
	Left	-0.67	-15.36	0.12	-11.33

B. Effect Size for Mean Crank Velocity (RPM)

		Day 1		Day 2	
		Bilat - Unilat A	Bilat - Unilat UN	Bilat - Unilat A	Bilat - Unilat Un
AT	Right	1.85	7.86	2.29	6.99
	Left	2.41	3.09	1.72	3.89
EX	Right	-0.11	1.50	0.32	2.69
	Left	-0.27	-4.51	-0.95	-0.86
PT	Right	2.06	-16.28	0.99	-12.89
	Left	1.99	-7.94	1.76	-8.12
FL	Right	-3.72	-8.63	-4.39	-8.78
	Left	-2.39	-6.35	-2.84	-6.12

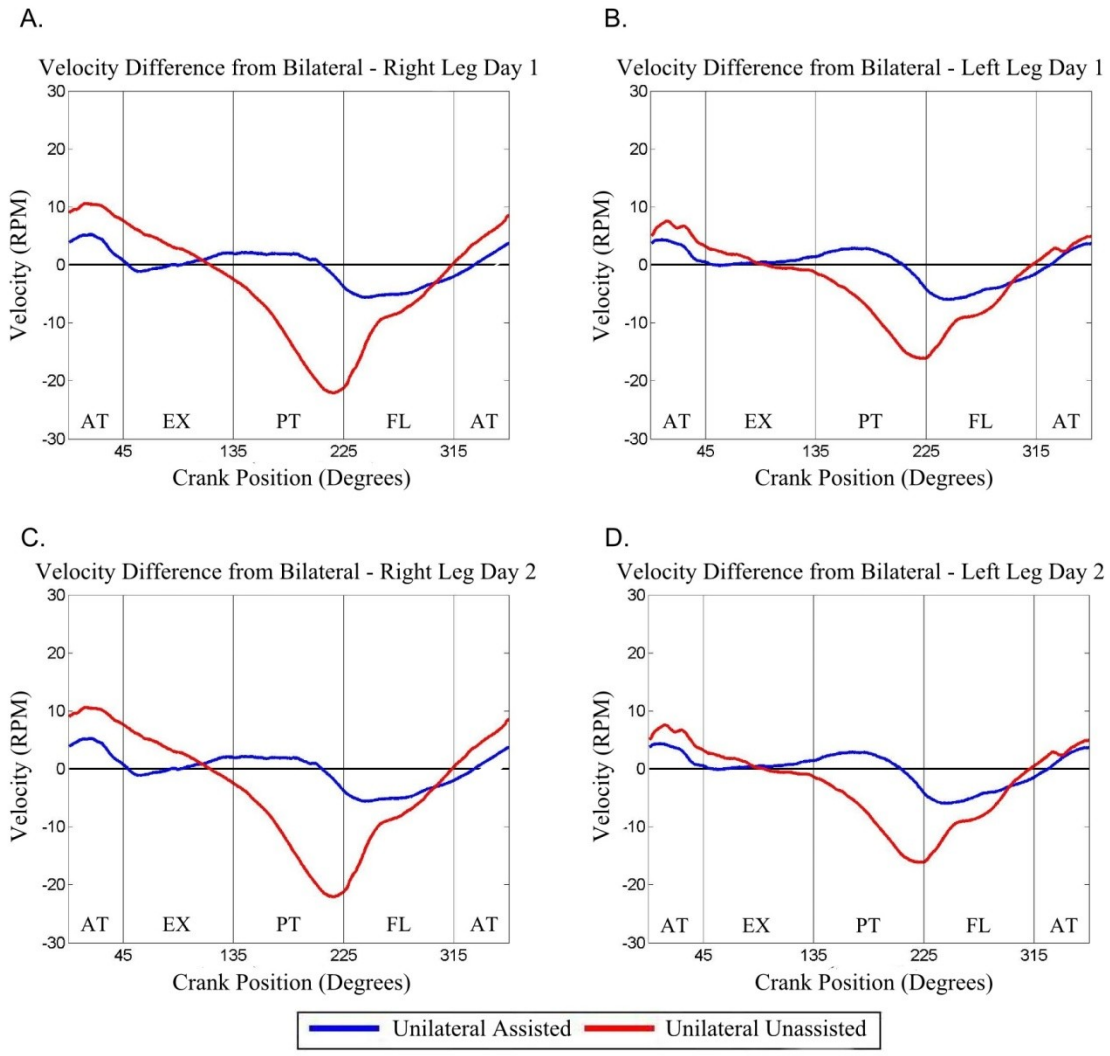

Figure 2.11: Difference of group average crank velocity profiles for bilateral minus unilateral assisted pedaling and bilateral minus unilateral unassisted pedaling (red). The data shown are differences of group averages of right (A) and left (B) pedaling on day 1, and right (C) and left (D) on day 2. Zero degrees represents the top-dead-center with respect to the unilateral pedaling leg, left or right. Vertical black lines indicate the four quadrants of the pedaling cycle, which are the anterior transition (AT), extension (EX), posterior transition (PT), and flexion (FL).

A representative example of muscle activity across the pedaling cycle during bilateral coupled, unilateral assisted pedaling, and unilateral unassisted pedaling performed by the right and left leg on two different days is shown in Figure 2.12. Without the assistance device, the spatiotemporal profile of EMG during unilateral pedaling was not well matched to coupled bilateral pedaling. Muscle activity tended to be elevated in the TA and RF, decreased in the BF, with little change in the VM. With the assistance device used in the unilateral conditions, the EMG profiles were much better matched. The normalized group average of EMG profiles for peak timing is shown in Figure 2.13. Timing of the EMG remained largely unaffected by the different conditions, with the only noticeable change being a delay of the peak during unilateral unassisted pedaling in BF. These observations were consistent for both right and left legs, and can be reproduced across days.

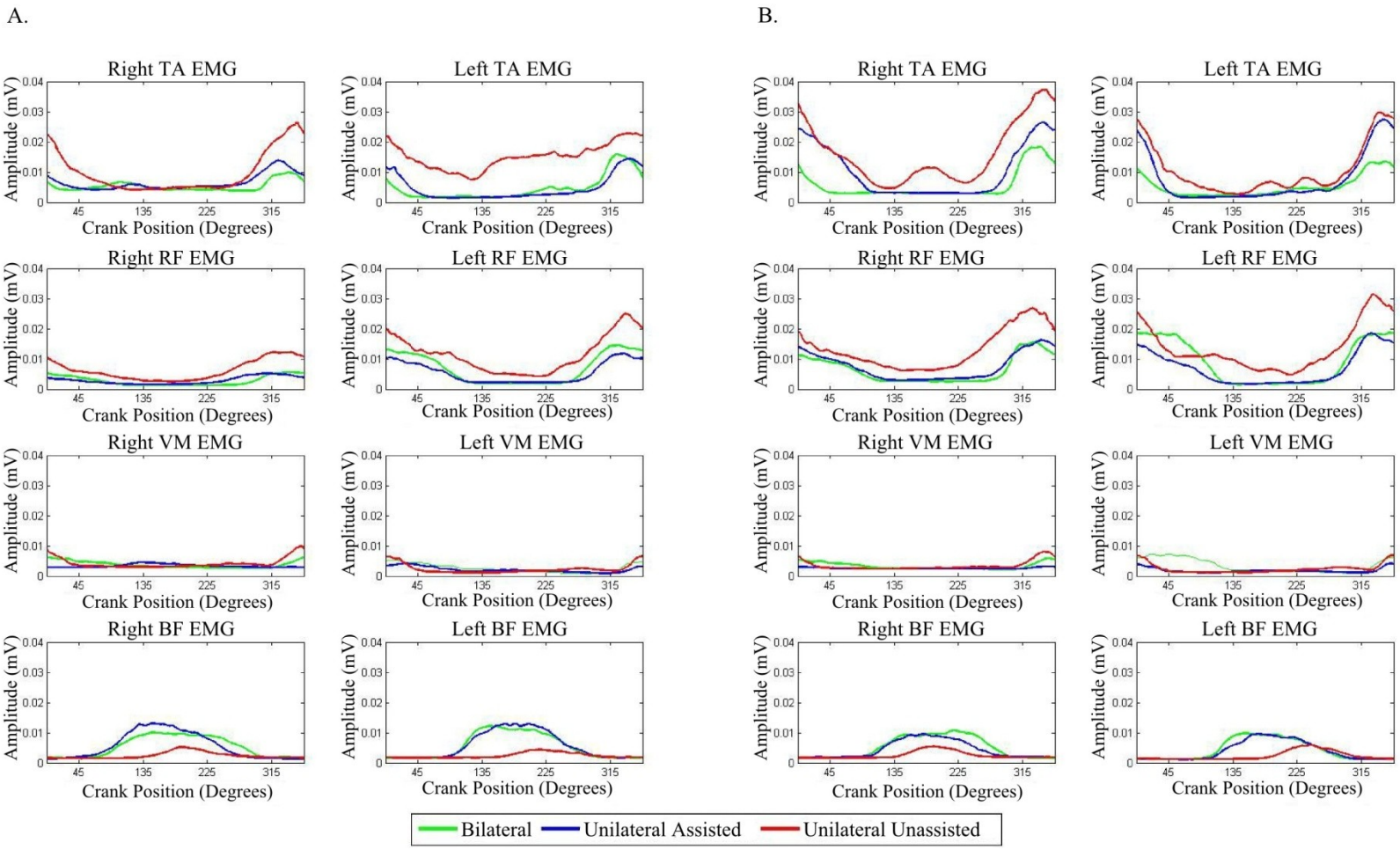

Figure 2.12 Representative example of EMG profiles during bilateral pedaling (green), unilateral assisted pedaling (blue), and unilateral unassisted (red). The data shown are from the same subject on day 1 (A) and day 2 (B) for EMG activity of the tibialis anterior (TA), rectus femoris (RF), vastus medialus (VM), biceps femoris (BF).

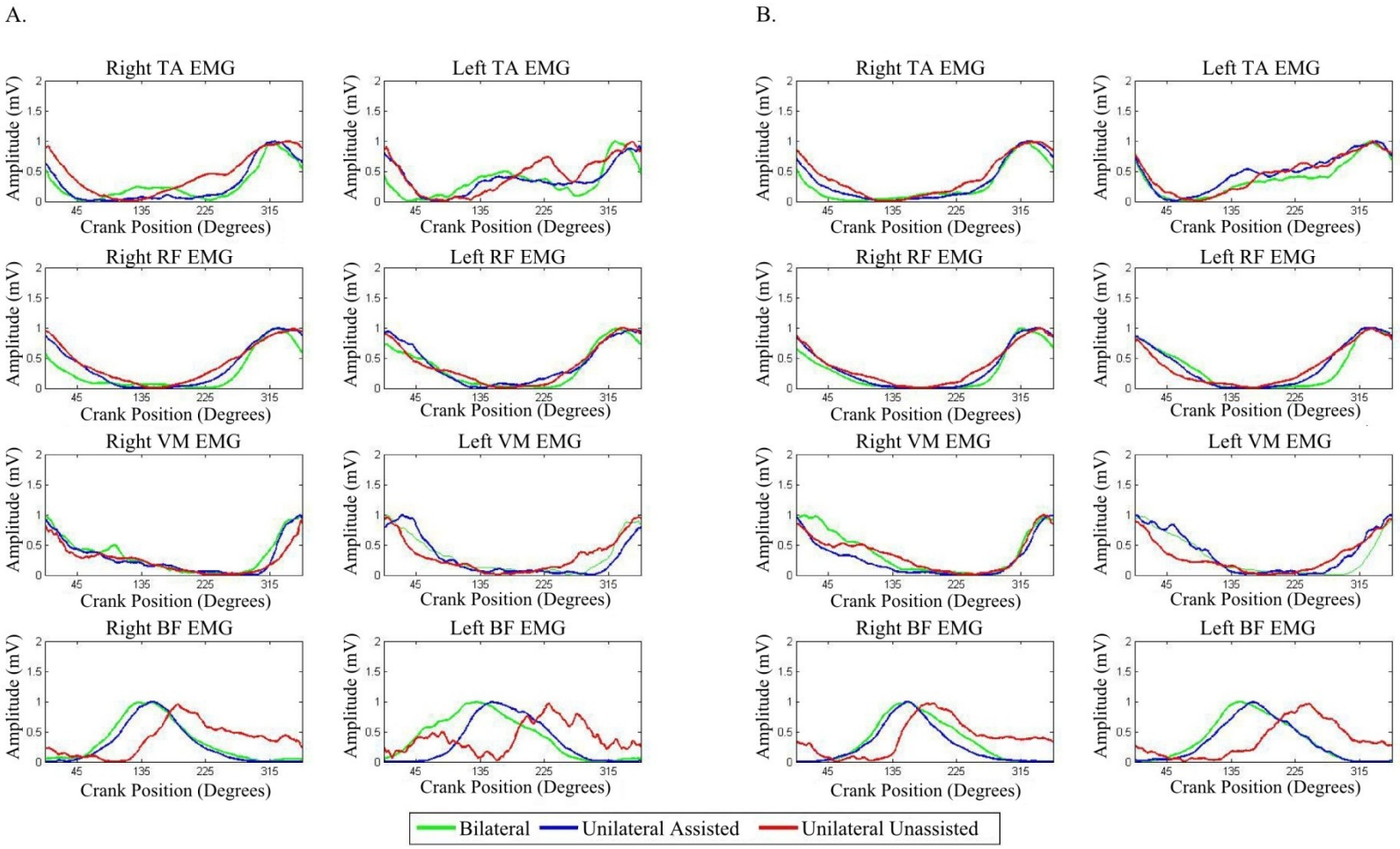

Figure 2.13 Normalized group average of EMG profiles to show peak timing during bilateral pedaling (green), unilateral assisted pedaling (blue), and unilateral unassisted (red). The data shown are from the same subject on day 1 (A) and day 2 (B) for EMG activity of the tibialis anterior (TA), rectus femoris (RF), vastus medialus (VM), biceps femoris (BF).

Peak EMG amplitude and sum of EMG across the pedaling cycle were examined quantitatively, and provided further support that unilateral assisted pedaling provided a good match to coupled bilateral pedaling. Peak EMG was the same between coupled bilateral and unilateral assisted pedaling in all muscles for right and left leg on day 1 (Figure 2.14A,B and Table 2.4A). On day 2, peak EMG was the same in all but one instance, left leg RF (Figure 2.15A,B and Table 2.5A). Without the assistance mechanism, peak EMG was different in right TA, RF, and BF, and left TA and RF on day 1. On day 2, it was different in right TA, RF, and BF, and left TA, RF, and BF. EMG sum was the same for bilateral coupled pedaling and unilateral assisted pedaling in all muscles on day 1 (Figure 2.14C,D and Table 2.4B), and the same in all muscles except the right RF on day 2 (Figure 2.15C,D and Table 2.5B). Without the assistance mechanism, EMG sum during unilateral pedaling was different in right TA and RF, and left TA and RF on day 1. On day 2, unilateral unassisted was different in right TA, RF, and BF, and left TA and RF. The effect size across muscles for bilateral pedaling compared to unilateral assisted pedaling ranged from 0.000 – 0.020 mV for peak EMG and 0.040 – 2.324 mV for sum of EMG. The effect size for bilateral pedaling compared to unilateral unassisted pedaling ranged from 0.002 – 0.017 mV for peak EMG and 0.139 – 3.508 mV for sum of EMG (Table 2.7).

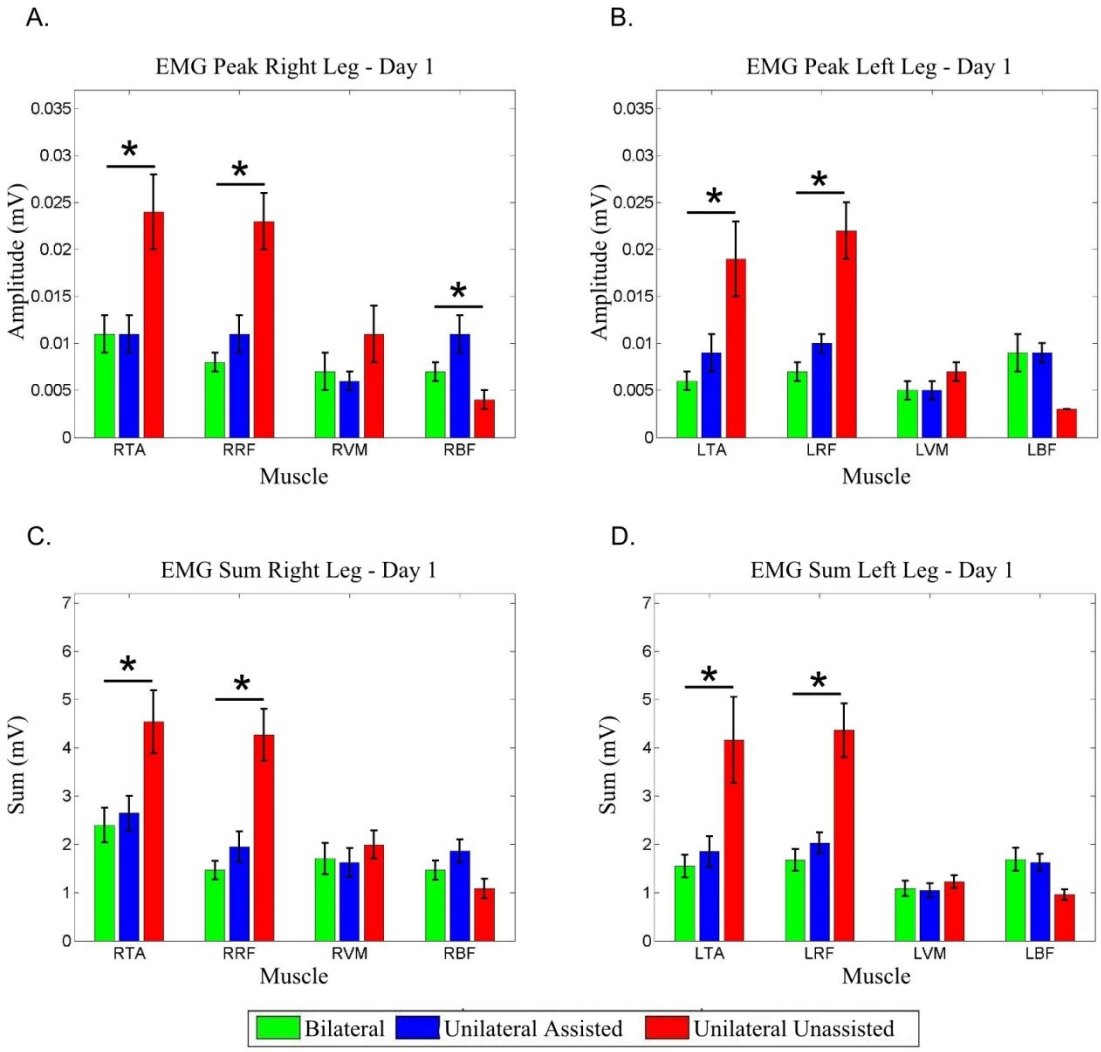

Figure 2.14 Mean (±SE) values on day 1 for the peak EMG of each muscle for right (A) and left (B) pedaling, and sum of EMG across the cycle of each muscle for right (C) and left (D) pedaling. The four muscles are tibialis anterior (TA), rectus femoris (RF), vastus medialus (VM), biceps femoris (BF). Statistical results are also shown for each quadrant, with * indicating a significant difference conditions at $P \leq 0.05$.

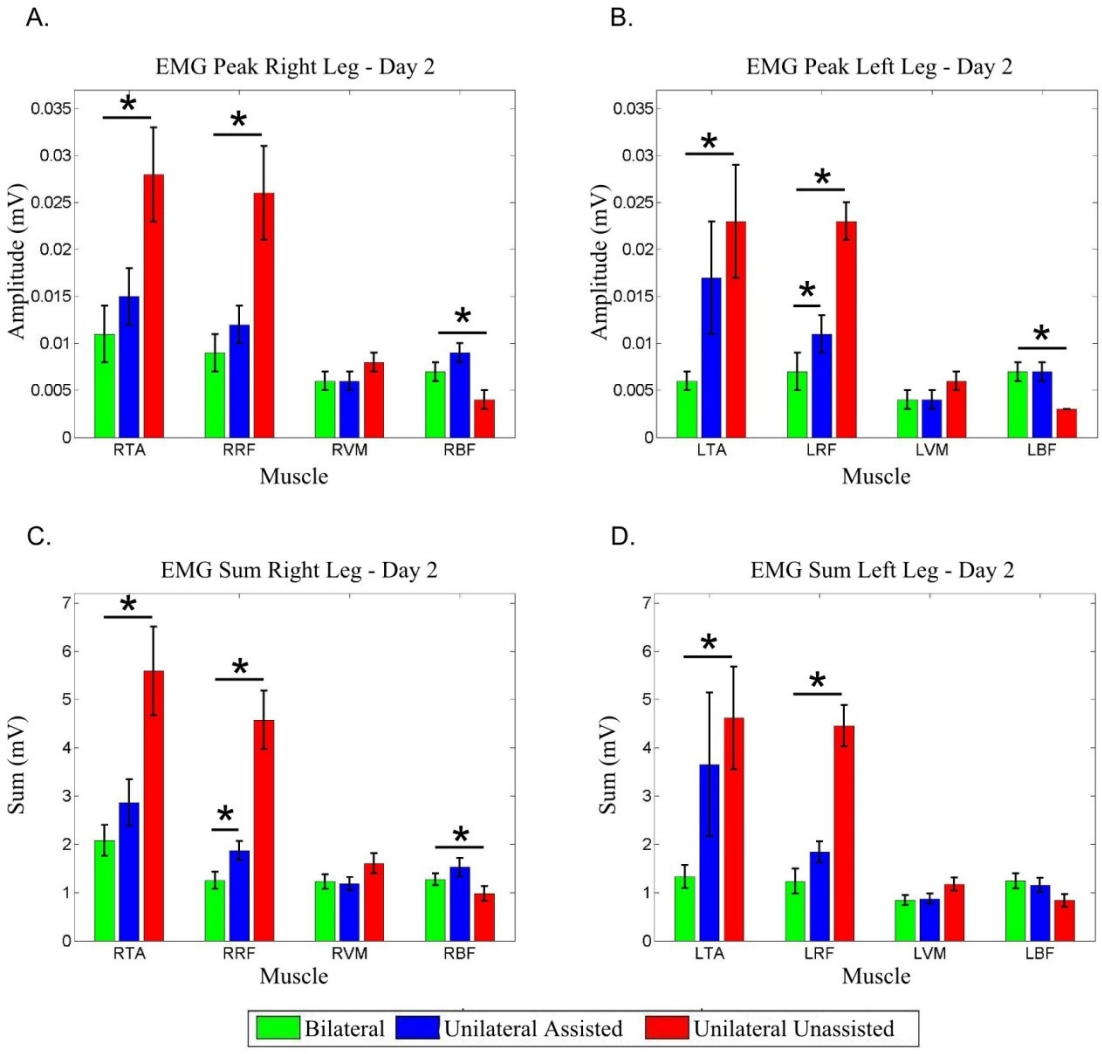

Figure 2.15 Mean (±SE) values on day 2 for the peak EMG of each muscle for right (A) and left (B) pedaling, and sum of EMG across the cycle of each muscle for right (C) and left (D) pedaling. The four muscles are tibialis anterior (TA), rectus femoris (RF), vastus medialus (VM), biceps femoris (BF). Statistical results are also shown for each quadrant, with * indicating a significant difference between conditions at $P \leq 0.05$.

Table 2.5 Group mean (±SE) values for EMG peak and EMG sum in each muscle across the entire pedaling cycle recorded on Day 1, and statistical results of the repeated measures ANOVA. TA = tibialis anterior, RF = rectus femoris, VM = vastus medialus, BF = biceps femoris, Bilat = bilateral coupled pedaling, Unilat A = unilateral assisted, Unilat Un = unilateral unassisted, '…' indications no post hoc due to non-significant global effect of condition

A. Day 1 EMG Peak

		Mean ± SE (mV)			P-Value		
		Bilat	Unilat A	Unilat Un	Global Effect	Bilat vs Unilat A	Bilat vs Unilat Un
TA	Right	0.011 ± 0.002	0.011 ± 0.002	0.024 ± 0.004	<0.001	1.000	0.001
	Left	0.006 ± 0.001	0.009 ± 0.002	0.019 ± 0.004	0.015	0.216	0.044
RF	Right	0.008 ± 0.001	0.011 ± 0.002	0.023 ± 0.003	<0.001	0.055	<0.001
	Left	0.007 ± 0.001	0.011 ± 0.001	0.022 ± 0.003	<0.001	0.071	0.002
VM	Right	0.007 ± 0.002	0.006 ± 0.001	0.011 ± 0.003	0.005	1.000	0.077
	Left	0.005 ± 0.001	0.005 ± 0.001	0.007 ± 0.001	0.116	…	…
BF	Right	0.007 ± 0.001	0.011 ± 0.002	0.004 ± 0.001	0.001	0.231	1.000
	Left	0.009 ± 0.002	0.009 ± 0.001	0.003 ± 0.000	0.004	1.000	0.086

B. Day 1 EMG Sum (mV)

		Mean ± SE (mV)			P-Value		
		Bilat	Unilat A	Unilat UN	Global Effect	Bilat vs Unilat A	Bilat vs Unilat Un
TA	Right	2.394 ± 0.358	2.644 ± 0.361	4.539 ± 0.652	0.001	0.217	0.004
	Left	1.549 ± 0.235	1.848 ± 0.320	4.164 ± 0.890	0.017	0.113	0.040
RF	Right	1.464 ± 0.194	1.948 ± 0.315	4.268 ± 0.542	<0.001	0.113	0.001
	Left	1.872 ± 0.283	2.337 ± 0.368	4.451 ± 0.509	<0.001	0.376	0.003
VM	Right	1.704 ± 0.328	1.623 ± 0.299	1.991 ± 0.288	0.034	1.000	0.312
	Left	1.087 ± 0.157	1.047 ± 0.145	1.226 ± 0.131	0.206	…	…
BF	Right	1.467 ± 0.200	1.859 ± 0.236	1.085 ± 0.201	0.002	0.313	0.070
	Left	1.686 ± 0.240	1.626 ± 0.174	0.958 ± 0.110	0.005	1.000	0.063

Table 2.6 Group mean (±SE) values for EMG peak and EMG sum in each muscle across the entire pedaling cycle recorded on Day 2, and statistical results of the repeated measures ANOVA. TA = tibialis anterior, RF = rectus femoris, VM = vastus medialus, BF = biceps femoris, Bilat = bilateral coupled pedaling, Unilat A = unilateral assisted, Unilat Un = unilateral unassisted, '…' indications no post hoc due to non-significant global effect of condition

A. Day 2 EMG Peak

		Mean ± SE (mV)			P-Value		
		Bilat	Unilat A	Unilat Un	Global Effect	Bilat vs Unilat A	Bilat vs Unilat Un
TA	Right	0.011 ± 0.003	0.015 ± 0.003	0.028 ± 0.005	<0.001	0.234	<0.001
	Left	0.006 ± 0.001	0.017 ± 0.006	0.023 ± 0.006	0.006	0.123	0.013
RF	Right	0.009 ± 0.002	0.012 ± 0.002	0.026 ± 0.005	0.001	0.113	0.003
	Left	0.07 ± 0.002	0.011 ± 0.001	0.022 ± 0.003	<0.001	0.043	<0.001
VM	Right	0.006 ± 0.001	0.006 ± 0.001	0.008 ± 0.001	0.048	1.000	0.206
	Left	0.004 ± 0.001	0.004 ± 0.001	0.006 ± 0.001	0.013	1.000	0.084
BF	Right	0.007 ± 0.001	0.009 ± 0.001	0.004 ± 0.001	0.001	0.744	0.039
	Left	0.007 ± 0.001	0.007 ± 0.001	0.003 ± 0.000	0.022	1.000	0.043

B. Day 2 EMG Sum

		Mean ± SE (mV)			P-Value		
		Bilat	Unilat A	Unilat UN	Global Effect	Bilat vs Unilat A	Bilat vs Unilat Un
TA	Right	2.082 ± 0.321	2.865 ± 0.480	5.590 ± 0.922	<0.001	0.120	0.002
	Left	1.328 ± 0.235	3.652 ± 1.49	4.617 ± 1.064	0.023	0.397	0.026
RF	Right	1.256 ± 0.176	1.870 ± 0.193	4.575 ± 0.604	<0.001	0.008	<0.001
	Left	1.243 ± 0.238	1.885 ± 0.201	4.295 ± 0.416	<0.001	0.103	<0.001
VM	Right	1.228 ± 0.153	1.187 ±0.136	1.608 ± 0.205	0.034	1.000	0.312
	Left	0.843 ± 0.100	0.873 ± 0.104	1.174 ± 0.141	0.206	…	…
BF	Right	1.275 ± 0.121	1.526 ±0.191	0.982 ± 0.155	0.002	0.313	0.070
	Left	1.241 ± 0.159	1.153 ± 0.149	0.837 ± 0.130	0.005	1.000	0.063

Table 2.7 Effect size values for EMG sum and EMG peak in each muscle across the entire pedaling cycle recorded on Day 1 and 2. TA = tibialis anterior, RF = rectus femoris, VM = vastus medialus, BF = biceps femoris, Bilat = bilateral coupled pedaling, Unilat A = unilateral assisted, Unilat Un = unilateral unassisted.

A. Effect Size for Peak EMG (mV)

		Day 1		Day 2	
		Bilat - Unilat A	Bilat - Unilat Un	Bilat - Unilat A	Bilat - Unilat Un
TA	Right	0.000	-0.013	-0.004	-0.017
	Left	-0.003	-0.013	-0.011	-0.017
RF	Right	-0.003	-0.015	-0.003	-0.017
	Left	-0.003	-0.015	-0.004	-0.016
VM	Right	0.001	-0.004	0.000	-0.002
	Left	0.000	-0.002	0.000	-0.002
BF	Right	-0.004	0.003	-0.020	0.003
	Left	0.000	0.006	0.000	0.004

B. Effect Size for Sum EMG (mV)

		Day 1		Day 2	
		Bilat - Unilat A	Bilat - Unilat UN	Bilat - Bilat vs Unilat A	Bilat - Bilat vs Unilat Un
TA	Right	-0.250	-2.145	-0.783	-3.508
	Left	-0.299	-2.615	-2.324	-3.289
RF	Right	-0.484	-2.804	-0.614	-3.319
	Left	-0.350	-2.690	-0.601	-3.222
VM	Right	-0.081	-0.387	0.041	-0.380
	Left	0.040	-0.139	-0.030	-0.331
BF	Right	-0.392	0.382	-0.251	0.293
	Left	0.060	0.728	0.088	0.404

2.5 Discussion

A novel device that allows for bilateral and unilateral assisted pedaling during fMRI scanning was developed and validated in this study. Based on a phantom scan experiment, our hypothesis was supported that the device did not affect the signal when in use in the MRI environment. Our second hypothesis was also supported, as the novel assistance mechanism was shown to accurately simulate the contribution of the non-contributing leg during unilateral pedaling by matching the velocity and EMG profiles to bilateral pedaling, with consistent results when used on the second day.

MRI Compatibility of the Pedaling Device

To use an experimental device in the MRI environment, it must be constructed of all non-magnetic materials for the safety of the subject and scanner. Beyond safety concerns, it was important to verify that the new device did not interfere with the MR signal during experiments, as this would contaminate the results. Ferromagnetic or conductive objects may induce changes in the homogeneity of the scanner's magnetic field that can lead to image distortion (Schenck 1996).

The changes in the signal to noise ratio did not exceed 2%, and previous studies have found changes in SNR's caused by MRI compatible devices were in the range of 1.8-7.95% (Chinzei et al. 1999, Khanicheh et al. 2005, Gassert et al. 2006, Suminski et al. 2007). Comparing the differences in signal intensity of the phantom images with and without the device is common practice for testing new devices, and the results here were consistent with what investigators have found (Chinxei et al. 1999, Flueckiger et al. 2005, Khanicheh et al. 2005, Izawa et al. 2006). When amplifying the intensity scale to 1% of

the original, the small differences were noticeable, but non-clustered and would be unlikely to be interpreted as task related brain activity.

Validation of Unilateral Pedaling

This experiment validated that the new pedaling device was able to simulate bilateral pedaling when people pedaled unilaterally. Unilateral pedaling without the assistance mechanism results in characteristics that were quite different from bilateral pedaling.

Specifically, for velocity, the posterior transition and flexion phase tended to be elevated during unassisted unilateral pedaling. During normal bilateral pedaling, the coupled leg would be doing the work and supporting the other leg during these phases. Without being coupled, the pedaling leg was affected by gravity and it was accelerated with less control. In contrast, when the assistance mechanism was engaged, the velocity during the posterior transition and flexion phase was brought close to the level seen during bilateral pedaling. In the right leg flexion phase, however, the mean velocity of unilateral assisted pedaling was still elevated slightly above the velocity during bilateral pedaling. The effect size was -3.72 and -4.39 RPM on day 1 and 2; compared to the pedal rate of 45 RPM, this represents less than a 10% change. Previous studies of pedaling during MRI have shown that differences in pedaling rate up to 15 RPM do not affect brain activity, so the small differences produced using the unilateral pedaling device would not be the cause of any changes in brain activity between conditions (Mehta 2012). The difference in velocity between assisted unilateral and bilateral pedaling in the flexion phase was much lower than between unassisted unilateral and bilateral,

suggesting that the assistance mechanism can be used to compensate for the missing leg during pedaling.

EMG results also showed a greater difference between unassisted unilateral pedaling and bilateral compared to assisted unilateral and bilateral pedaling. Unassisted unilateral pedaling was characterized by increased muscle activity by the tibialis anterior and rectus femoris, no change in the vastus medialis, and a decrease in the biceps femoris. These changes in activity would related to increased muscle activity required to flex the leg and pull it up through the flexion phase into the anterior transition, as this would be when the coupled leg would normally be doing the work. The decrease in biceps femoris activity would relate to not needed to push the coupled leg during the extension phase. By simulating the presence of the non-contributing leg, muscle activity with the assistance mechanism engaged matched the activity during bilateral pedaling. The tibialis anterior and rectus femoris no longer had increased activity to pull the leg through the flexion and anterior transition phase, and bicep femoris activity returned as it was needed during extension. Unilateral assisted pedaling resulted in no significant change from bilateral in the tibialis anterior, vastus medialis, and biceps femoris. The rectus femoris did show a significant difference in two instances. These differences occurred in left leg peak on day 1, with an effect size of -0.004 mV, and right leg sum on day 2, with an effect size of -0.614 mV. These effect sizes are much lower compared to the unilateral unassisted condition, with -0.016 mV and -3.319 mV respectively. Timing of muscle activity was largely unchanged for any condition, meaning that the patterns of muscle activity did not change throughout the pedaling cycle, only the amplitude of the activity.

Repeatability

Achieving similar results for velocity and EMG profiles from day 1 to day 2 showed that the use of the device was repeatable and we could expect the performance to be the same during future experiments involving fMRI scanning.

Limitations

Adjustment of the device was performed through trial and error to find the best assistance and workload level, and angle of the eccentric pulley. Another method to make these selections would be to create a model of the system. The model would include the weight of the user's leg and foot, muscle and joint resistance, effects of gravity, and the elastic properties of the rubber bands. Modeling the bilateral pedaling first will determine when and how much torque is produced and applied to each leg. Subsequently, the model of the assistance mechanism can then be calibrated to match the bilateral model. However, it may be difficult to accurately model the mechanical properties of the users' legs.

Another method to match the bilateral and unilateral conditions is to actually measure the torque produced at the crank, a common practice in pedaling studies. One method to find the crank torque is to measure normal and shear forces directly applied to the pedals, and calculate torque based on the pedal position and crank arm length. The complication is that traditional 6-axis force sensors add substantial weight at the pedals, which would change the model of the system and affect the calibration of the assistance mechanism. The sensors could not be left on permanently because they are not MRI compatible. To overcome this complication, other force sensors could be developed that

are light weight enough or MRI compatible. Alternatively, crank torque could be determined in other ways including measuring deformation on the crank arm. These two methods however may not be accurate enough.

During validation experiments, only four muscles on each leg were measured and may not have captured all the activity involved in the pedaling task, particularly in the unilateral uncoupled task. The task showed elevated TA and RF at the beginning of the posterior transition, which would be contributing to the pulling the leg up in the transition after deceleration from the posterior transition and flexion stage. No muscle activity was shown that could explain the extension and posterior transition phase that would make up for the absence of BF activity. Looking at the velocity profile, there is a large acceleration caused by gravity starting at the end of the extension phase, and the momentum from this can make up for the missing muscle activity. Muscles responsible for hip flexion and extension may also be involved, which were not measured. Particularly, subjects reported extensive use of the iliopsoas, however this muscle is deep and difficult to measure. Additionally, any trunk muscles involved in stabilization were not measured either.

Conclusions

A novel device was developed that allows for conventional coupled bilateral pedaling and unilateral pedaling. The results of a phantom scan show that the device does not interfere with MRI signal acquisition. Validation experiments showed that the assistance mechanism was able to accurately simulate the contribution of the non-contributing leg during unilateral pedaling by matching the velocity and EMG profiles to

bilateral pedaling, with consistent results when used on the second day. Based on these results, the device is ready for use in MRI experiments of lower extremity motor control.

Chapter 3 – FMRI Study of Unilateral vs. Bilateral Pedaling

3.1 Introduction

Using functional imaging and electrophysiological techniques, it is possible to examine human brain activity during locomotor activities, such as walking, running, or pedaling. Techniques include functional magnetic resonance imaging (fMRI) (Mehta et al. 2012, Promjunyakul et al. *in prep*), near infrared spectroscopy (NIRS) (Miyai et al. 2001, Suzuki et al. 2004, Suzuki et al. 2008), positron emission tomography (PET) (Christensen et al. 2001), electroencephalography (EEG) (Jain et al. 2013, Peterson et al. 2012, Gwin et al. 2010), and transcranial magnetic stimulation (TMS) (Petersen et al. 1998, Schubert et al. 1999, Capaday et al. 1999, Petersen et al. 2001, Pyndt and Nielsen 2003). The primary motor (M1) and somatosensory (S1) cortices, supplemental motor area (SMA), premotor area (PMA), and cerebellum (Cb) have consistently been shown to be active during locomotion (Fukuyama et al. 1997, Williamson et al. 1997, Christensen et al. 2000, Miyai et al. 2001, Suzuki et al. 2004, Mihara et al. 2007, Suzuki et al. 2008, Harada et al. 2009, Mehta et al. 2012).

Prior work in our laboratory has used fMRI to examine human brain activity during pedaling in individuals with chronic post stroke hemiparesis, in an effort to understand supraspinal contributions to the control and recovery of locomotor like movements of the lower extremities. Our results demonstrated that the volume of pedaling related brain activity was reduced in people post-stroke compared to age-matched controls. In contrast, unilateral ankle or knee movement produced normal activation volumes (Promjunyakul et al. *in prep*). While it is possible that reduced brain

activation volume during post-stroke pedaling reflects enhanced reliance on spinal pattern generating circuits for the production and maintenance of locomotor-like movements of the legs, it is also possible that this observation was caused by stroke related changes in task performance.

It is well documented that during conventional bilateral pedaling, the non-paretic leg of people post-stroke contributes more than half the mechanical work required to accelerate the crank (Brown et al. 1998, Brown et al. 1999, Kautz et al. 2005, Schindler-Ivens et al. 2008, Liang et al. 2013). This stroke related behavioral adaptation is effective for successful task performance because, during conventional bilateral pedaling, the left and right pedals are mechanically coupled, making it possible for the non-paretic limb to accelerate both pedals. Hence, it is possible that the reduced brain activation volume observed during pedaling post stroke may simply reflect the reduced contribution from the paretic limb. If this were the case, unilateral pedaling with the non-paretic limb only would produce brain activation similar to that seen during conventional, bilateral pedaling. Unilateral pedaling with the paretic limb only would produce brain activity in regions not active during bilateral pedaling or unilateral pedaling with the non paretic limb.

Further studies in our laboratory are planned to examine whether reduced pedaling related brain activation volume post-stroke is due to enhanced spinal control of this task or behavioral compensation. To this end, people with stroke will pedal with the non-paretic limb only and with the paretic limb only. Comparison will be made between brain activation observed during these movements and during conventional bilateral

pedaling. However, prior to beginning these studies, we thought it prudent to understand normal control of unilateral pedaling, which is the focus of the present study.

During bilateral locomotor tasks, brain activation has been shown to be symmetrically activated between left and right hemispheres in the regions M1S1, BA6, and Cb for healthy, able-bodied individuals (Christensen et al. 2000, Miyai et al. 2001, Suzuki et al. 2004, Mihara et al. 2007, Suzuki et al. 2008, Mehta et al. 2009, Mehta et al. 2012). Comparisons of brain activity during unilateral and bilateral locomotor tasks have not been previously looked at directly, but we can draw hypotheses from other lower extremity motor studies.

One might assume that unilateral pedaling would produce brain activation that was distributed contralateral to the moving limb with approximately half the volume of that seen during bilateral pedaling. However, prior work examining brain activity during unilateral knee, ankle, and toe movements suggest that these assumptions may be inaccurate. These studies have found that activation is lateralized to the contralateral M1S1 and ipsilateral Cb, but the extent of lateralization differs between these studies. For example, studies of ankle and toe movement produced low group average laterality indices (LI of 1 is completely lateral, LI of 0 is completely bilateral) in M1S1 of 0.23 – 0.25 toward the contralateral side (Luft et al. 2002, Sahyoun et al. 2004). Another found knee, ankle, and toe activation laterality to be 0.28 – 0.59 (Kapreli et al. 2006). One study found average lateralization related to ankle movement to be much higher at 0.81 – 0.85 (Kim et al. 2006). Cerebellar activity has shown laterality indices of 0.27 – 0.59 (Luft et al. 2002, Kapreli et al. 2006). Laterality of SMA activity during lower extremity movement is also inconsistent across studies, reported as completely contralateral, low

laterality to the contralateral side, and bilaterally activated (Luft et al. 2002, Sahyoun et al. 2004, Kim et al. 2006, Kapreli et al. 2006). These data provide no clear framework explaining supraspinal control of unilateral movements, particularly during a continuous, multi-joint task like pedaling. However, they do suggest that unilateral movements are not under strict contralateral control. Hence, there may be brain regions that are activated during both unilateral left and right, and bilateral movements of the lower extremities.

The purpose of this study was to compare brain activation associated with unilateral and bilateral pedaling in individuals with a healthy nervous system. We hypothesize that if unilateral pedaling was similarly controlled as unilateral single joint movements of the lower extremities, then activation will show laterality towards contralateral M1S1and BA6 and ipsilateral Cb, but laterality indices will be less than 1 indicating that some activity exists in ipsilateral M1S1 and BA6 and contralateral Cb. Along with the laterality change, the volume of activation during unilateral pedaling will decrease due to the decreased muscle activity needed to move one leg compared to two. Also, because there will be brain activation in both hemispheres during unilateral pedaling, we also hypothesize that there will be a common area in the brain that will be active during right and left unilateral and bilateral pedaling. Intensity of activation in this common area will be decreased in unilateral compared to bilateral pedaling for both right and left conditions, due to decreased muscle activity of the task.

3.2 Methods

Instrumentation and Data Recording

The pedaling device, described in Chapter 2, was outfitted with dual position encoders to monitor each side of the crank (model: TD 5207, Micronor Inc. Newbury Park, CA). Crank data were recorded using a 16-bit an analog-to-digital converter board (Micro 1401mkII, Cambridge Electronic Design) sampled at 2000 Hz using Spike2 data acquisition software on a Windows XP PC.

A 3T short bore scanner (Discovery MR750 3T, General Electric Healthcare) was used with a single channel transmit/receive split head coil assembly (Model 2376114, General Electric Healthcare). For functional imaging (T2* weighted), echo-planar imaging was used to collect thirty-six slices of data along the sagittal plane (repetition time (TR): 2000 ms, echo time (TE): 25 ms, flip angle: 77º, 64 x 64 matrix, 4 mm slice thickness, and field of view (FOV): 24 cm, 3.75 x 3.75 x 4.00 mm slice thickness). Each run consisted of 109 TR repetitions. A full brain anatomical scan (T1 weighted) was also performed after the first two conditions (TR: 9.5 ms, TE: 25 ms, flip angle: 12°, 256 x 244 matrix, resolution: 1 mm^3). The anatomical scan was used to localize the functional data to physiological sections of the brain. Presentation software was used to sync the scanner with the audio timing cues during the experiment.

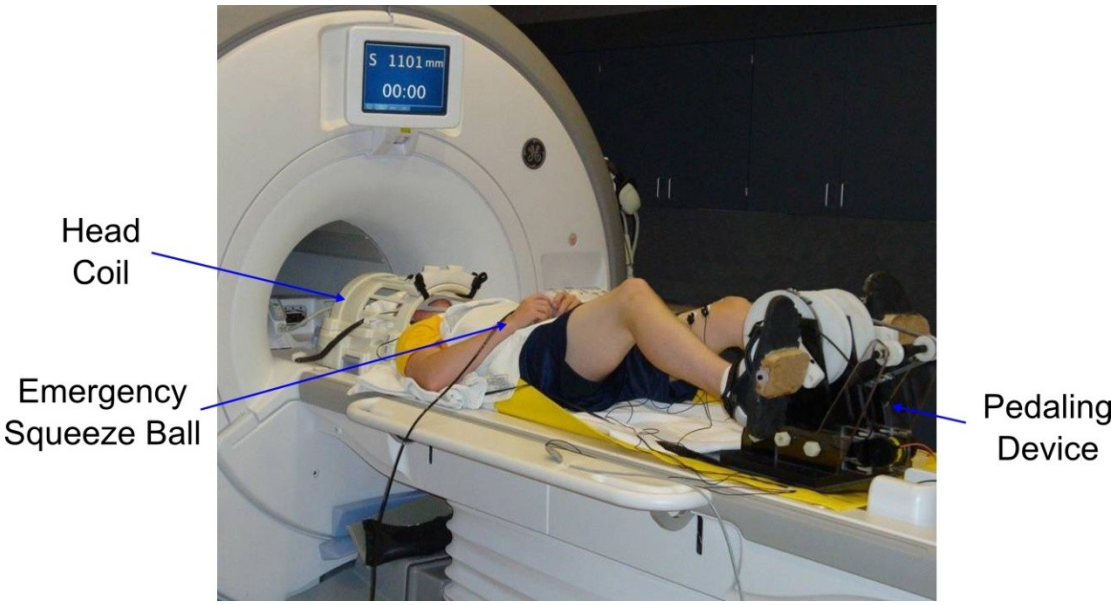

Figure 3.1: Experimental setup for MRI sessions. Subject lies supine on the MRI scanner bed with feet strapped to the device pedals. A backboard runs under the subject to stabilize the device, straps and padding are used to limit head movement of the subject.

Procedure

Eleven able-bodied subjects participated, the same group who previously participated in the validation experiments (6 male, 5 female, 21 years of age or older, mean age of 25). The subjects were familiarized with the procedure within 6 days prior to the MRI session. The subjects lay supine with feet secured to the pedals on the scanner bed. Steps were then taken to limit the amount of head movement while the subject was pedaling, as this could cause artifacts in the data. To stabilize the head, a vacuum bead pillow was used inside the radiofrequency (RF) coil, along with additional padding and a chin strap. A large chest strap was also used to prevent excessive body movement. Cushioning was used under the back and around the shoulders to provide comfort during the experiment. An emergency squeeze ball was given to the subject that

could be used at any time to signal the operator of a problem. MRI experimental setup is shown in Figure 3.1.

Bilateral, right unilateral assisted, and left unilateral assisted pedaling were performed during fMRI scanning. The order of the conditions was counterbalanced between subjects. An anatomical MRI scan was performed between the second and third condition. The experiment was performed as a block design. For each run, an 18 second resting block came first, followed by 5 pairs of 20 second pedaling and 20 second resting blocks. Each run was performed 3 times per condition. A pacing tone was used to keep the pedaling rate constant at 45 revolutions per minute (RPM), to prevent changes in neural activity caused by different pedaling rates (Mehta et al. 2012). The tone was played during the entire run, with audio cues saying "pedal" and "rest" indicating when the subject should be pedaling. The pedaling rate was calculated after each run, and the run was repeated if it was not within 43-48 RPM. The experimental data collection sheet can be found in Appendix B.

Data Analysis

FMRI data were processed using Analysis of Functional NeuroImages (AFNI) software (Cox 1996). MRI files received from the scanner were in Digital Imaging and Communication in Medicine (DICOM) format, and were first converted to 3D images using *to3d* [time: zt, number of points (slices) in the z-direction: 36, number of points in the t-direction (time): 109 TRs, TR time: 2000ms, alt+z]. A time series of each individual voxel was aligned to the same temporal origin within each TR using *3dTshift* to perform a 7th order Lagrange polynomial interpolation [align each slice to tzero (time

offset): 0, ignore the first 4 TRs, heptic]. Multiple runs of the same condition were concatenated together, and the first 4 TR's were removed for each run to eliminate non-steady state magnetization artifacts using *3dTcat.* The concatenated functional data for each condition was registered to the single experimental run that was closest to the anatomical scan using iterative linearized weighted least squares technique with *3dvolreg* [heptic, base: 0].

A multiple linear regression analysis was performed to determine which voxels had pedaling related signal changes due to neural activity. *3dDeconvolve* was used to perform a voxel-wise analysis with the model of the hemodynamic response function (HRF) based on the task timing as a variable of interest and head position as a variable of no interest. As previously described, only data during the resting blocks was used, catching the hemodynamic response on its trailing edge to reduce any effects of head movement, referred to as the delayed non-movement model (Mehta et al. 2009). The time series equation was $y = \beta_0 + \beta_1 x_1 + \beta_2 x_2 + \ldots + \beta_7 x_7 + \varepsilon$, where x_1 was the delayed non-movement model and x_2-x_7 were the head position data in 6 directions (roll, pitch, yaw, linear x, y, z).

To identify a voxel as being statistically active, a Monte Carlo simulation was performed using *Alphasim* to set the individual voxel p-value and cluster size to maintain a family wise Type 1 error rate of $p<0.05$ [voxel dimensions: 3.75x3.75x4mm, fwhmx: 4.32, fwhmy: 4.33, fwhmz: 3.20, T-threshold: 2.85, cluster size: 7 voxels x 56.25 μL/voxel = 393.75 μL].

Regions of interest (ROI) were drawn on the anatomical image of the brain for each subject, outlining primary motor and primary sensory areas (M1S1), Brodmann's

Area 6 (BA6), and the cerebellum (Cb). These areas were defined by previously described anatomical boundaries (Wexler et al. 1997, Schmahmann et al. 1999). The ROIs were resampled in the resolution of the functional images, and applied as masks in the original space of each subject as opposed to transforming to a standardized coordinate system to avoid distortions that could be created. To test the hypotheses, measures were taken within these ROIs. First, laterality indices were calculated to test that activation would show laterality towards contralateral M1S1 and BA6 and ipsilateral Cb, but laterality indices will be less than 1 indicating that some activity exists in ipsilateral M1S1 and BA6 and contralateral Cb. Laterality index was based on the difference in volume active voxels between left and right hemisphere (Eq. 1).

$$LI = \frac{Right-Left}{Right+Left}$$ Eq. 1: Laterality index of activation

The laterality index will always fall between -1 and 1. An LI of -1 indicated the activation was completely in the left hemisphere, 0 was perfectly bilateral, and 1 was completely in the right hemisphere. Next, volume was calculated as the number of voxels active in each ROI multiplied by the volume of one voxel, 56.25μL. This was to test the hypothesis that the volume of activation during unilateral pedaling would decrease due to the decreased muscle activity needed to move one leg compared to two.

For each subject, the common areas of activation across conditions were identified. Any voxels that were active during all three pedaling conditions were included in the common area mask. The common area mask was convolved with the regions of interest in each subject to find the common area of activation in each brain area, $M1S1_{com}$, $BA6_{com}$, and Cb_{com}. The volume is the same in all three conditions, and

the intensity for each condition is found by convolving the common area ROI masks with the functional data for each condition.

To test the hypothesis that intensity of activation in this common area would be decreased in unilateral compared to bilateral pedaling for both right and left conditions, percent signal change was calculated. Percent signal change in the amplitude of the BOLD signal compared to baseline was calculated using *3dcalc* and the equation 100*(d/((a+b+c)/3))*step(1-abs((d/((a+b+c)/3)))), where a-c were the baseline constants for each run within one condition, d was the sub-brick containing the regression coefficient, and the step function controlled outflow if the baseline was close to 0. Voxels that were outside of the brain, negatively correlated, or with a signal change greater than 10% were ignored.

To generate group data for each condition, individual datasets were manually transformed to Talairach coordinate system (Talairach and Tournoux 1988). The functional datasets were then blurred using a 4 mm full width half maximum (FWHM) Gaussian filter using *3dmerge.* A t-test was performed on each group using *3dTtestx,* which gave a threshold for voxels being active across the group with an error rate of 0.05, and created an averaged dataset. Group data were not used for statistical analysis, and were only for visualization.

Repeated measures analysis of variances (ANOVA) and Bonferroni post-hoc tests were computed for each ROI across pedaling conditions for each variable. Statistical analyses used a significance level of $P<0.05$.

3.3 Results

All eleven subjects completed the experiment, however two datasets were excluded from analysis due to excessive head movement. Hence, data from 5 females and 4 males are shown here. Mean pedaling rate for each run of pedaling performed by each subject fell between 43 – 48 RPM. Pedaling rate was found to be significantly different between bilateral and left unilateral pedaling. The group mean (±SE) values were 44.99 (±0.14), 45.50 (±0.33), and 45.96 (±0.24) RPM for bilateral coupled, right unilateral, and left unilateral pedaling, respectively. Despite the significant result, the mean difference in pedaling rate between all three conditions was within 1 RPM so it would not have an effect on the results, as a previous study has shown that differences up to 15 RPM do not produce a difference in brain activation (Mehta et al. 2012).

During the bilateral, coupled pedaling condition, significant pedaling related brain activity was observed in the medial aspects of M1S1 and BA6 and in Cb lobules I, II, III, IV, V and VIII. As shown in the representative example (Figure 3.2A) and the group data (Figure 3.3A), activation in each region was distributed approximately equally across the left and right sides of the brain. The observation that the quantity of brain activity was comparable across the left and right sides of the brain during bilateral pedaling was supported quantitatively by group mean (SE) values for laterality index of -0.057 (0.036), -0.036 (0.061), and -0.036 (0.077) for M1SI, BA6, and Cb, respectively. These values were not significantly different from zero ($P \geq$ the smallest P-value of the 3 comparisons). See Figure 3.4A and Table 3.1A.

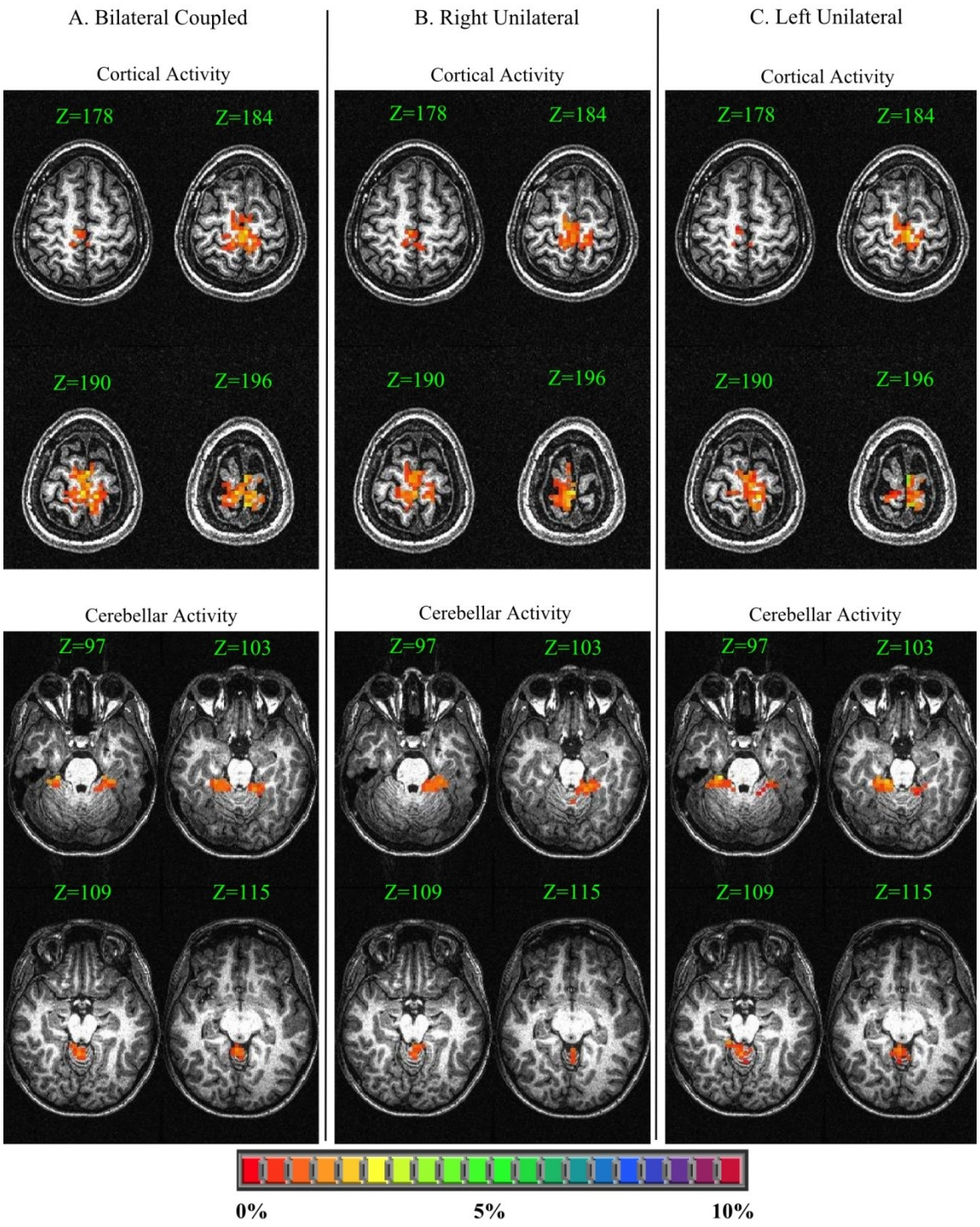

Figure 3.2: Representative example from a single subject (C10) displaying pedaling related brain activity during bilateral, coupled pedaling (A) and unilateral pedaling with the right (B) and left (C) legs. Eight different slices in the axial plane are shown to display representative activity in M1SI, BA6, and Cb. Colors represent percent signal change from baseline.

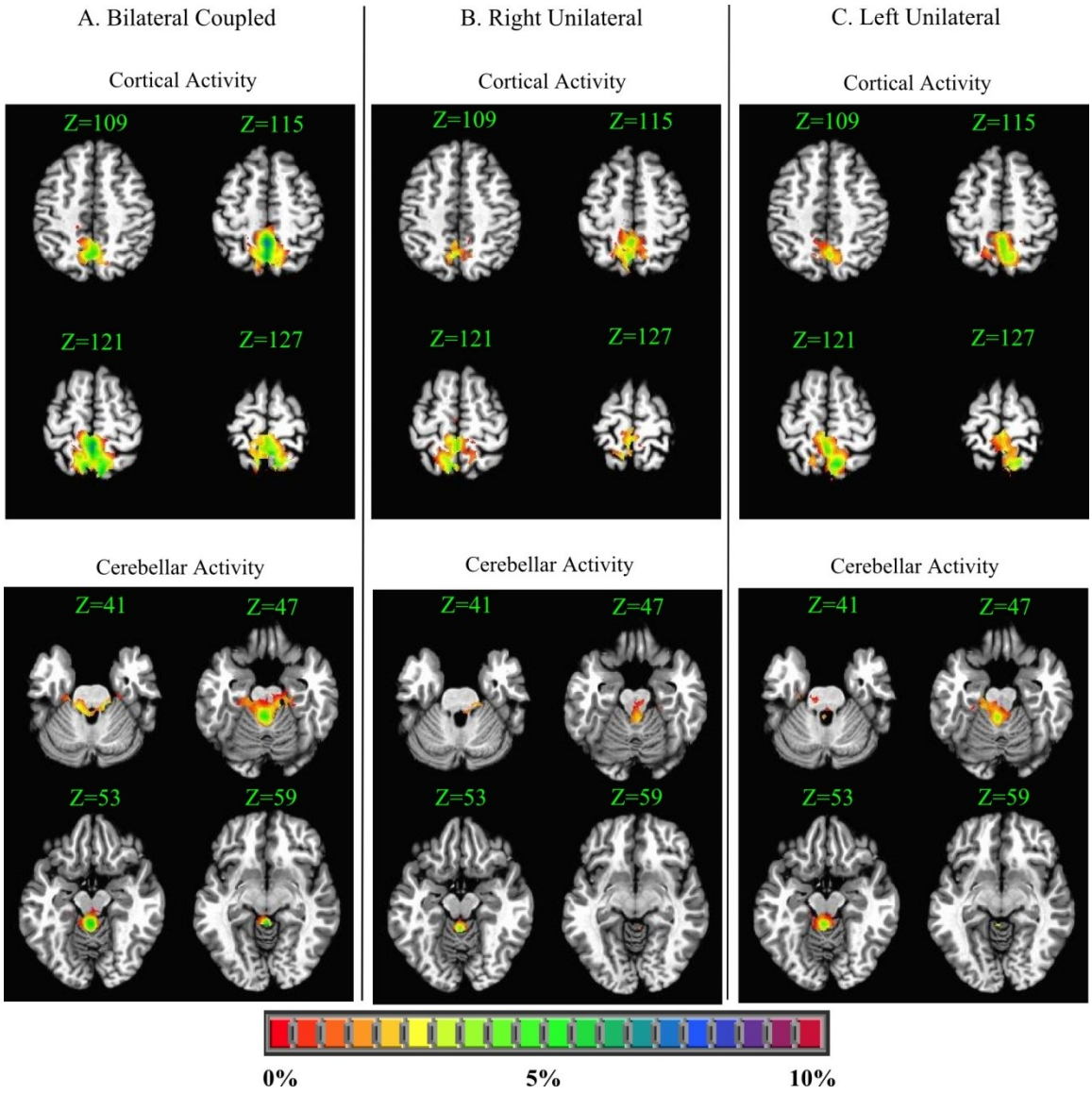

Figure 3.3: Group average displaying pedaling related brain activity during bilateral, coupled pedaling (A) and unilateral pedaling with the right (B) and left (C) legs. Data are shown in Talairach space on a standard brain. Eight different slices in the axial plane are shown to display representative activity in M1SI, BA6, and Cb. Colors represent percent signal change from baseline.

Table 3.1: Group mean (±SE) values for activation laterality, activation volume, and mean intensity of activation in the common area for bilateral coupled, right unilateral, and left unilateral pleading, along with statistical results of the repeated measures ANOVA between conditions.

Bilat (B) = bilateral coupled pedaling, Right (R) = right unilateral pedaling, Left (L) = left unilateral pedaling, M1S1 = primary motor and sensory cortex, BA6 = Brodmann's area 6, Cb = cerebellum, '…' indications no post hoc due to non-significant global effect of condition

A. Activation Laterality

	Bilat LI	Right LI	Left LI	Bilat vs 0 P-Value	Global BvRvL P-Value	Bilat vs Rright P-Value	Bilat vs Left P-Value
M1S1	-0.057±0.036	-0.389±0.111	0.332±0.064	0.150	< 0.01	0.03	<0.01
BA6	-0.036±0.061	-0.136±0.122	0.078±0.063	0.571	0.21	0.03	0.01
Cb	-0.036±0.077	-0.46±0.142	-0.444±0.121	0.652	<0.01	…	…

B. Activation Volume

	Bilat µL	Right µL	Left µL	Common Area µL	Global BvRvL P-Value	Bilat vs Rright P-Value	Bilat vs Left P-Value
M1S1	10556±1336	7631±1490	7856±1643	3000±805	0.04	0.18	0.16
BA6	5031±1027	3444±691	4819±1405	1394±403	0.21	…	…
Cb	6900±2322	4843±1948	6731±2608	1663±989	0.22	…	…

C. Activation Mean Intensity of Common Region

	Bilat % change	Right % change	Left % change		Global BvRvL P-Value	Bilat vs Rright P-Value	Bilat vs Left P-Value
M1S1	1.863±0.152	1.468±0.080	1.435±0.080		0.01	0.08	0.01
BA6	1.867±0.234	1.421±0.081	1.401±0.108		0.05	0.13	0.22
Cb	1.456±0.068	1.320±0.087	1.201±0.115		0.01	0.04	0.03

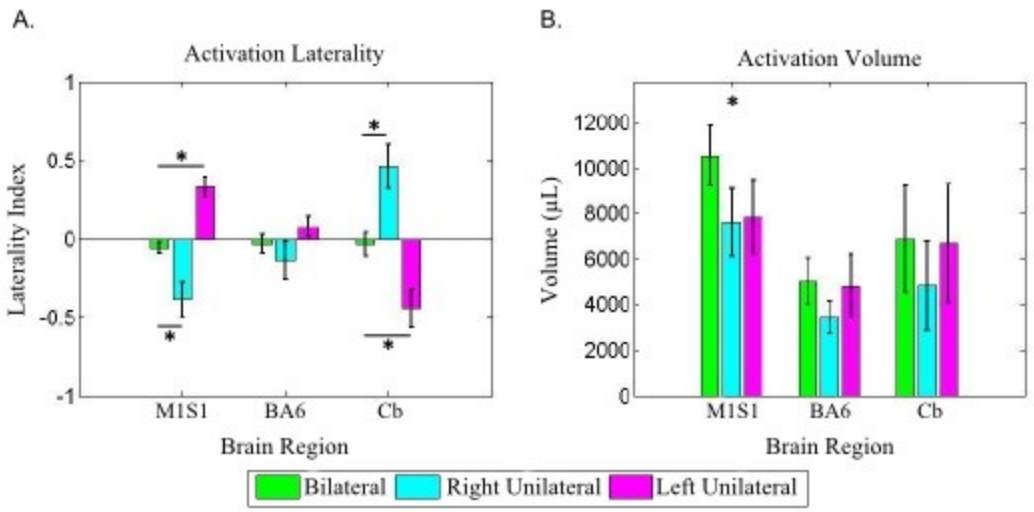

Figure 3.4: Group mean (SE) data for laterality of activation (A) and volume of activation (B) in M1S1, BA6, and Cb during bilateral, coupled pedaling (green) and unilateral pedaling with the right (blue) and left (pink) limbs. Asterisks indicate significant differences between conditions at $P \leq 0.05$.

During unilateral pedaling with the left or right leg, brain activity was observed in the same regions as during bilateral pedaling, namely M1S1, BA6, and Cb (Figures 3.2B,C and Figure 3.3B,C). Our hypotheses compared laterality, volume, and mean intensity within these regions. In BA6, brain activity was bilaterally distributed during unilateral pedaling, as was seen during bilateral pedaling, which was contrary to our hypothesis. However, in M1S1 and Cb, brain activity during unilateral pedaling was more lateralized than in bilateral pedaling such that M1S1 activity was more substantial in the cortex contralateral to the moving limb and Cb activity was more substantial ipsilateral to the moving limb, in agreement with our hypothesis. Of interest is the observation that some ipsilateral M1S1 activity and some contralateral Cb activity remained present during unilateral pedaling. These observations are visually evident in Figures 3.2B,C and 3.3B,C. Moreover, Figure 3.4A and Table 3.1A show that mean (SE)

values for laterality index during unilateral pedaling were significantly different than in bilateral pedaling. However these values did not approach +1 or -1, which would indicate purely unilateral brain activity. Also, neither right nor left pedaling resulted in activation lateralized more to their corresponding hemisphere, determined by comparing the absolute value of the laterality (P-values: 0.62 for M1S1, 0.08 for BA6, 0.81 for Cb).

Quantitative measures of brain activation volume in each active region further support an incomplete shift to unilateral brain activity during unilateral pedaling. During unilateral pedaling, there was no significant decrease in activation volume in BA6 or Cb as compared to bilateral pedaling, contrary to our hypothesis (Figure 3.4B). In M1S1, there was a tendency for lower activation volume during unilateral pedaling, as statistical significance was achieved with the global test of between-group differences ($P=0.04$, repeated measures ANOVA). However, pair-wise comparisons between groups failed to reach statistical significance ($P\geq0.16$, Figure 3.4B and Table 3.1C). The modest shift in laterality index observed during unilateral pedaling, coupled with non-significant decreases in activation volume associated with unilateral pedaling likely reflect a partial, but not complete, lateralization of brain activity during unilateral pedaling.

As indicated above, brain activity during unilateral pedaling was not completely lateralized and activation volume was not significantly decreased compared to bilateral pedaling. Together, these observations suggest the existence of common regions of brain activation for bilateral and unilateral pedaling, as predicted in our hypothesis. Indeed, the map of common areas of brain activity across all conditions displayed in Figure 3.5 shows that portions of M1S1, BA6, and Cb lobules I, II, III, and V were active across all three conditions examined. The activation volume common to all three conditions was

smaller than the activation volume for any single condition, as shown in Table 3.2B. In the active areas that were common to all conditions, mean activation intensity was significantly higher in M1S1 and Cb during bilateral pedaling compared to unilateral pedaling with either the left or right leg, supporting the hypothesis (Figure 3.6 and Table 3.1C.) In BA6, there was a significant global effect of condition on activation mean intensity, but no significant between condition effects were observed with the post-hoc tests.

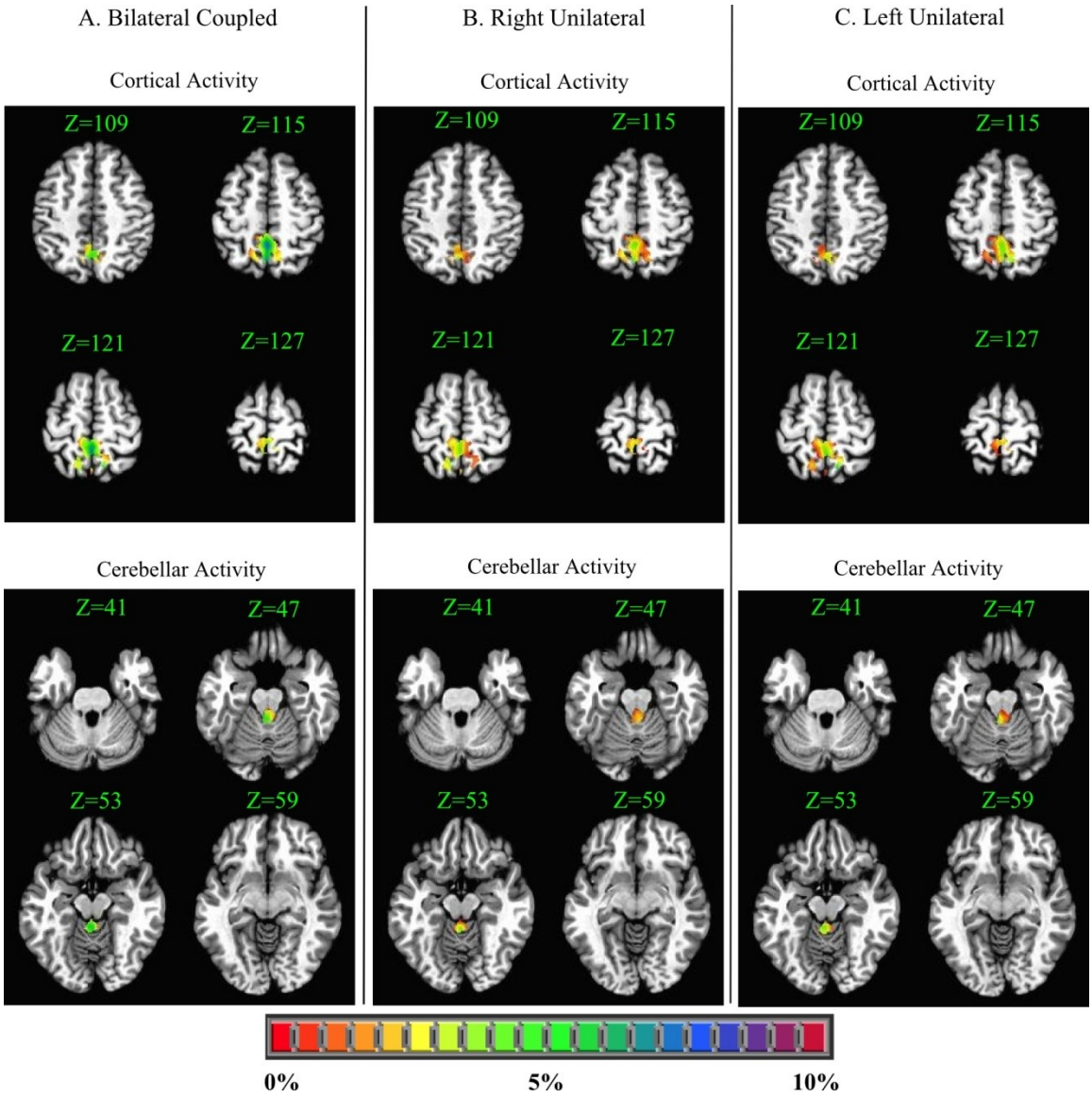

Figure 3.5: Group average displaying pedaling related brain activity during bilateral, coupled pedaling (A) and unilateral pedaling with the right (B) and left (C) legs only in the active regions common to all three pedaling conditions. Data are shown in Talairach space on a standard brain. Eight different slices in the axial plane are shown to display representative activity in M1SI, BA6, and Cb. Colors represent percent signal change from baseline.

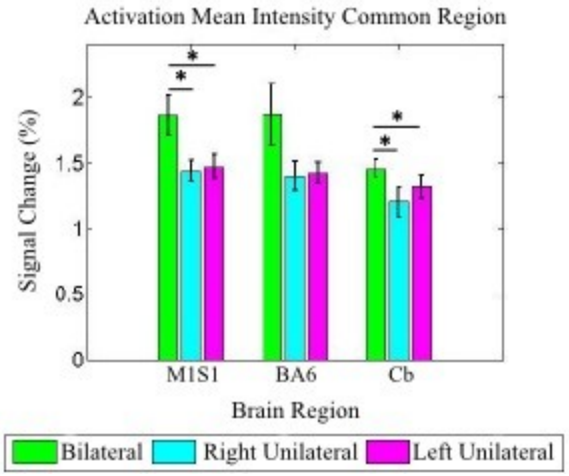

Figure 3.6: Group mean (SE) data for mean activation intensity during bilateral, coupled pedaling (green) and unilateral pedaling with the right (blue) and left (pink) legs. The data shown were extracted from active regions of M1S1, BA6, and Cb common to all three pedaling conditions. Asterisks indicate significant differences between conditions at $P \leq 0.05$.

3.4 Discussion

This study compared brain activation during coupled bilateral, right unilateral, and left unilateral pedaling, with differences found in the laterality and mean intensity of activation. Task related brain activity was seen in the sensorimotor cortex (M1S1), Brodmann's area 6 (BA6, including supplementary motor area and premotor area), and the cerebellum (Cb). Supporting our first hypothesis, the laterality of activation was shifted to the contralateral M1S1 and ipsilateral Cb during unilateral pedaling, however in contrast with our hypothesis, BA6 showed no significant lateralization in activity. Additionally, there was no difference in the magnitudes of the laterality shift in right and left pedaling, and bilateral pedaling was not shifted to either hemisphere. Our second hypothesis of a reduced volume during unilateral pedaling was rejected, as our results showed no significant change in any brain area, although it neared a significant decrease

in M1S1 for unilateral pedaling. We expected to see reduced activation volume when one leg was active versus both legs. Mean intensity in the common area of activation was lower in M1S1, BA6, and Cb for right and left unilateral compared to bilateral pedaling.

Laterality of Activation

Pedaling bilaterally showed symmetrical activation in the brain, while pedaling with only one leg resulted in changes in laterality of activation. Symmetrical brain activity during bilateral locomotion has been shown previously in other studies involving able-bodied individuals (Christensen et al. 2000, Miyai et al. 2001, Suzuki et al. 2004, Mihara et al. 2007, Suzuki et al. 2008, Mehta et al. 2009, Mehta et al. 2012). The brain activation in unilateral pedaling was shifted to the contralateral hemisphere in M1S1 and the ipsilateral hemisphere in Cb during unilateral pedaling. The laterality indices for M1S1 and Cb show that activation was not completely shifted to one hemisphere in either right or left legged pedaling, meaning that the activation was still partially bilateral in both cases. These laterality results are similar to previous studies that looked at single joint flexion of the lower extremities of able-bodied individuals (Luft et al. 2002, Sahyoun et al. 2004, Kim et al. 2006), but are less lateralized than other studies have shown (Kapreli et al. 2006, Kim et al. 2006). Contrary to what previous studies have found, activity was more bilaterally activated in BA6. Possible physiological explanations related to corticospinal pathways and upper motor neurons, as well as technical limitations exist for the laterality results we found in M1S1, Cb, and BA6.

About 75% of descending pathways from the motor cortex are part of the lateral corticospinal tract (Ropper et al. 2009). From the motor cortex, most of the lateral corticospinal tract crosses to control motor function on opposite sides of the body. Activation in M1S1 was shifted to the contralateral hemisphere during the unilateral pedaling. M1S1 has direct descending pathways to distal motor neurons, and has contralateral control over the arms and legs utilizing the crossed lateral corticospinal tract. However, there is evidence that up to 10% of the lateral corticospinal tract remains uncrossed (Nyberg-Hansen 1966). This has been supported in animal studies, namely cats and monkeys, which have found corticospinal tracts to extend ipsilaterally all the way down to the lumbar segments of the spinal cord (Kuypers and Brinkman 1970, Ralston and Ralston 1985, Dum and Strick 1996, Armand et al. 1997, Lacroix et al. 2004). Although the exact extent of the prevalence and role of these uncrossed lateral corticospinal tracts in humans is not fully known, they may relate to the M1S1 activation in the ipsilateral hemisphere during unilateral locomotion. Several studies of stroke patients using fMRI, PET, TMS, and NIRS have shown increased ipsilateral activation during hand movement, which may indicate the utilization of preexisting uncrossed pathways to compensate for contralateral cortex damage (Kato et al. 2002, Chollet et al. 1991, Weiller et al. 1992, Caramia et al. 1996, Cramer et al. 1997, Netz et al. 1997, Cao and Zhou 1998).

The remaining 25% of descending pathways comprise the medial corticospinal tract, which originates in the medial portions of the motor cortex and descends uncrossed (Ropper et al. 2009). This pathway is connected to areas that are typically activated bilaterally, including the trunk. The trunk is involved in control of posture, which is a

major component to human locomotion. While our experimental design of pedaling removed the need for postural control, the related brain areas may have still been active as they normally would be during locomotion.

Another possible pathway, the lateral reticulospinal tract descends bilaterally from the lateral reticular formation, which receives input from the cerebral cortex and transmits signals that initiate locomotion (Kandel et al. 2000, Lundy-Ekman 2007). This pathway has been linked to inhibiting flexor and facilitating extensor muscle activity during walking (Noga et al. 2003). This could also be a pathway for bilateral cortical input for locomotion.

Activity in the ipsilateral hemisphere of M1S1 may be related to inhibitory signals rather than excitatory. Through interhemispheric connections, one hemisphere can directly inhibit efferent neurons from firing in the other hemisphere, or first trigger interneurons that in turn inhibit the efferents (Ferbert et al. 1992, Kandel et al. 2000, Zafiris et al 2002). Since pedaling is normally a bilateral task, inhibition may be needed to prevent the idle leg from moving during unilateral pedaling. The contralateral hemisphere may inhibit the ipsilateral hemisphere to keep one leg idle. Efferent neurons that do not fire would not have shown up in the MRI scan, but any interneurons firing in the ipsilateral hemisphere would. Unfortunately, it is not possible with fMRI to distinguish between efferent and interneuron activity.

For locomotion, the cerebellum is thought to be involved in the generation and coordination of appropriate limb movement, regulation of balance, and adaptation of posture and locomotion through practice (Morton and Bastian 2004, Jayaram et al. 2011). Motor control from the cerebellum is ipsilateral (Lundy-Ekman 2007), which correlates

to our findings that Cb activation during unilateral pedaling was shifted to the ipsilateral side. The cerebellum may also play a role in acquisition and discrimination of sensory data relating to motor control, and can be active in response to sensory stimuli in the absence of movement (Fox et al. 1985, Gao et al. 1996, Naito et al. 2002, Mehta et al. 2012). Sensory processing for the pedaling and idle leg may have contributed to the result that Cb activation was not completely in one hemisphere.

The supplementary motor (SMA) has been connected to postural control (Massion 1992), predictable movements from memory, motor planning, and execution of gait in humans (Deiber et al. 1999, Jenkins et al. 2000, Miyai et al. 2001, Sahyoun et al. 2004). The pre-motor area (PMA) is related to planning of movements guided by sensory cues (Elsinger et al. 2006). These areas would have been active during our pedaling task, as it is a familiar, locomotor task performed by memory that involves sensory feedback, and it is also externally cued. During unilateral, non locomotor lower extremity tasks, SMA and PMA show bilateral activity (Luft et al. 2002, Sahyoun et al. 2004, Ciccarelli et al. 2005, Mehta et al. 2009). During the preparation of walking cued by verbal instruction, both PMA and SMA show greater activity compared to before walking without a cue. Our task involved auditory cues for when to pedal and the pace, which could be related to this activity. Since locomotion is typically performed with both legs, SMA and PMA may have activated bilaterally in preparation for movement, even when only one leg actually performed the task.

Being right side dominant did not result in a greater lateral shift during either right or left leg pedaling, despite what was seen in other studies of lower motor control (Kapreli et al. 2006, Rocca and Filippi 2010). This is likely due to the difference in task.

Locomotion is performed bilaterally, with each leg in a pattern of alternating, reciprocal flexion and extension. This may be less likely to lead to a dominant hemisphere for brain activation compared to discrete motor tasks of leg joint flexion and extension that could be more representative of a unilateral task, such as kicking. Dominance has shown a greater effect in brain activation relating to upper extremity movements (Allison et al. 2000, Reddy et al. 2000, Nirkko et al. 2001, Hamzei et al. 2002, Babiloni et al. 2003, Rogers et al. 2004), which supports the view that upper limb motor control is not a proper model for lower motor tasks, particularly locomotion. Repeating this study with a group of left side dominant subjects would help to fully investigate these differences.

Some of the bilateral activity during unilateral pedaling could also be due to a technical limitation of the imaging system. The spatial resolution in the anterior-posterior and left-right directions is 3.75 mm, and some of the activation may have been incorrectly included in the wrong region if it occurred on the very edge of one hemisphere or on the border between M1S1 and BA6.

Volume of Activation

Contrary to our hypothesis, brain activation volume did not statistically decrease during unilateral pedaling in M1, S1, or Cb. The volume of brain activation from one legged pedaling is not half of bilateral pedaling activation, even though unilateral pedaling is half of the task performed in bilateral pedaling. Because the activation during unilateral tasks was present in both hemispheres, bilateral pedaling is not simply the summation of left and right pedaling. There is an overlap in the active areas and they would be counted twice during summation. A better way to look at it is by summing the

volume that is active in right or left pedaling (RL), counting the common area only once. As a result, there was no difference between bilateral or RL activation.

Because there was a laterality shift in M1S1 and Cb during unilateral pedaling, we would have expected either the total volume in these areas to decrease with respect to bilateral pedaling, or in the hemisphere the activation was shifted to the volume would have to be greater. However, no change in total volume of these areas was found, and the hemispheres with lateralized activity did not increase in activation volume, as shown by the RL data.

Common Area and Intensity of Activation

Since the unilateral pedaling tasks resulted in activity in both hemispheres, there is a common area that is active across all three conditions, bilateral, right, and left legged pedaling. The common area is present in M1S1, BA6, and Cb. This common area may have underlying control of locomotion and will be active during any related motor task. Arguments have been made for the existence of a central pattern generator at the cortical level, so it is possible that the common area found in this study is related to CPGs (Yuste et al. 2005). The common area may also be related to stabilization of the trunk or non-participating leg during the unilateral conditions. Further studies could be done to measure how much stabilization is occurring using EMG. MRI experiments could also be performed that better restrain the subject so no stabilization is needed, or that increase the need to stabilize the trunk or leg to see how brain activity changes under these conditions.

In bilateral pedaling compared to unilateral pedaling, there was increased mean intensity in M1S1, BA6 and Cb within the common region. Since these regions are active during all conditions, the intensity may be higher during bilateral pedaling simply because it requires a greater amount of movement and coordination compared to unilateral pedaling. Another possible explanation is the task complexity. Task complexity has been studied in the upper limb during fMRI by comparing a single finger movement to more complex sequential movements of multiple fingers (Wexler et al. 1997, Elsinger et al., 2006). Their results showed that the more complex task did elicit greater intensity of activation. In our study, the increased intensity during bilateral compared to unilateral pedaling might be because bilateral pedaling requires coordination between the two legs and may be considered a more complex task than unilateral pedaling. The increased intensity could be caused by the active neurons firing more rapidly to deal with the increased movements or complexity of the task (Wexler et al. 1997, Elsinger et al. 2006), or by an increased number of neurons firing within the resolution of the voxel. However, it is also possible that the unilateral assisted task could be more complex, since it is less familiar that the bilateral task.

Limitations

One limitation in this study is the resolution of the functional data collected. At 3.75 x 3.75 x 4 mm, there may have been some overlap of activity into different brain regions, since the anatomical spacing between them is only a few millimeters. Some of the activity volume measured for the common region or in laterality calculations may have been caused by overlap into the longitudinal fissure between the two hemispheres

where there are no neurons that could be active. A strip of voxels could be removed from the functional data that cover the longitudinal fissure during analysis to eliminate any effects it might have had on the common area or laterality. It is also possible to improve the spatial resolution in future experiments. Spatial resolution is the field of view divided by the frequency domain sampling matrix size. Resolution can be increased by narrowing the field of view to look at only the sensorimotor cortex where activity is expected to be. Also, if an MRI scanner with a stronger magnetic field is used, the matrix size can be increased without affected the SNR, as would occur if the field strength was not increased.

Conclusion

This study used a new pedaling device to compare brain activity between conventional coupled bilateral, unilateral right, and unilateral left pedaling in neurologically intact, able-bodied individuals. Active brain areas were identified for each condition, with any differences in laterality, volume, and mean intensity identified. Additionally, a common region that was active across all three conditions was shown. This knowledge will lay the groundwork for future studies involving people with stroke, where they will pedal with the non-paretic limb only and with the paretic limb only to examine any changes in brain control of locomotion.

CHAPTER 4: CONCLUSIONS

In this study, a new device was developed to study the brain control of locomotion by determining the specific areas of control for each limb independently. The device is MRI compatible and allows for coupled bilateral pedaling and uncoupled unilateral pedaling. The device was validated to show that during unilateral pedaling, the assistance mechanism was able to simulate the presence of the non-contributing leg. An fMRI experiment comparing brain activation during bilateral and unilateral pedaling with able-bodied, neurologically intact individuals was also performed using the device. Mainly, the results found a shift in laterality of activation in M1S1 and Cb during unilateral pedaling, a common region that was active during all conditions, and increased activation intensity in the common region during bilateral pedaling in M1S1, BA6, and Cb.

Additional studies could be performed to further our understanding of normal control of locomotion using the new unilateral pedaling device. To test if any of the brain activation is related to stabilization and postural control, an experiment can be designed that destabilizes the leg, increasing the demand on stabilization muscles. One or both legs could be placed on unstable or changing surfaces that need constant adjustment, and could also be done while one leg is pedaling. Passive unilateral pedaling could also be performed to look at activation related to sensory feedback, with or without the second leg also pedaling. There are also ways to increase task complexity, by making the task more unfamiliar. The crank can be coupled 90° out of phase or the assistance mechanism could be adjusted so that it does not properly simulate bilateral pedaling. Uncoupled bilateral pedaling tasks can also be performed by using the assistance

mechanisms on both sides, but keeping the crank uncoupled. By keeping the two limbs uncoupled, one leg will be unable to drive or influence the other leg. This may be particularly useful for studies involving people with stroke, as the non-paretic limb will not be able to compensate for the paretic limb.

Our laboratory previously found that the volume of bilateral pedaling related brain activity was reduced in people post-stroke compared to age-matched controls, and laterality of activation was unchanged. The reduced volume in people post-stroke is similar in size and position to the common area of activation found in the present study. If the common area is related to some underlying control of locomotion, it may play a role in recovery after stroke and be responsible for producing the impaired locomotion. Using the unilateral pedaling device, the next study can examine whether reduced pedaling related brain activation volume post-stroke is due to a change in brain control involving the common area that leads to behavioral compensation or if it is due to enhanced spinal control of this task. People with stroke will pedal with the non-paretic limb only, the paretic limb only, and with both limbs in conventional bilateral pedaling. By pedaling with the paretic limb only, brain activation will not be mixed with activation that is related to the non-paretic limb as with the bilateral pedaling task, and any influence the non-paretic leg may have on the paretic leg's task performance will be removed. This work will hopefully increase our understanding of the changes in locomotor control strategies of the brain following stroke.

BIBLIOGRAPHY

Ahlsio B, Britton M, Murray V, Theorell T. (1984). Disablement and quality of life after stroke. Stroke 15:886-890.

Allison, J. D., Meador, K. J., Loring, D. W., Figueroa, R. E., & Wright, J. C. (2000). Functional MRI cerebral activation and deactivation during finger movement. Neurology, 54(1), 135-135.

Armand J, Olivier E, Edgley SA, Lemon RN. (1997). Postnatal develop- ment of corticospinal projections from motor cortex to the cervical enlargement in the macaque monkey. J Neurosci 17:251–66.

Armstrong DM and Drew T. (1984). Discharges of pyramidal tract and other motor cortical neurones during locomotion in the cat. The Journal of Physiology 346:471-495.

Babiloni, F., Babiloni, C., Carducci, F., Romani, G. L., Rossini, P. M., Angelone, L. M., & Cincotti, F. (2003). Multimodal integration of high-resolution EEG and functional magnetic resonance imaging data: a simulation study.Neuroimage, 19(1), 1-15.

Balasubramanian CK, Bowden MG, Neptune RR, Kautz SA. (2007). Relationship between step length asymmetry and walking performance in subjects with chronic hemiparesis. Archives of Physical Medicine and Rehabilitation 88(1):43-49.

Barbeau H and Rossignol S. (1987). Recovery of locomotion after chronic spinalization in the adult cat. Brain Research 412(1):84-95.

Belanger M, Patla AE. (1987). Phase-dependent compensatory responses to perturbation applied during walking in humans. Jornal of Motor Behavior 19(4): 434-453.

Bowden MG, Balasubramanian CK, Behrman AL, Kautz SA. (2008). Validation of a speed-based classification system using quantitative measures of walking performance poststroke. Neurorehabilitation and Neural Repair 22(6):672-675.

Boynton GM, Engel SA, Glover GH, Heeger DJ. (1996). Linear systems analysis of functional magnetic resonance imaging in human V1. The Journal of Neuroscience 16(13):4207-4221.

Brown DA, Kautz SA, Dairaghi CA. (1997). Muscle activity adapts to anti-gravity posture during pedalling in persons with post-stroke hemiplegia. A Journal of Neurology 120:825-837.

Brown, D. A., & Kautz, S. A. (1998). Increased workload enhances force output during pedaling exercise in persons with poststroke hemiplegia. Stroke, 29(3), 598-606.

Brown, D. A., & Kautz, S. A. (1999). Speed-dependent reductions of force output in people with poststroke hemiparesis. Physical therapy, 79(10), 919-930.

Brown TG. (1911). The intrinsic factors in the act of progression in the mammal. Proceedings of the Royal Society B: Biological Sciences 84(572):308-319.

Calancie B, Needham-Shropshire B, Jacobs P, Willer K, Zych G, Green BA. (1994). Involuntary stepping after chronic spinal cord injury. evidence for a central rhythm generator for locomotion in man. A Journal of Neurology 117:1143-1159.

Cao, J., & Zhou, D. (1998). Stability analysis of delayed cellular neural networks. Neural networks, 11(9), 1601-1605.

Capaday C, Lavoie BA, Barbeau H, Schneider C, Bonnard M. (1999). Studies on the corticospinal control of human walking. I. responses to focal transcranial magnetic stimulation of the motor cortex. Journal of Neurophysiology 81(1):129-139.

Caramia MD, Palmieri MG, Giacomini P, Iani C, Dally L, Silvestrini M. (2000). Ipsilateral activation of the unaffected motor cortex in patients with hemiparetic stroke. Clin Neurophysiol 111:1990–6.

Chinzei K, Kikinis R, Jolesz FA. (1999) MR compatibility of mechatronic devices: Design criteria. In: Proceedings of the second international conference on medical image computing and computer-assisted intervention. p. 1020–31.

Chollet, F., DiPiero, V., Wise, R. J. S., Brooks, D. J., Dolan, R. J., & Frackowiak, R. S. J. (1991). The functional anatomy of motor recovery after stroke in humans: a study with positron emission tomography. Annals of neurology, 29(1), 63-71.

Christensen LO, Andersen JB, Sinkjaer T, Nielsen J. (2001). Transcranial magnetic stimulation and stretch reflexes in the tibialis anterior muscle during human walking. The Journal of Physiology 531:545-557.

Christensen LO, Johannsen P, Sinkjaer T, Petersen N, Pyndt HS, Nielsen JB. (2000). Cerebral activation during bicycle movements in man. Experimental Brain Research 135(1):66-72.

Ciccarelli O, Toosy AT, Marsden JF, Wheeler-Kingshott CM, Sahyoun C, Matthews PM, et al. (2005). Identifying brain regions for integrative sensorimotor processing with ankle movements. Experimental Brain Research 166:31-42.

Cox RW. (1996). AFNI: Software for analysis and visualization of functional magnetic resonance neuroimages. Computers and Biomedical Research, an International Journal 29(3):162-173.

Cramer, S. C., Nelles, G., Benson, R. R., Kaplan, J. D., Parker, R. A., Kwong, K. K., ... & Rosen, B. R. (1997). A functional MRI study of subjects recovered from hemiparetic stroke. Stroke, 28(12), 2518-2527.

Daskalakis, Z. J., Christensen, B. K., Fitzgerald, P. B., Roshan, L., & Chen, R. (2002). The mechanisms of interhemispheric inhibition in the human motor cortex. *The Journal of physiology*, *543*(1), 317-326.

Deiber, M.P., Honda, M., Ibanez, V., Sadato, N., & Hallett, M. (1999). Mesial motor areas in self-initiated versus externally triggered movements examined with fMRI: Effect of movement type and rate. Journal of Neurophysiology, 81(6), 3065–3077.

Dettmann MA, Linder MT, Sepic SB. (1987). Relationships among walking performance, postural stability, and functional assessments of the hemiplegic patient. American Journal of Physical Medicine 66(2):77-90.

Dietz V, Colombo G, Jensen L, Baumgartner L. (1995). Locomotor capacity of spinal cord in paraplegic patients. Annals of Neurology 37(5):574-582.

Dietz V, Colombo G, Jensen L. (1994). Locomotor activity in spinal man. Lancet 344(8932):1260-1263.

Dimitrijevic MR, Gerasimenko Y, Pinter MM. (1998). Evidence for a spinal central pattern generator in humans. Annals of the New York Academy of Sciences 860:360-376.

Dobkin, B. H., Harkema, S., Requejo, P., & Edgerton, V. R. (1994). Modulation of locomotor-like EMG activity in subjects with complete and incomplete spinal cord injury. *Journal of neurologic rehabilitation*, *9*(4), 183-190.

Drew T. (1988). Motor cortical cell discharge during voluntary gait modification. Brain Research 457(1):181-187.

Dum RP, Strick PL. (1996). Spinal cord terminations of the medial wall motor areas in macaque monkeys. J Neurosci 16:6513–25.

Duysens, J., & Van de Crommert, H. W. (1998). Neural control of locomotion; thecentral pattern generator from cats to humans. Gait & Posture, 7(2), 131-141.

Elsinger, C. L., Harrington, D. L., & Rao, S. M. (2006). From preparation to online control: reappraisal of neural circuitry mediating internally generated and externally guided actions. Neuroimage, 31(3), 1177-1187.

Ferbert, A., Priori, A., Rothwell, J. C., Day, B. L., Colebatch, J. G., & Marsden, C. D. (1992). Interhemispheric inhibition of the human motor cortex. *The Journal of physiology*, *453*(1), 525-546.

Flueckiger M, Bullo M, Chapuis D, Gassert R, Perriard Y. (2005) fMRI compatible haptic interface actuated with traveling wave ultrasonic motor. In: 2005 IEEE industry applications conference. p. 2075–82.

Forssberg H and Grillner S. (1973). The locomotion of the acute spinal cat injected with clonidine i.v. Brain Research 50(1):184-186.

Forssberg H. (1985). Ontogeny of human locomotor control. I. infant stepping, supported locomotion and transition to independent locomotion. Experimental Brain Research 57(3):480-493.

Fox, P. T., Raichle, M. E., & Thach, W. T. (1985). Functional mapping of the human cerebellum with positron emission tomography. Proceedings of the National Academy of Sciences, 82(21), 7462-7466.

Fukuyama H, Ouchi Y, Matsuzaki S, Nagahama Y, Yamauchi H, Ogawa M, Kimura J, Shibasaki H. (1997). Brain functional activity during gait in normal subjects: A SPECT study. Neuroscience Letters 228(3):183-186.

Gao, J.H., Parsons, L.M., Bower, J.M., Xiong, J., Li, J., & Fox, P.T. (1996). Cerebellumimplicated in sensory acquisition and discrimination rather than motor control. Science (New York, N.Y.), 272(5261), 545–547.

Gassert R, Moser R, Burdet E, Bleuler H. (2006) MRI/fMRI-compatible robotic system with force feedback for interaction with human motion. IEEE/ASME Trans Mechatronics,11(2):216–24.

Go, A. S., Mozaffarian, D., Roger, V. L., Benjamin, E. J., Berry, J. D., Borden, W. B., ... & Turner, M. B. (2013). Heart disease and stroke statistics—2013 update a report from the American Heart Association. Circulation, 127(1), e6-e245.

Gordon KE, Wu M, Kahn JH, Dhaher YY, Schmit BD. (2009). Ankle load modulates hip kinetics and EMG during human locomotion. Journal of Neurophysiology 101(4):2062-2076.

Grillner S and Rossignol S. (1978). On the initiation of the swing phase of locomotion in chronic spinal cats. Brain Research 146(2):269-277.

Gwin JT, Gramann K, Makeig S, Ferris DP. (2010). Removal of movement artifact from high-density EEG recorded during walking and running. Journal of Neurophysiology 103:3526-3534.

Haacke EM, Brown RW, Thompson MR, Venkatesan R. (1999) Magnetic resonance imaging: physical principles and sequence design. New York: Wiley.

Hamzei, F., Dettmers, C., Rzanny, R., Liepert, J., Büchel, C., & Weiller, C. (2002). Reduction of excitability ("inhibition") in the ipsilateral primary motor cortex is mirrored by fMRI signal decreases. Neuroimage, 17(1), 490-496.

Harada T, Miyai I, Suzuki M, Kubota K. (2009). Gait capacity affects cortical activation patterns related to speed control in the elderly. Experimental Brain Research 193(3):445-454.

Herzog W, Nigg BM, Read LG, Olsson E. (1989). Asymmetries in ground reaction force patterns in normal human gait. Medicine and Science in Sports and Exercise 21:110-114.

Hollnagel C, Brugger M, Vallery H, Wolf P, Dietz V, Kollias S, Riener R. (2011). Brain activity during stepping: A novel MRI-compatible device. Journal of Neuroscience Methods 201:12-130.

Huettel, S. A., Song, A. W., & McCarthy, G. (2004). *Functional magnetic resonance imaging* (Vol. 1). Sunderland: Sinauer Associates.

Izawa, J., Shimizu, T., Aodai, T., Kondo, T., Gomi, H., Toyama, S., & Ito, K. (2006). MR compatible manipulandum with ultrasonic motor for fMRI studies. In *Robotics and Automation, 2006. ICRA 2006. Proceedings 2006 IEEE International Conference on* (pp. 3850-3854). IEEE.

Jain S, Gourab K, Schindler-Ivens S, Schmit BD. (2013). EEG during pedaling: Evidence for cortical control of locomotor tasks. Clinical Neurophysiology 124(2):379-390.

Jain, S., Gourab, K., Schindler-Ivens, S., & Schmit, B. D. (2012). EEG during pedaling: Evidence for cortical control of locomotor tasks. Clinical Neurophysiology

Jayaram G, Galea JM, Bastian AJ, Celnik P. (2011). Human locomotor adaptive learning is proportional to depression of cerebellar excitability Cerebral Cortex 21(8):1901-1909.

Jenkins, I. H., Jahanshahi, M., Jueptner, M., Passingham, R. E., & Brooks, D. J. (2000). Self-initiated versus externally triggered movements. II. the effect of movement predictability on regional cerebral blood flow. Brain: A Journal of Neurology, 123 (Pt 6)(Pt 6), 1216-1228.

Kandel, E. R., Schwartz, J. H., & Jessell, T. M. (2000).Principles of neural science. (4 ed.). McGraw-Hill/Appleton & Lange.

Kapreli E, Athanasopoulos S, Papathanasiou M, Van Hecke P, Strimpakos N, Gouliamos A, Peeters R, Sunaert S. (2006). Lateralization of brain activity during lower limb joints movement. an fMRI study. NeuroImage 32(4):1709-1721.

Kato, H., Izumiyama, M., Koizumi, H., Takahashi, A., & Itoyama, Y. (2002). Near-Infrared Spectroscopic Topography as a Tool to Monitor Motor Reorganization After Hemiparetic Stroke A Comparison With Functional MRI.Stroke, 33(8), 2032-2036.

Kautz SA and Brown DA. (1998). Relationships between timing of muscle excitation and impaired motor performance during cyclical lower extremity movement in post- stroke hemiplegia. Brain 121:515-526.

Kautz, S. A., Duncan, P. W., Perera, S., Neptune, R. R., & Studenski, S. A. (2005). Coordination of hemiparetic locomotion after stroke rehabilitation.Neurorehabilitation and neural repair, 19(3), 250-258.

Khanicheh A, Muto A, Trantafyllou C, Weinberg B, Astrakas L, Tzika A, et al. (2005) MR compatible ERF driven hand rehabilitation device. In: Proceedings of the 2005 IEEE 9th international conference on rehabilation robotics.

Kim, Y. H., You, S. H., Kwon, Y. H., Hallett, M., Kim, J. H., & Jang, S. H. (2006). Longitudinal fMRI study for locomotor recovery in patients with stroke.*Neurology*, *67*(2), 330-333.

Kuypers HG, Brinkman J. (1970) Precentral projections to different parts of the spinal intermediate zone in therhesus monkey. Brain Res 24:29–48.

Lacroix, S., Havton, L. A., McKay, H., Yang, H., Brant, A., Roberts, J., & Tuszynski, M. H. (2004). Bilateral corticospinal projections arise from each motor cortex in the macaque monkey: a quantitative study. Journal of Comparative Neurology, 473(2), 147-161.

Liang, J. N., & Brown, D. A. (2013). Impaired foot-force direction regulation during postural loaded locomotion in individuals post-stroke. Journal of neurophysiology.

Luft, A. R., Smith, G. V., Forrester, L., Whitall, J., Macko, R. F., Hauser, T. K., ... & Hanley, D. F. (2002). Comparing brain activation associated with isolated upper and lower limb movement across corresponding joints. *Human brain mapping*, *17*(2), 131-140.

Lundy-Ekman, L. (2009). Neuroscience, fundamentals for rehabilitation. (3rd ed.). W.B. Saunders Company.

Marchal-Crespo L, Hollnagel C, Brugger M, Kollias S, Riener R. (2011). An fMRI pilot study to evaluate brain activation associated with locomotion adaptation. IEEE/RSJ International Conference on Rehabilitation Robotics, Zurich Switzerland.

Massion, J. (1992). Movement, posture and equilibrium: interaction and coordination. Progress in neurobiology, 38(1), 35-56.

Mehta JP, Verber MD, Wieser JA, Schmit BD, Schindler-Ivens SM. (2009). A novel technique for examining human brain activity associated with pedaling using fMRI. Journal of Neuroscience Methods 179(2):230-239.

Mehta JP, Verber MD, Wieser JA, Schmit BD, Schindler-Ivens SM. (2012). The effect of movement rate and complexity on functional magnetic resonance signal change during pedaling. Motor Control 16(2):158-175.

Mihara M, Miyai I, Hatakenaka M, Kubota K, Sakoda S. (2007). Sustained prefrontal activation during ataxic gait: A compensatory mechanism for ataxic stroke? NeuroImage 37(4):1338-1345.

Miyai I, Suzuki M, Hatakenaka M, Kubota K. (2006). Effect of body weight support on cortical activation during gait in patients with stroke. Experimental Brain Research 169(1):85-91.

Miyai I, Tanabe HC, Sase I, Eda H, Oda I, Konishi I, Tsunazawa Y, Suzuki T, Yanagida T, Kubota K. (2001). Cortical mapping of gait in humans: A near-infrared spectroscopic topography study. NeuroImage 14(5):1186-1192.

Miyai I, Yagura H, Hatakenaka M, Oda I, Konishi I, Kubota K. (2003). Longitudinal optical imaging study for locomotor recovery after stroke. Stroke 34(12):2866-2870.

Miyai I, Yagura H, Oda I, Konishi I, Eda H, Suzuki T, Kubota K. (2002). Premotor cortex is involved in restoration of gait in stroke. Annals of Neurology 52(2):188- 194.

Morton SM and Bastian AJ. (2004). Cerebellar control of balance and locomotion. The Neuroscientist 10(3):247-259.

Naito, E., Kochiyama, T., Kitada, R., Nakamura, S., Matsumura, M., Yonekura, Y., et al. (2002). Internally simulated movement sensations during motor imagery activate corti- cal motor areas and the cerebellum. The Journal of Neuroscience: The Official Journal of the Society for Neuroscience, 22(9), 3683–3691

Netz, J., Lammers, T., & Hömberg, V. (1997). Reorganization of motor output in the non-affected hemisphere after stroke. Brain, 120(9), 1579-1586.

Nielsen JB. (2003). How we walk: Central control of muscle activity during human walking. The Neuroscientist 9(3):195-204.

Nirkko, A. C., Ozdoba, C., Redmond, S. M., Bürki, M., Schroth, G., Hess, C. W., & Wiesendanger, M. (2001). Different ipsilateral representations for distal and proximal movements in the sensorimotor cortex: activation and deactivation patterns. Neuroimage, 13(5), 825-835.

Noga, B. R., Kriellaars, D. J., Brownstone, R. M., & Jordan, L. M. (2003). Mechanism for activation of locomotor centers in the spinal cord by stimulation of the mesencephalic locomotor region. Journal of neurophysiology, 90(3), 1464-1478.

Nyberg-Hansen, R. (1966). Functional organization of descending supraspinal fibre systems to the spinalcord. Anatomical observations and physiological correlations. Ergebnisse der Anatomie und Entwicklungsgeschichte, 39(2), 3

Nyberg-Hansen, R. (1966). Sites of termination of interstitiospinal fibers in the cat. An experimental study with silver impregnation methods. Archives italiennes de biologie, 104(1), 98.

Pang MYC and Yang JF. (2000). The initiation of the swing phase in human infant stepping: Importance of hip position and leg loading. The Journal of Physiology 528:389-404.

Pearson KG. (1995). Proprioceptive regulation of locomotion. Current Opinion in Neurobiology 5(6):786-791.

Petersen N, Christensen LO, Nielsen J. (1998). The effect of transcranial magnetic stimulation on the soleus H reflex during human walking. The Journal of Physiology 513:599-610.

Petersen NT, Butler JE, Marchand-Pauvert V, Fisher R, Ledebt A, Pyndt HS, Hansen NL, Nielsen JB. (2001). Suppression of EMG activity by transcranial magnetic stimulation in human subjects during walking. The Journal of Physiology 537:651-656."

Petersen, T. H., Willerslev‐Olsen, M., Conway, B. A., & Nielsen, J. B. (2012). The motor cortex drives the muscles during walking in human subjects. The Journal of Physiology, 590(10), 2443-2452.

Peterson TH, Willerslev-Olsen M, Conway BA, Nielsen JB. (2012). The motor cortex drives the muscles during walking in human subjects. The Journal of Physiology 590:2443-2452.

Promjunyakul, N. O., Schmit, B. D., & Schindler-Ivens, S. (2013). Changes in hemodynamic responses in chronic stroke survivors do not affect fMRI signal detection in a block experimental design. Magnetic resonance imaging.

Pyndt HS and Nielsen JB. (2003). Modulation of transmission in the corticospinal and group ia afferent pathways to soleus motoneurons during bicycling. Journal of Neurophysiology 89(1):304-314.

Raasch CC, Zajac FE, Ma B, Levine WS. (1997). Muscle coordination of maximum-speed pedaling. Journal of Biomechanics 30(6):595-602.

Ralston DD, Ralston HJ 3rd. (1985) The terminations of corticospinal tract axons in the macaque monkey. J Comp Neurol 242:325–37.

Reddy H, Narayanan S, Matthews PM, Hoge RD, Pike GB, Duquette P, Antel J, Arnold DL. (2000) Relating axonal injury to functional recovery in MS. Neurology 54:236–9.

Rocca, M. A., & Filippi, M. (2010). FMRI correlates of execution and observation of foot movements in left-handers. Journal of the neurological sciences, 288(1), 34-41.

Rogers, L. M., Brown, D. A., & Gruben, K. G. (2004). Foot force direction control during leg pushes against fixed and moving pedals in persons post-stroke. Gait & posture, 19(1), 58-68.

Ropper, A. H., Adams, R. D., Samuels, M. A., & Victor, M. (2009). Adams and victor\'s principles of neurology. (9 ed.). McGraw-Hill Professional.

Sahyoun, C., Floyer-Lea, A., Johansen-Berg, H., Matthews, P.M., (2004) Towards an understanding of gait control: brain activation during the anticipation, preparation and execution of foot movements. NeuroImage 21, 568–575.

Schenck F. (1996) The role of magnetic susceptibility in magnetic resonance imag- ing: MRI magnetic compatibility of the first and second kinds. Med Phys, 23(6):815–50.

Schindler-Ivens, S., Brown, D. A., Lewis, G. N., Nielsen, J. B., Ondishko, K. L., & Wieser, J. (2008). Soleus H-reflex excitability during pedaling post-stroke.Experimental Brain Research, 188(3), 465-474.

Schmahmann, J. D., Doyon, J., McDonald, D., Holmes, C., Lavoie, K., Hurwitz, A. S., ... & Petrides, M. (1999). Three-dimensional MRI atlas of the human cerebellum in proportional stereotaxic space. Neuroimage, 10(3), 233-260.

Schmit, B. D., & Benz, E. N. (2002). Extensor reflexes in human spinal cord injury: activation by hip proprioceptors. *Experimental brain research*, *145*(4), 520-527.

Schubert M, Curt A, Colombo G, Berger W, Dietz V. (1999). Voluntary control of human gait: Conditioning of magnetically evoked motor responses in a precision stepping task. Experimental Brain Research 126(4):583-588.

Schubert M, Curt A, Jensen L, Dietz V. (1997). Corticospinal input in human gait: Modulation of magnetically evoked motor responses. Experimental Brain Research 115:234-246.

Shik ML, Severin FV, Orlovskii GN. (1966). Control of walking and running by means of electric stimulation of the midbrain Biofizika 11(4):659-666.

Sherrington, C. S. (1910). Flexion-reflex of the limb, crossed extension-reflex, and reflex stepping and standing. *The Journal of physiology*, *40*(1-2), 28.

Stephens M and Yang J. (1999). Loading during the stance phase of walking in humans increases the extensor EMG amplitude but does not change the duration of the step cycle. Experimental Brain Research 124:363-370.

Suminski A, Zimbelman J, Scheidt R. (2007) Design and validation of a MR-compatible pneumatic manipulandum. J Neurosci Methods, 163:255–66.

Suzuki M, Miyai I, Ono T, Kubota K. (2008). Activities in the frontal cortex and gait performance are modulated by preparation. an fNIRS study. NeuroImage 39(2):600-607.

Suzuki M, Miyai I, Ono T, Oda I, Konishi I, Kochiyama T, Kubota K. (2004). Prefrontal and premotor cortices are involved in adapting walking and running speed on the treadmill: An optical imaging study. NeuroImage 23(3):1020-1026.

Talairach J, Tournoux P. (1988) Co-planar stereotaxic atlas of the human brain: 3- dimensional proportional system—an approach to cerebral imaging. New York: Thieme Medical Publishers.

Ting LH, Christine RC, Brown DA, Kautz SA, Zajac FE. (1998). Sensorimotor state of the contralateral leg affects ipsilateral muscle coordination of pedaling. Journal of Neurophysiology 80:1341-1351.

Van der Loos HF, Kautz SA, Scwandt D, Anderson J, Chen G, Bevly D. (2002). A split-crank, servomotor-controlled bicycle ergometer design for studies in human biomechanics. IEEE/RSJ International Conference on Intelligent Robots and Systems, Lausanne, Switzerland: IEEE 1409–1414.

Weiller, C., Chollet, F., Friston, K. J., Wise, R. J., & Frackowiak, R. S. (1992). Functional reorganization of the brain in recovery from striatocapsular infarction in man. Annals of neurology, 31(5), 463-472.

Wexler BE, Fulbright RK, Lacadie CM, Skudlarski P, Kelz MB, Constable RT, Gore JC. (1997). An fMRI study of the human cortical motor system response to increasing functional demands. Magnetic Resonance Imaging 15(4):385-396.

Whelan PJ. (1996). Control of locomotion in the decerebrate cat. Progress in Neurobiology 49(5):481-515.

Williamson JW, Nobrega AC, McColl R, Mathews D, Winchester P, Friberg L, Mitchell JH. (1997). Activation of the insular cortex during dynamic exercise in humans. The Journal of Physiology 503:277-283."

Wu M, Gordon K, Kahn JH, Schmit BD. (2011). Prolonged electrical stimulation over hip flexors increases locomotor output in human SCI. Clinical Neurophysiology 122(7):1421-1428.

Yang JF, Stephens MJ, Vishram R. (1998). Infant stepping: A method to study the sensory control of human walking. The Journal of Physiology 507(3):927-937.

Yuste, R., MacLean, J. N., Smith, J., & Lansner, A. (2005). The cortex as a central pattern generator. *Nature Reviews Neuroscience*, *6*(6), 477-483.

APPENDIX A – DEVICE DETAILS

Table A1: Parts list

Part	Quantity	Material, Details	Source
Base	1	UHMW	Midland Plastics
Upright	4	PC	Midland Plastics
Middle Block 1	2	UHMW	Midland Plastics
Middle Block 2	1	UHMW	Midland Plastics
Crankshaft	2	POM	Midland Plastics
Coupler	1	POM	Midland Plastics
Centric Pulley	2	POM	Midland Plastics
Eccentric Pulley	2	POM	Midland Plastics
Crank Arm	2	POM	Midland Plastics
Pedal	2	Oak	Midland Plastics
Pedal Shaft	2	POM	Midland Plastics
Pulley Shaft	1	Acrylic	Midland Plastics
Side Support	2	PC	Midland Plastics
Center Support	1	UHMW	Midland Plastics
Small Pulley	2	POM	Midland Plastics
Encoder Upper	2	PC	Midland Plastics
Encoder Lower	2	PC	Midland Plastics
Large Bearing	4	POM, glass ID: 1”, OD: 2” PN: 6455K14	McMaster-Carr
Small Bearing	4	POM, glass ID: 5/8”, OD: 1 1/8” PN: 6455K78	McMaster-Carr
Encoder Pulley	4	PC 80MXL, Bore: 0.313” (modified to 6mm), Diameter: 2.017” Belt width: 1/4" PN: A 6M16-080DF2510	Spd-si
Encoder Belt	2	Neoprene 80MXL PN: 7959K21	McMaster-Carr
Encoder	2	PN: TD 5207	Micronor
Friction Strap	2	1/2” Nylon strap PN: 87975K52	McMaster-Carr
Elastic Bands	-	Vulcanized Rubber 8 1/2” x 1/8” PN: 97425	Amazon
Small Fasteners	-	Nylon, 1/4 x 20	McMaster-Carr
Threaded rod, nuts	3,6	Nylon, 3.4” x 10	McMaster-Carr

UHMW: Ultra-high molecular weight polyethylene
POM: polyoxymethylene (Commonly Delrin ®)
PC: Polycarbonate

Base

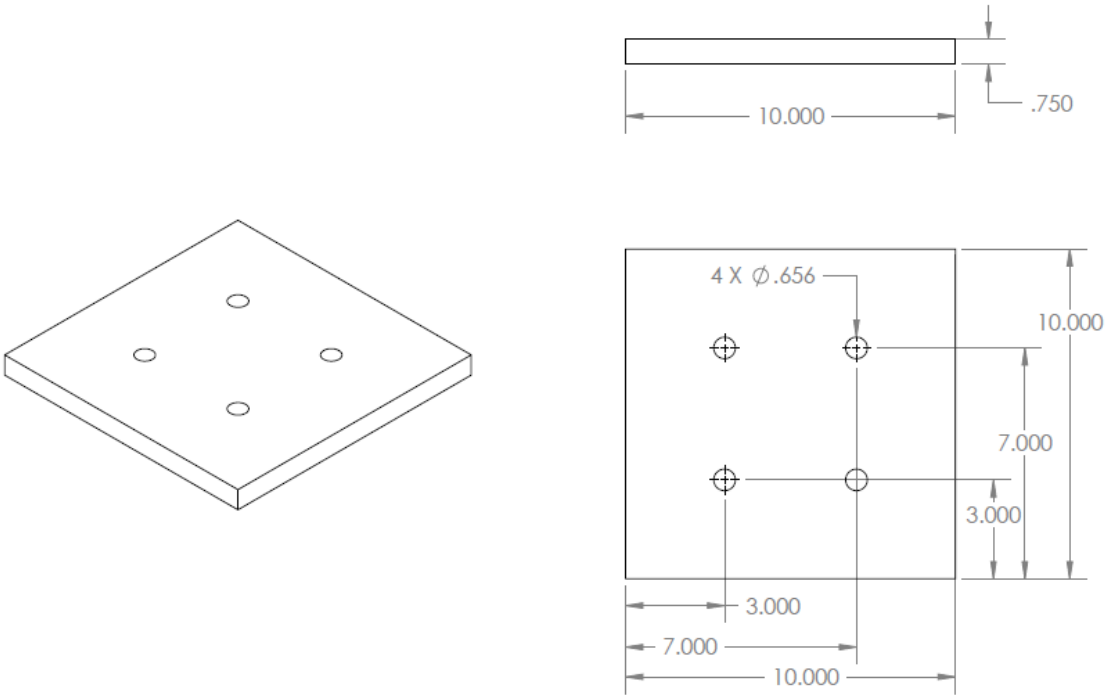

Upright

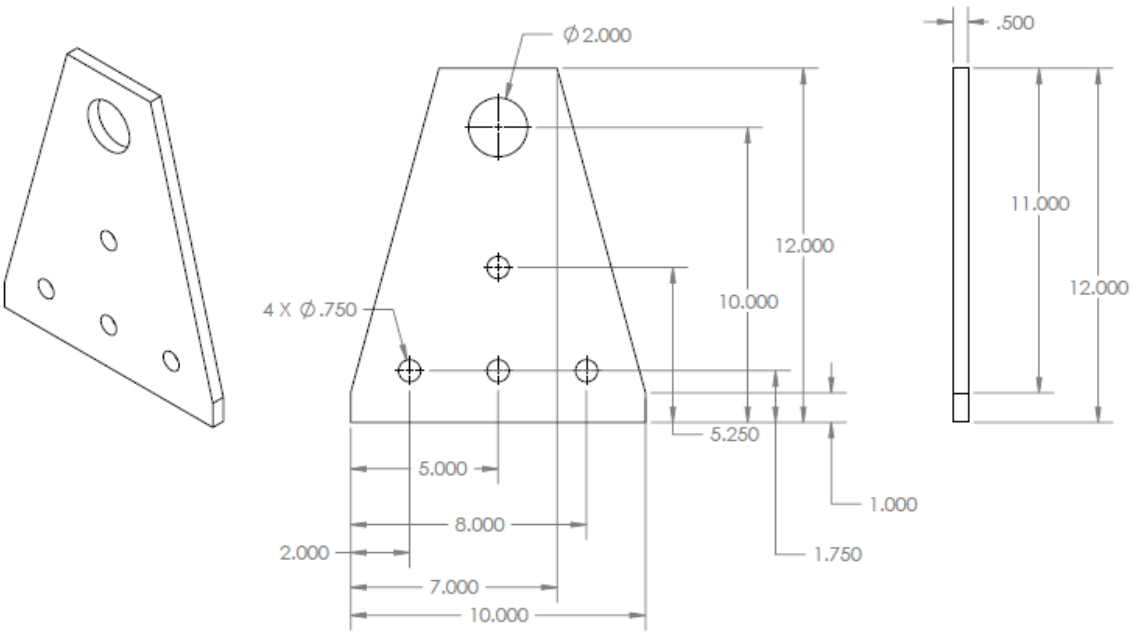

Middle Block 1

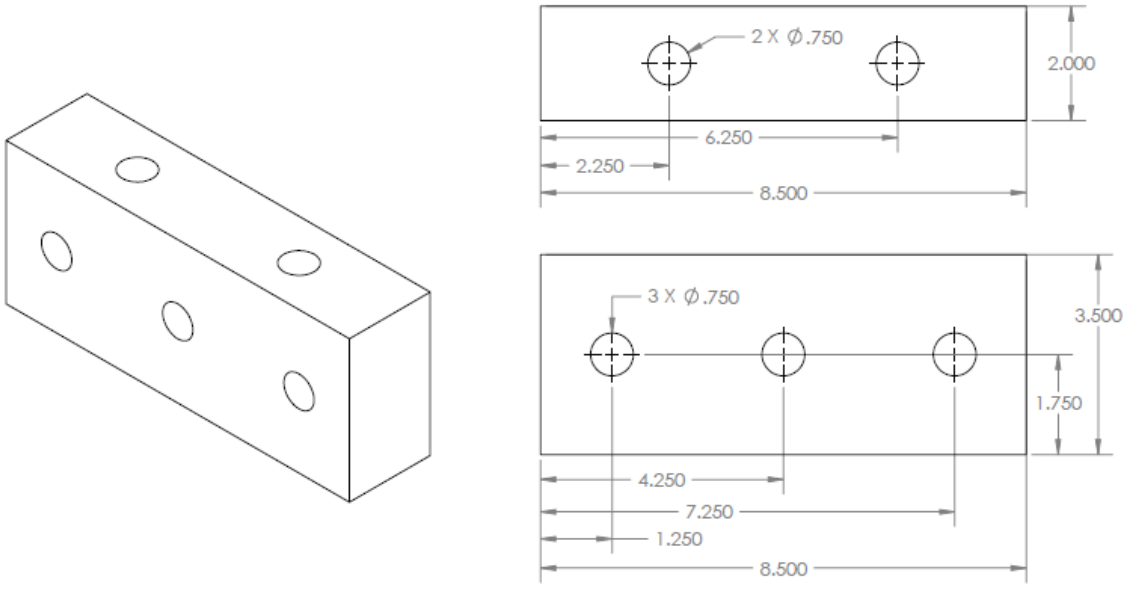

Middle Block 2

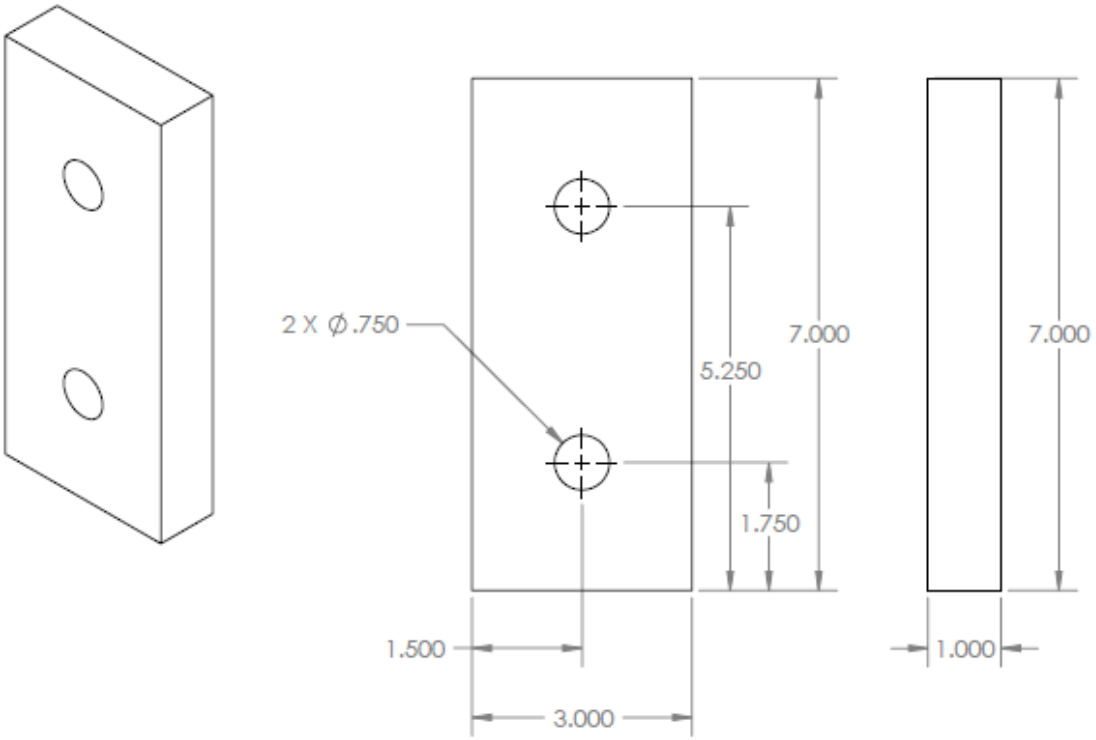

Crankshaft

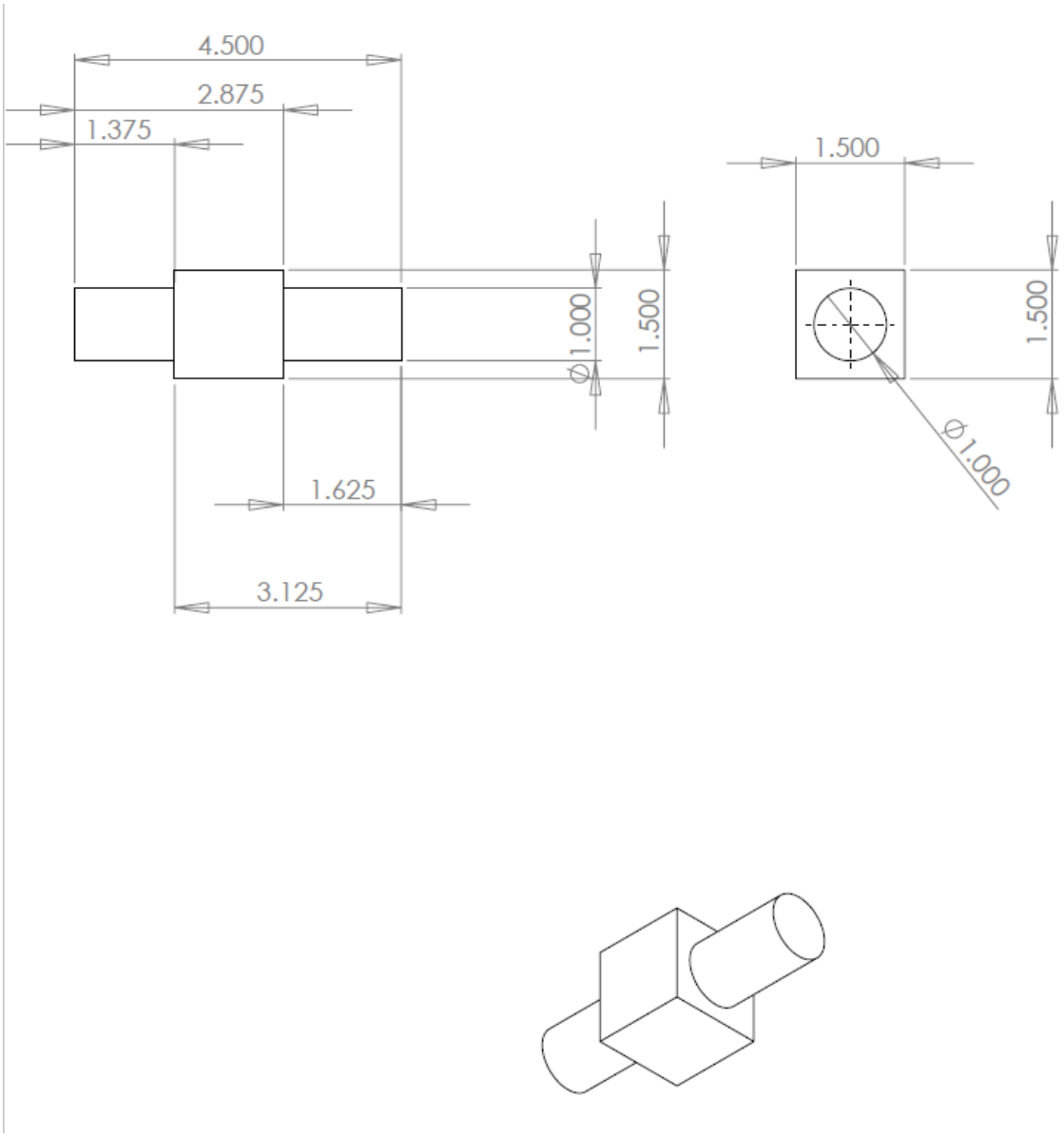

Coupler

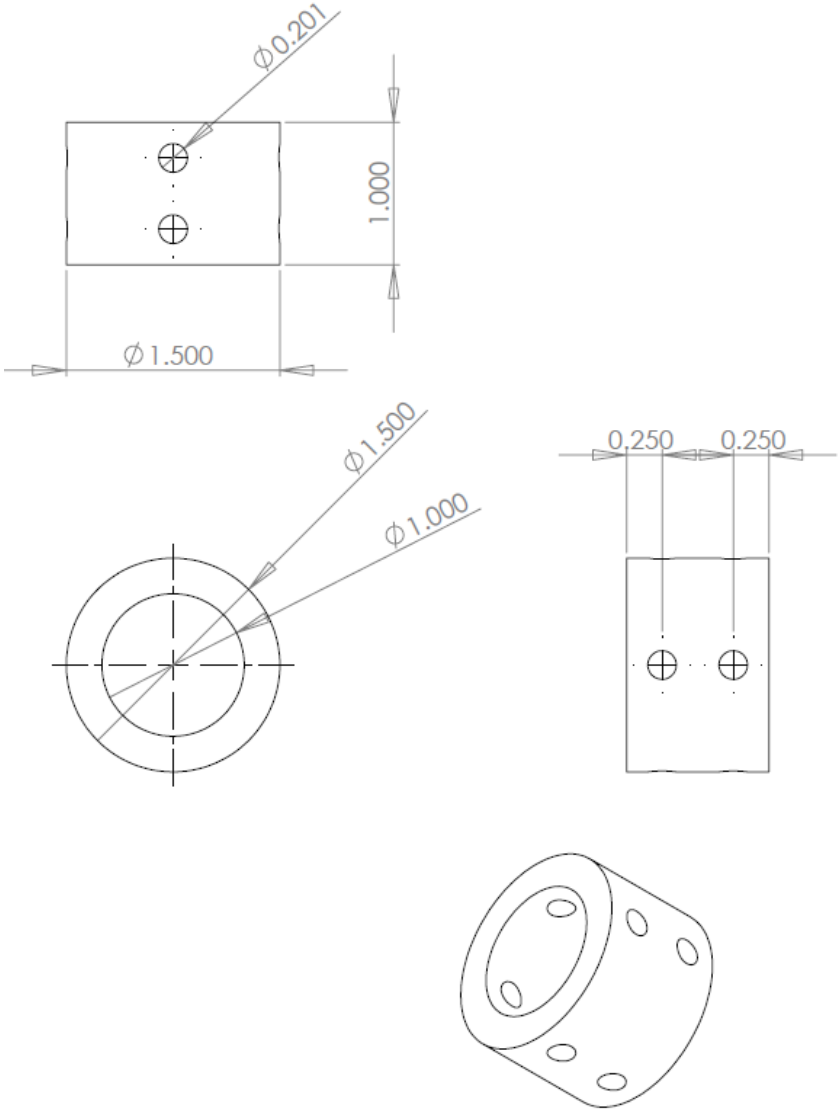

Centric Pulley

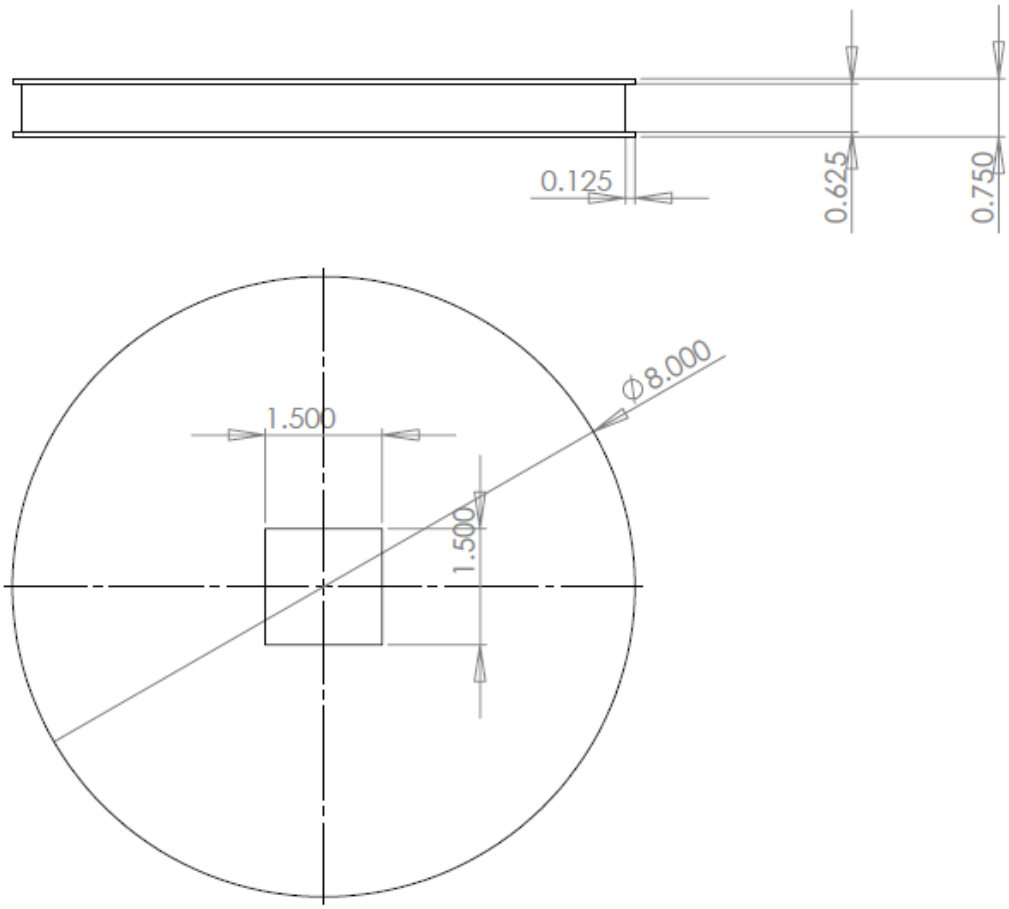

Eccentric Pulley

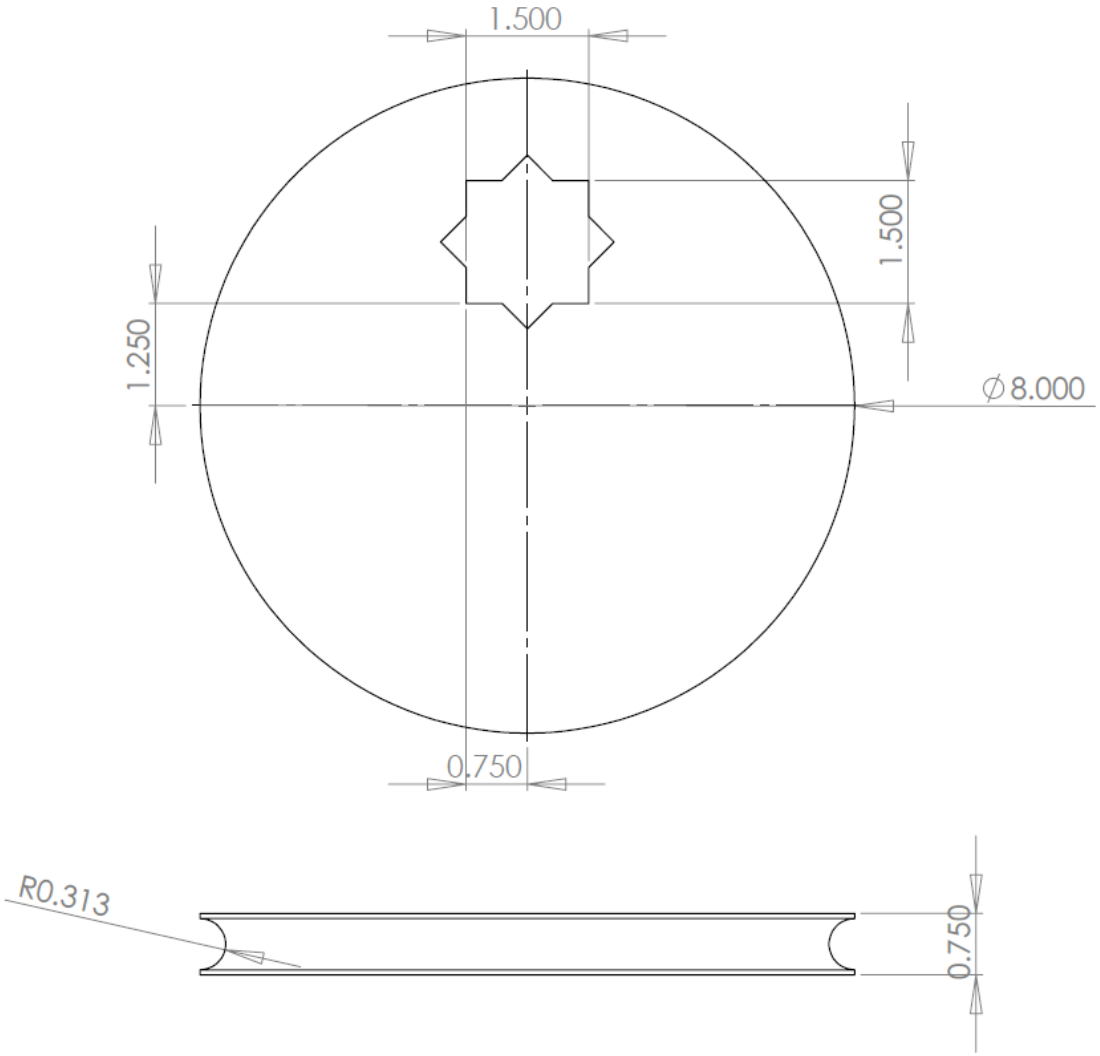

Crank Arm

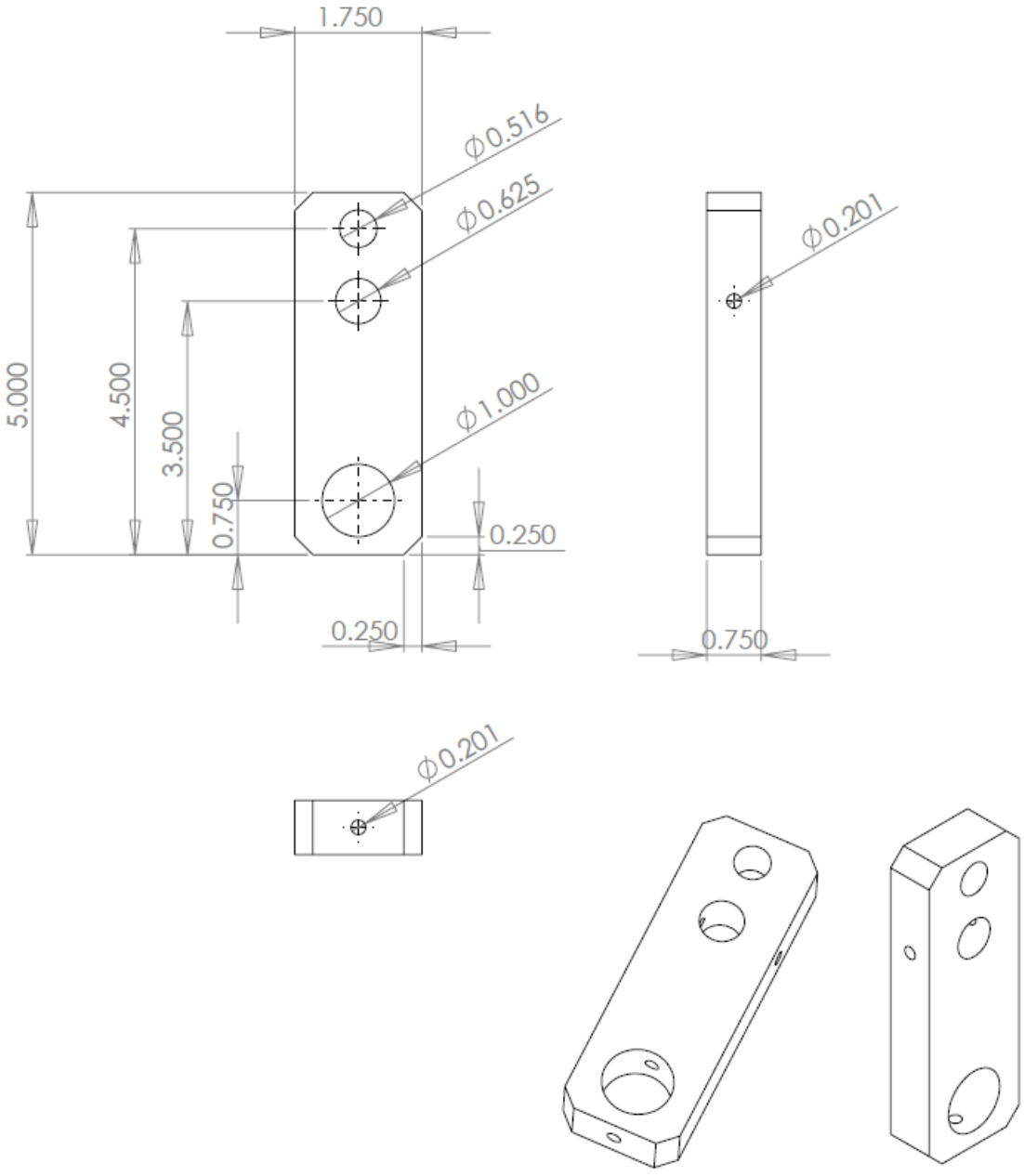
1.750
ϕ0.516
ϕ0.625
ϕ1.000
5.000
4.500
3.500
0.750
0.250
0.250
ϕ0.201
0.750
ϕ0.201

Pedal

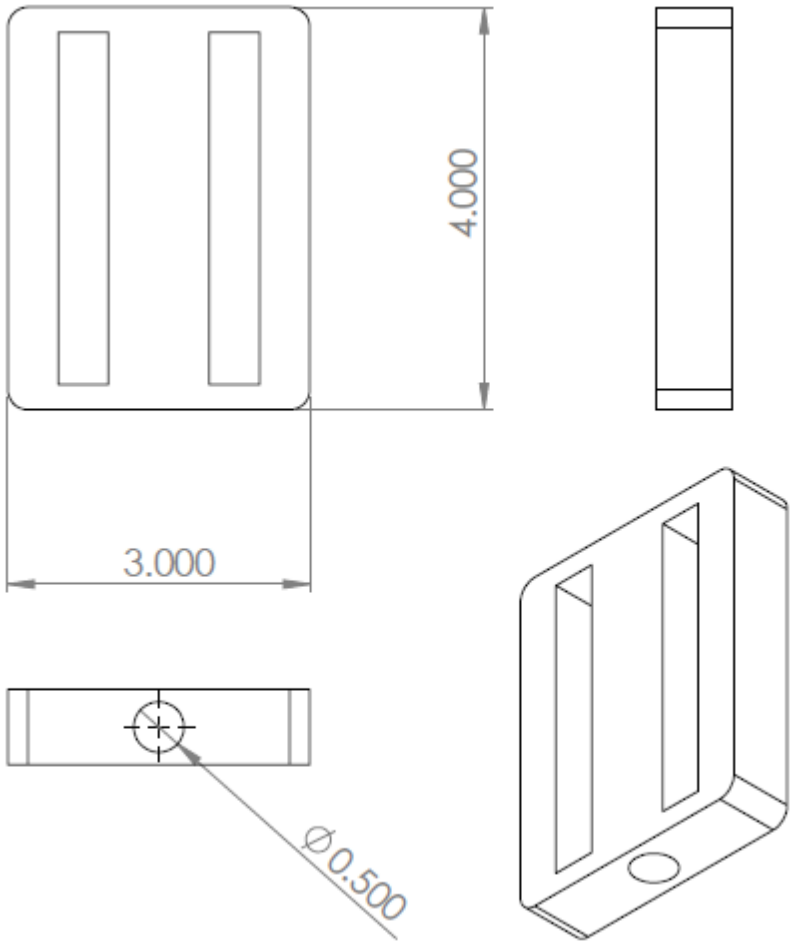

Pedal Shaft

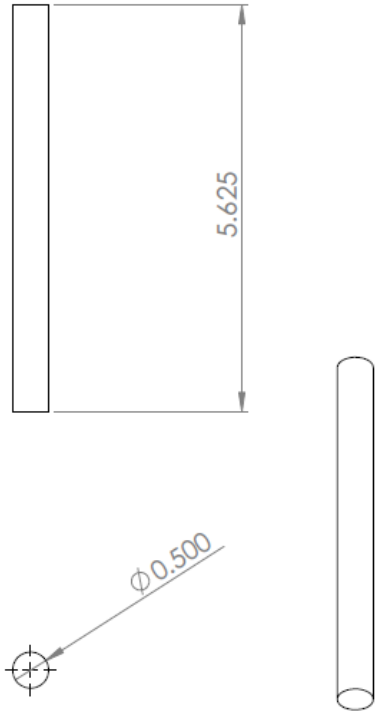

Pulley Shaft

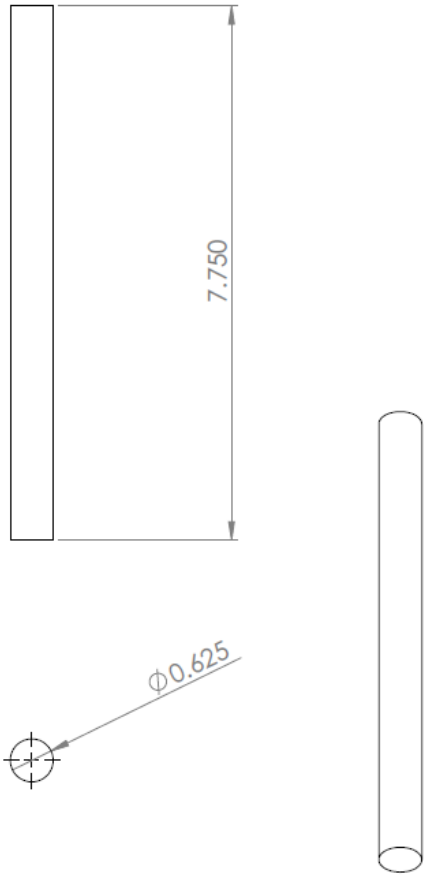

Side Support

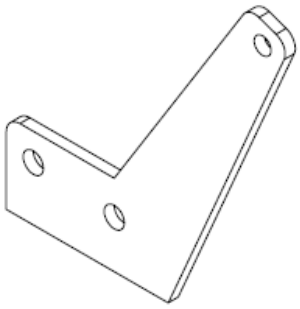

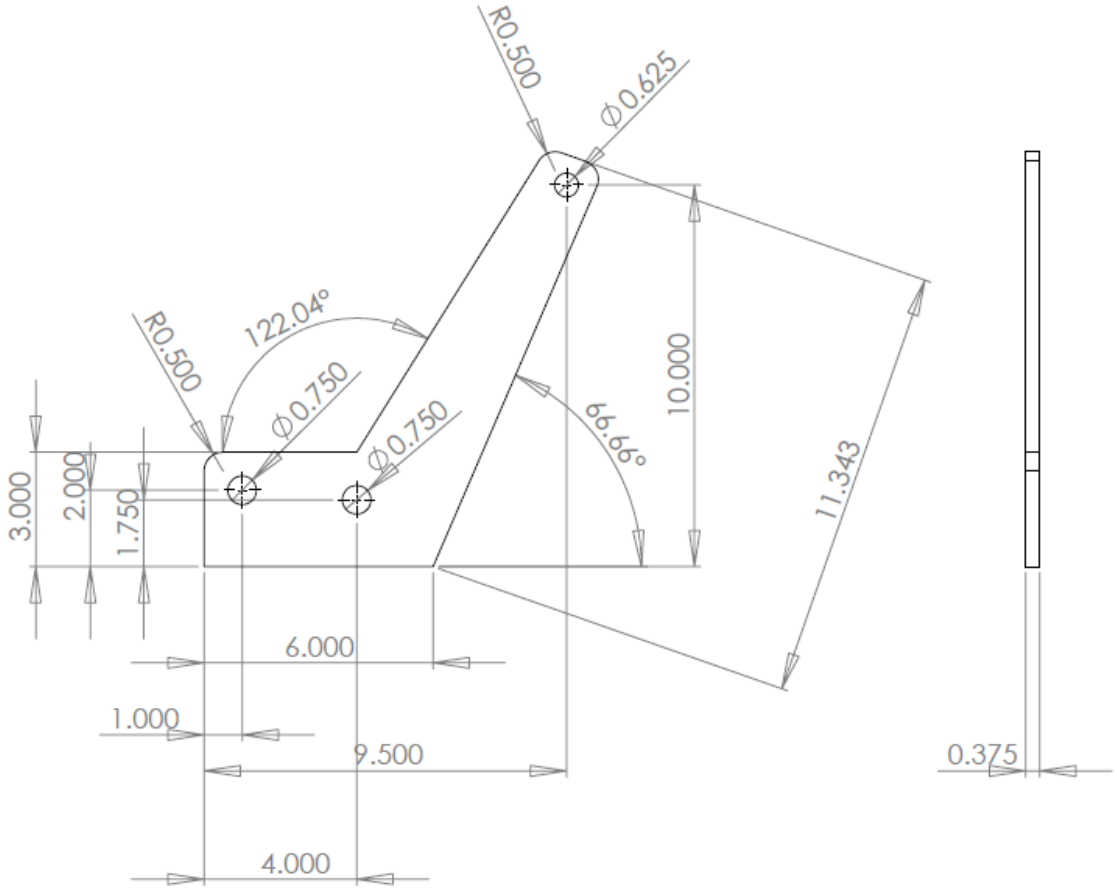

Center Support

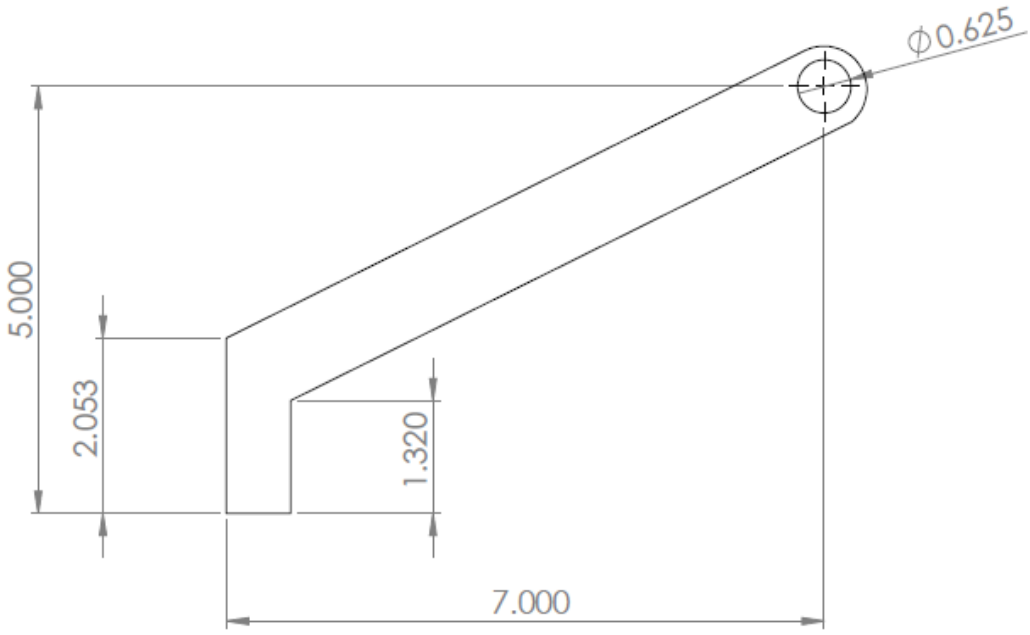

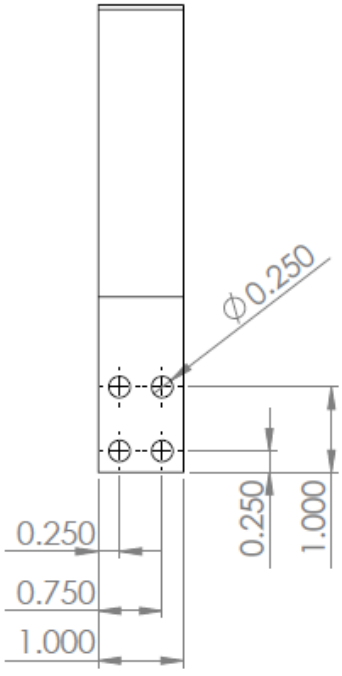

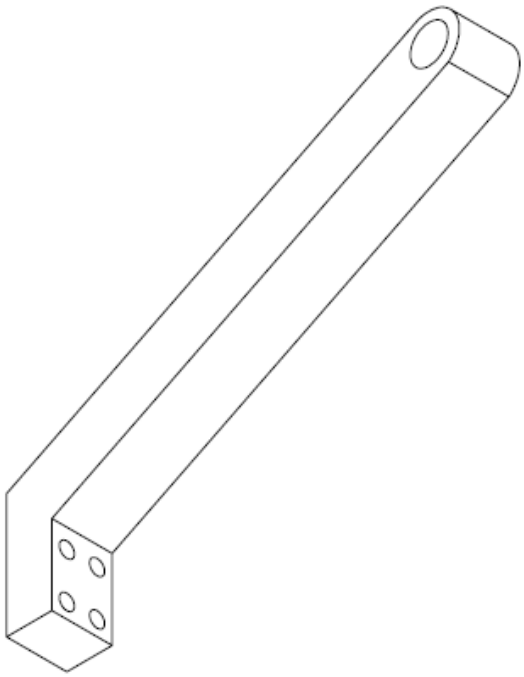

Small Pulley

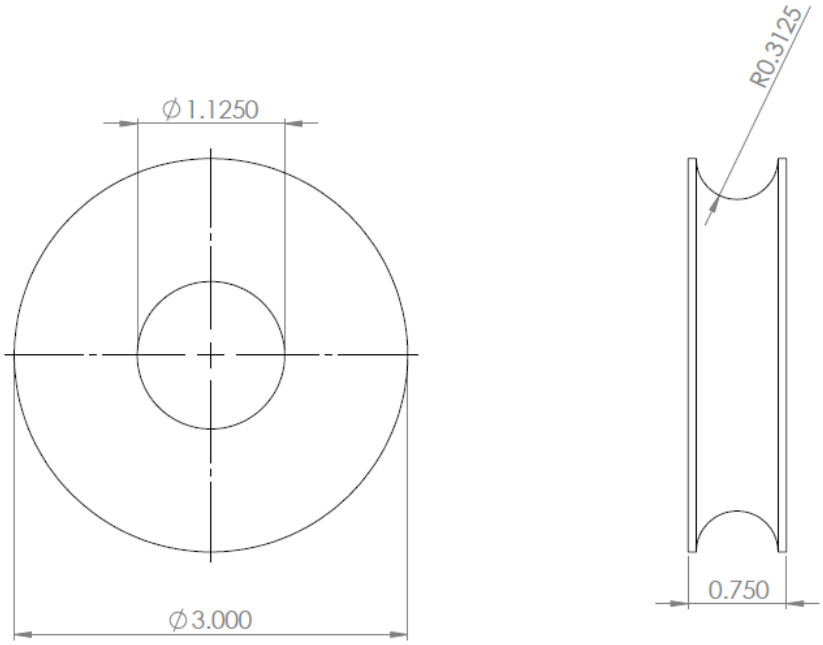

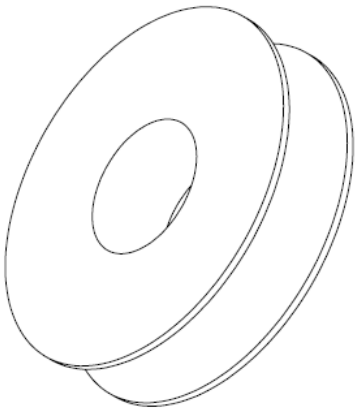

Encoder Upper

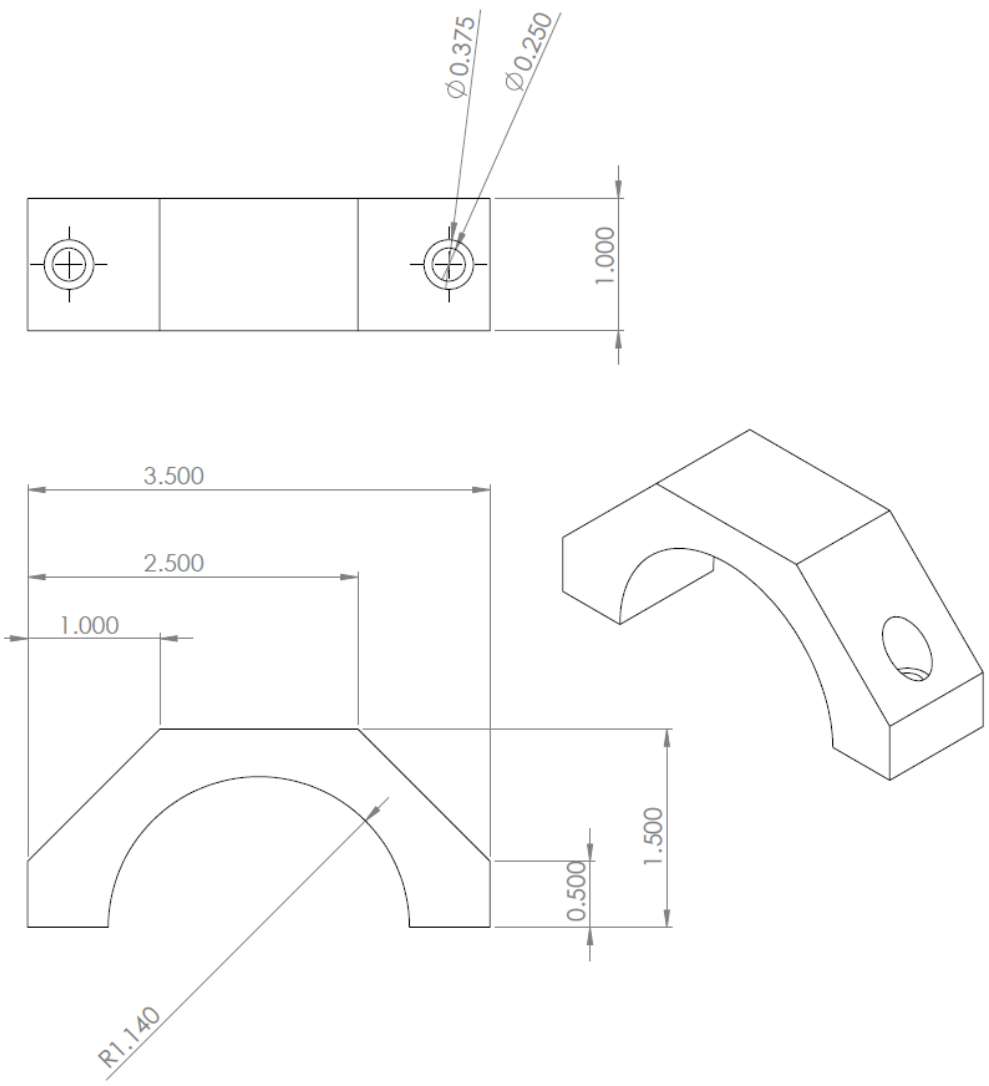

Encoder Lower

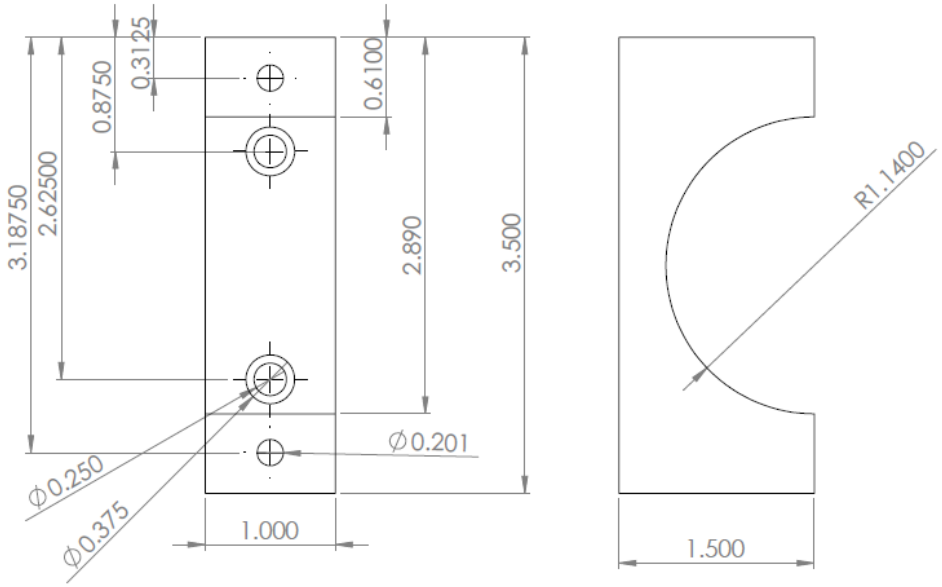

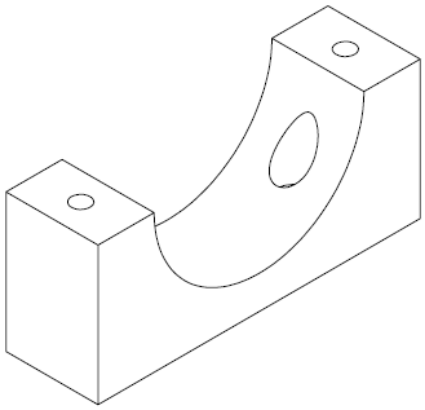

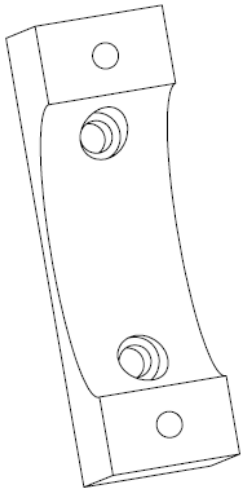

APPENDIX B: SUBJECTS AND DATA COLLECTION SHEETS

Table B1: Subject Information

Experiment Code	Gender	Age	Height	Height (in)	Weight (lbs)
BA C01	F	33	5'2"	62	105
BA C02	M	21	6'	72	200
BA C03	F	21	5'9"	69	160
BA C04	F	21	4"11"	59	100
BA C05	M	21	5'10"	70	160
BA C06	M	25	5'10"	70	140
BA C07	M	29	5'11"	71	170
BA C08	F	26	5'6"	66	125
BA C09	M	32	6'1"	73	150
BA C10	F	21	5'4"	64	130
BA C11	M	26	5'7"	67	172
MEAN		25.1			

Validation Data Collection Sheet:

Subject ID: ____________________
Date: ____________________ Begin Time: ____________________ End Time: ____________________

- -

Run	Condition	B #	Load	File Name	RPM	Comments
1	Bilateral	-	L			
2	Bilateral	-	L			
3	Bilateral	-	M			
4	Bilateral	-	M			
5	Bilateral	-	H			
6	Bilateral	-	H			
7	Right	10	L			
8	Right	10	L			
9	Right	8	L			
10	Right	8	L			
13	Right	6	L			
14	Right	6	L			
15	Left	10	L			
16	Left	10	L			
17	Left	8	L			
18	Left	8	L			
21	Left	6	L			
22	Left	6	L			

Additional Comments:
____
____
____
____

FMRI Data Collection Sheet:

Unilateral Pedaling Experiment: fMRI Parameters Sheet

Experiment Code: _____ PI: Schindler-Ivens S.

Date: _____/_____/_____ Start Time (24-hr): _____Technician: _____

Scanner: __Short bore 3T__ Gradient Coil: __GE Head__ RF Coil: __GE head coil__

Phantom Scan

Scan Type: ___GE-EPI___ TE (ms): ___25___ TR (ms): _____2000__ Flip: 77___

NEX: __1____

Plane: __Sag__ FOV (mm): __240__ Matrix: __64 x 64__ Thickness (mm):__4__

Slices:__36__

Location: First:_____ Last:_____

Timing: # Reps: _____ Number of scans: _____

Run #	Conditions	Time	Notes
1	Right Unilateral Pedaling		
2	Right Unilateral Pedaling		
3	Right Unilateral Pedaling		
4	Left Unilateral Pedaling		
5	Left Unilateral Pedaling		
6	Left Unilateral Pedaling		
	Anatomical		
7	Bilateral Pedaling		
8	Bilateral Pedaling		
9	Bilateral Pedaling		

APPENDIX C: INDIVIDUAL RESULTS FOR VALIDATION EXPERIMENTS

Subject C01

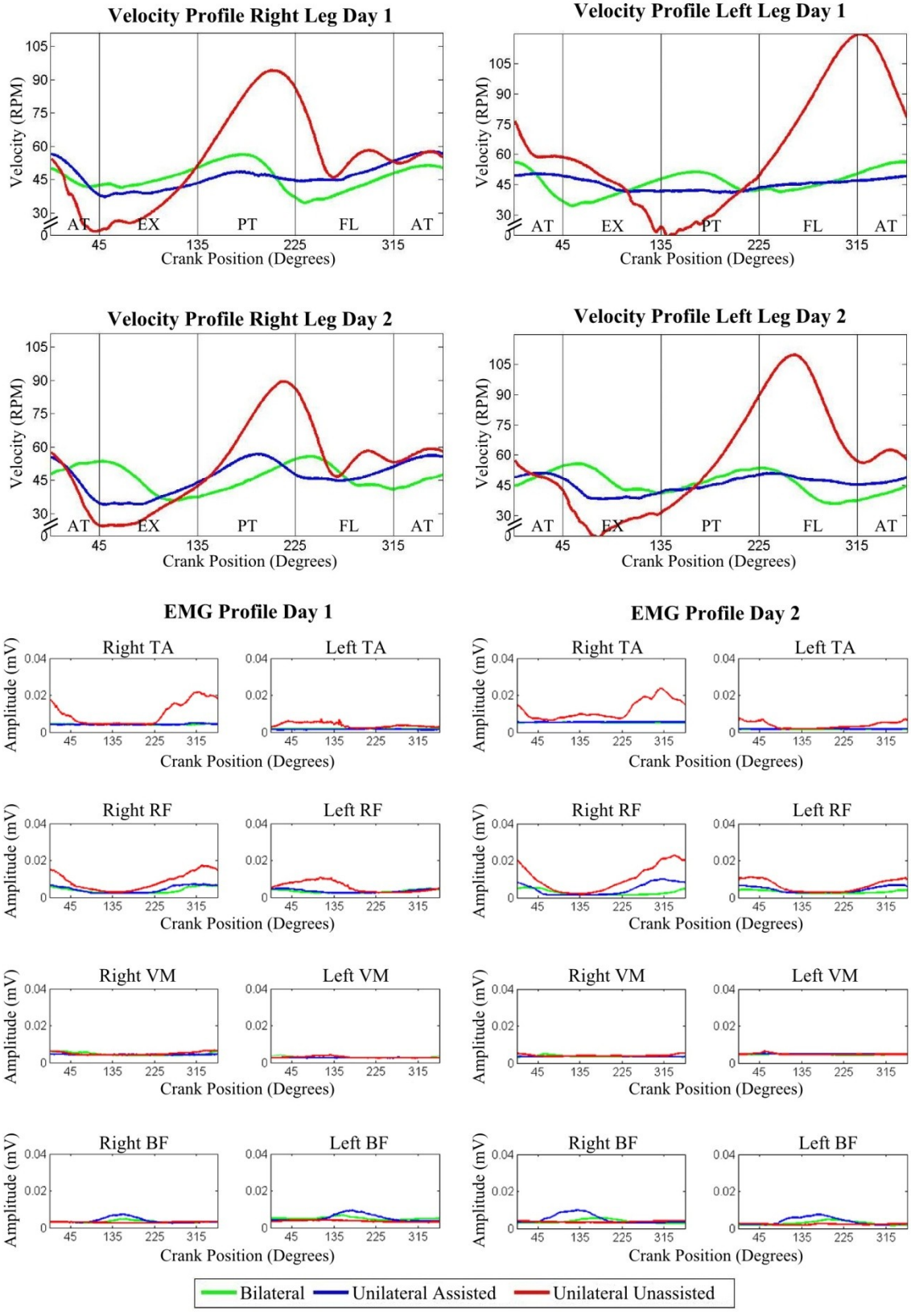

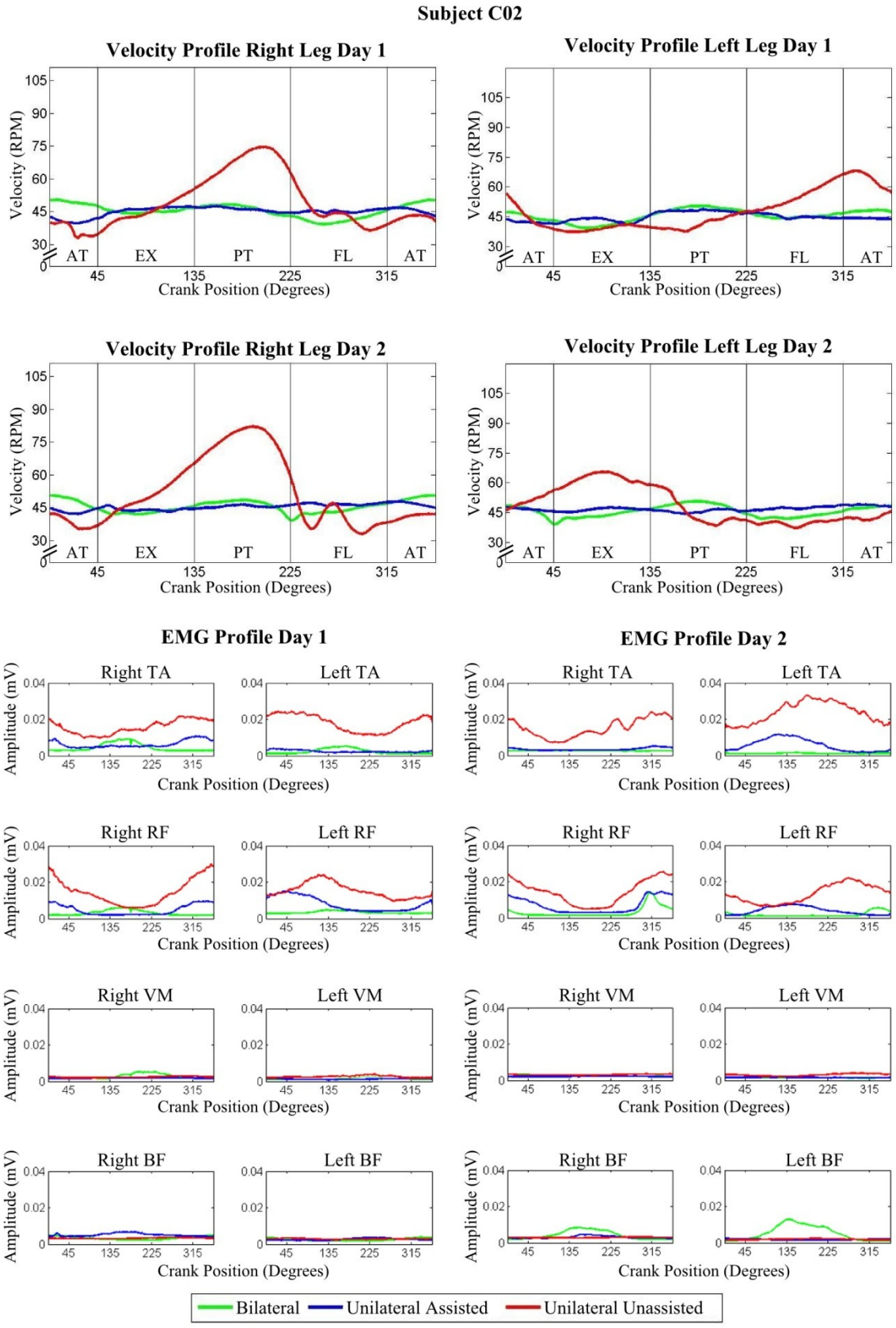
Subject C02
Velocity Profile Right Leg Day 1
Velocity Profile Left Leg Day 1
Velocity Profile Right Leg Day 2
Velocity Profile Left Leg Day 2
Velocity (RPM)
105
90
75
60
45
30
0
AT
EX
PT
FL
AT
45
135
225
315
Crank Position (Degrees)
EMG Profile Day 1
EMG Profile Day 2
Right TA
Left TA
Right RF
Left RF
Right VM
Left VM
Right BF
Left BF
Amplitude (mV)
0.04
0.02
0
Bilateral
Unilateral Assisted
Unilateral Unassisted

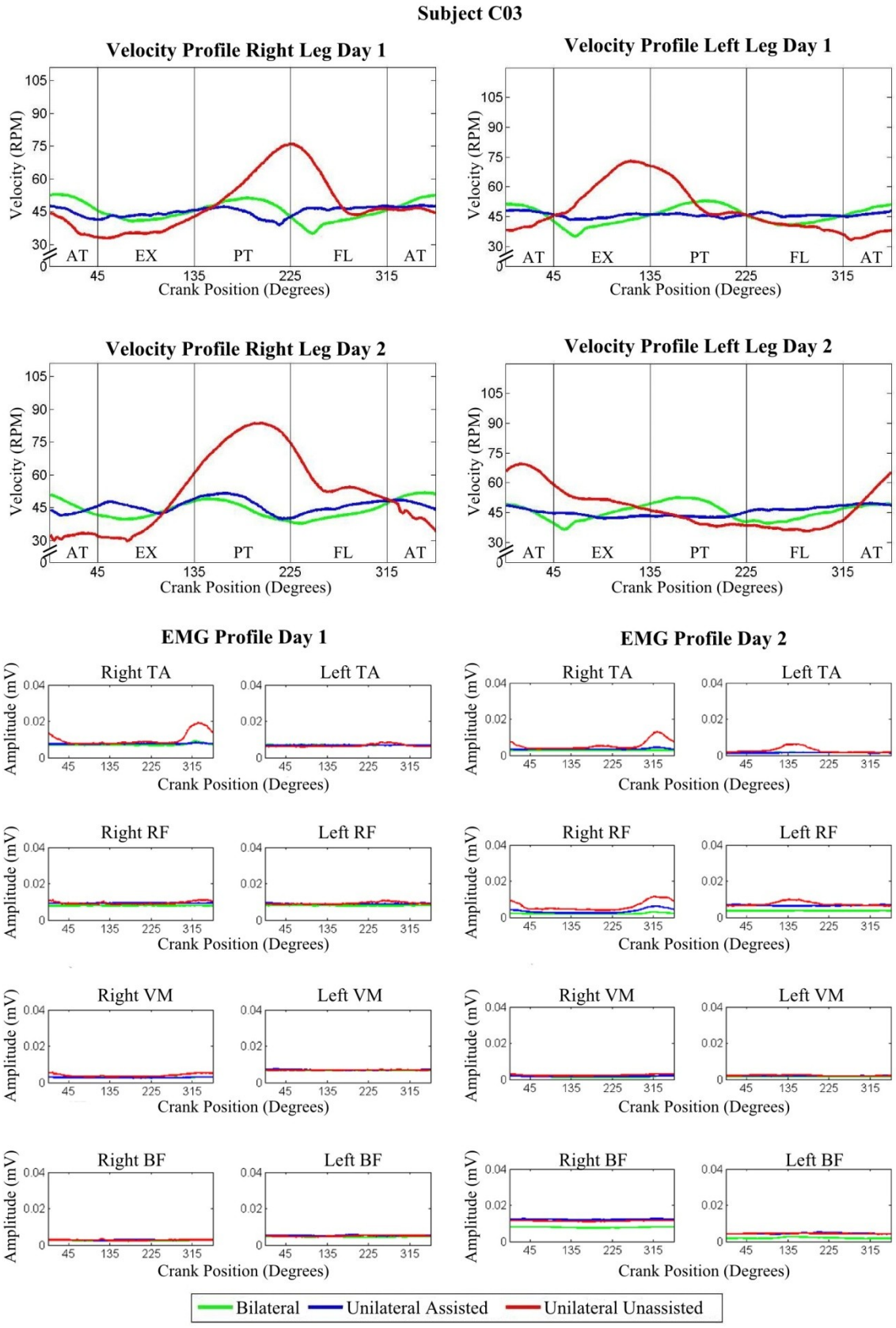
Subject C03
Velocity Profile Right Leg Day 1
Velocity Profile Left Leg Day 1
Velocity Profile Right Leg Day 2
Velocity Profile Left Leg Day 2
Velocity (RPM)
105
90
75
60
45
30
0
AT
EX
PT
FL
AT
45
135
225
315
Crank Position (Degrees)
EMG Profile Day 1
EMG Profile Day 2
Right TA
Left TA
Right RF
Left RF
Right VM
Left VM
Right BF
Left BF
Amplitude (mV)
0.04
0.02
0
Bilateral
Unilateral Assisted
Unilateral Unassisted

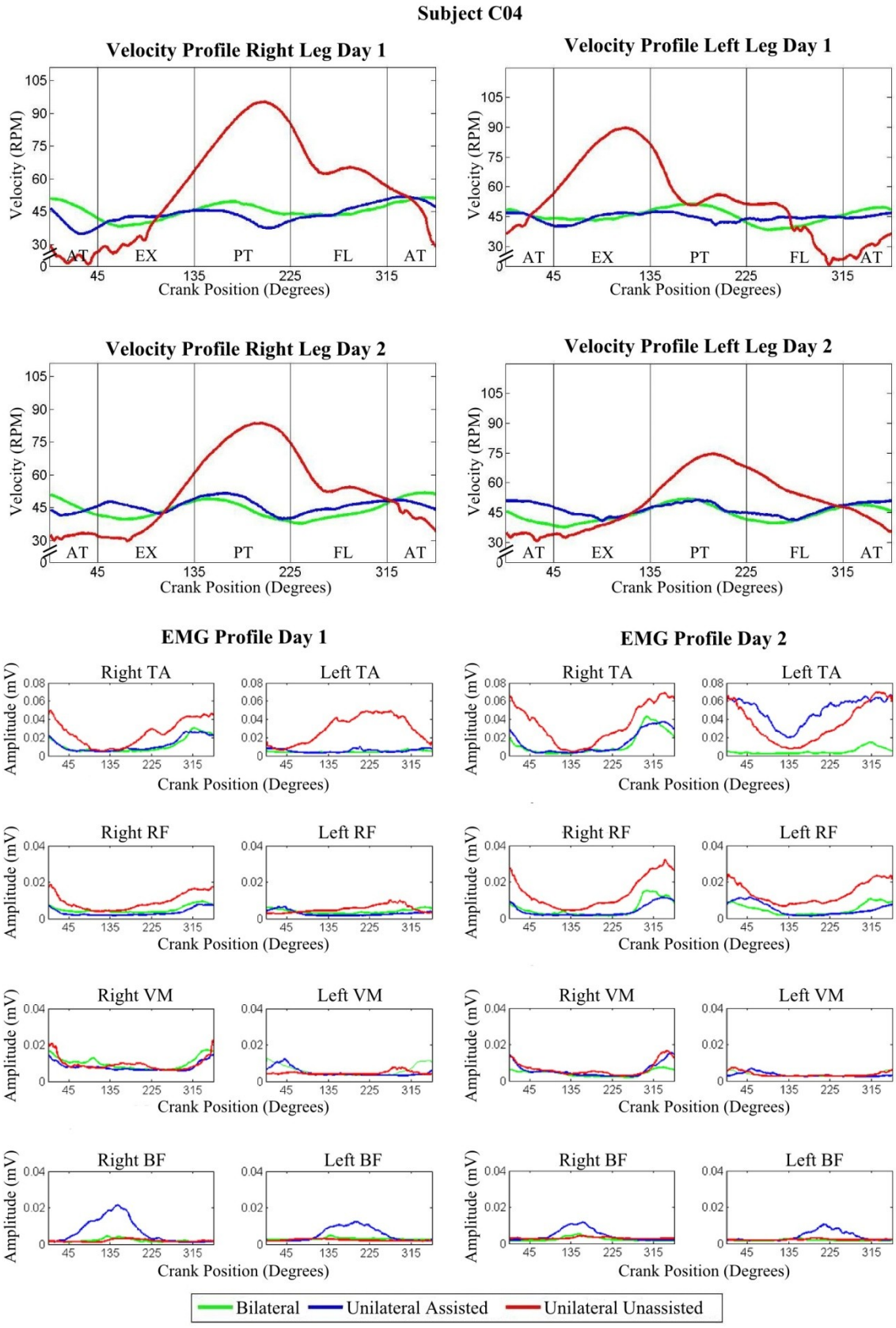
Subject C04
Velocity Profile Right Leg Day 1
Velocity Profile Left Leg Day 1
Velocity Profile Right Leg Day 2
Velocity Profile Left Leg Day 2
Velocity (RPM)
AT
EX
PT
FL
AT
Crank Position (Degrees)
EMG Profile Day 1
EMG Profile Day 2
Right TA
Left TA
Right RF
Left RF
Right VM
Left VM
Right BF
Left BF
Amplitude (mV)
Bilateral
Unilateral Assisted
Unilateral Unassisted

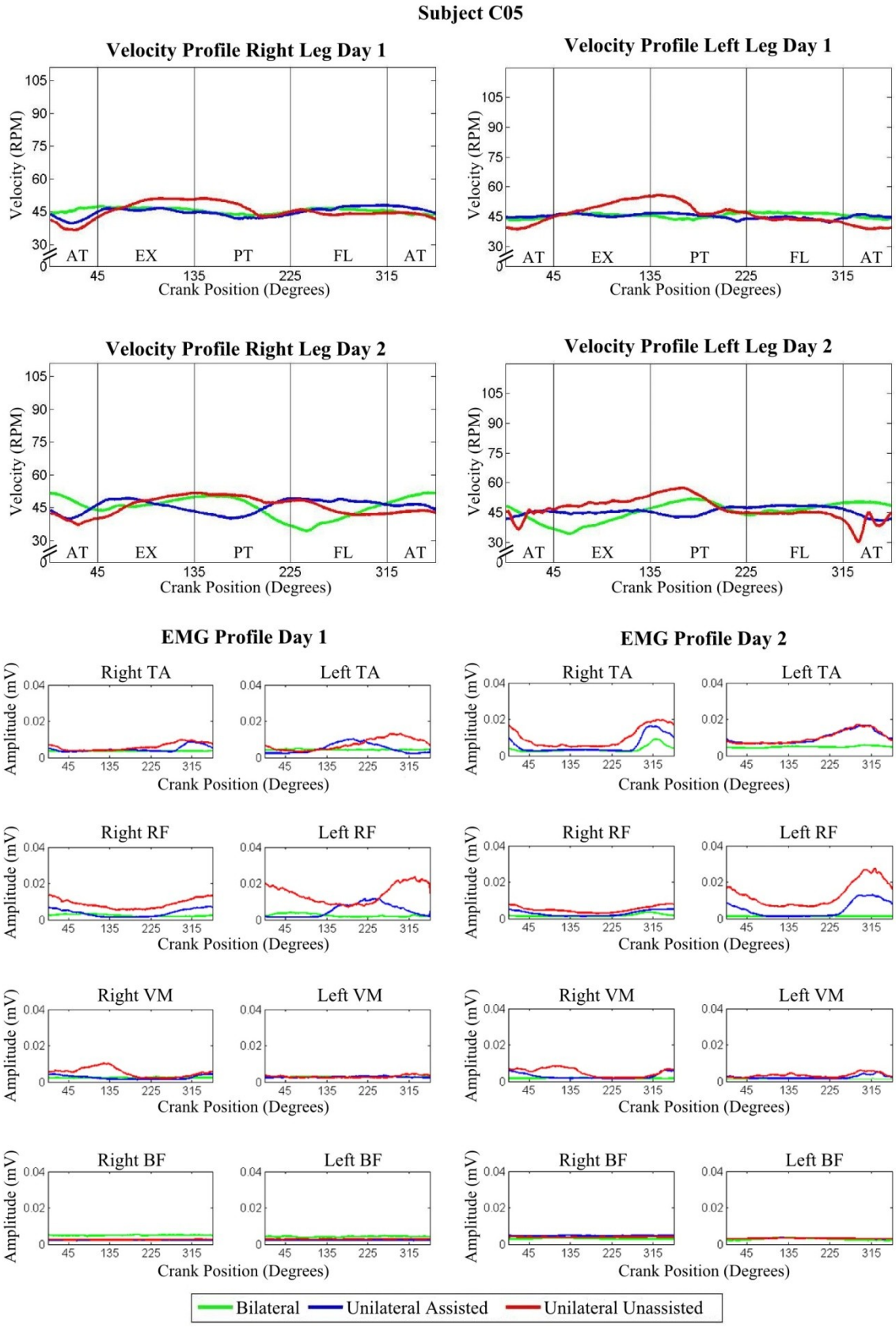
Subject C05
Velocity Profile Right Leg Day 1
Velocity Profile Left Leg Day 1
Velocity Profile Right Leg Day 2
Velocity Profile Left Leg Day 2
Velocity (RPM)
105
90
75
60
45
30
0
AT
EX
PT
FL
AT
45
135
225
315
Crank Position (Degrees)
EMG Profile Day 1
EMG Profile Day 2
Right TA
Left TA
Right RF
Left RF
Right VM
Left VM
Right BF
Left BF
Amplitude (mV)
0.04
0.02
0
Bilateral
Unilateral Assisted
Unilateral Unassisted

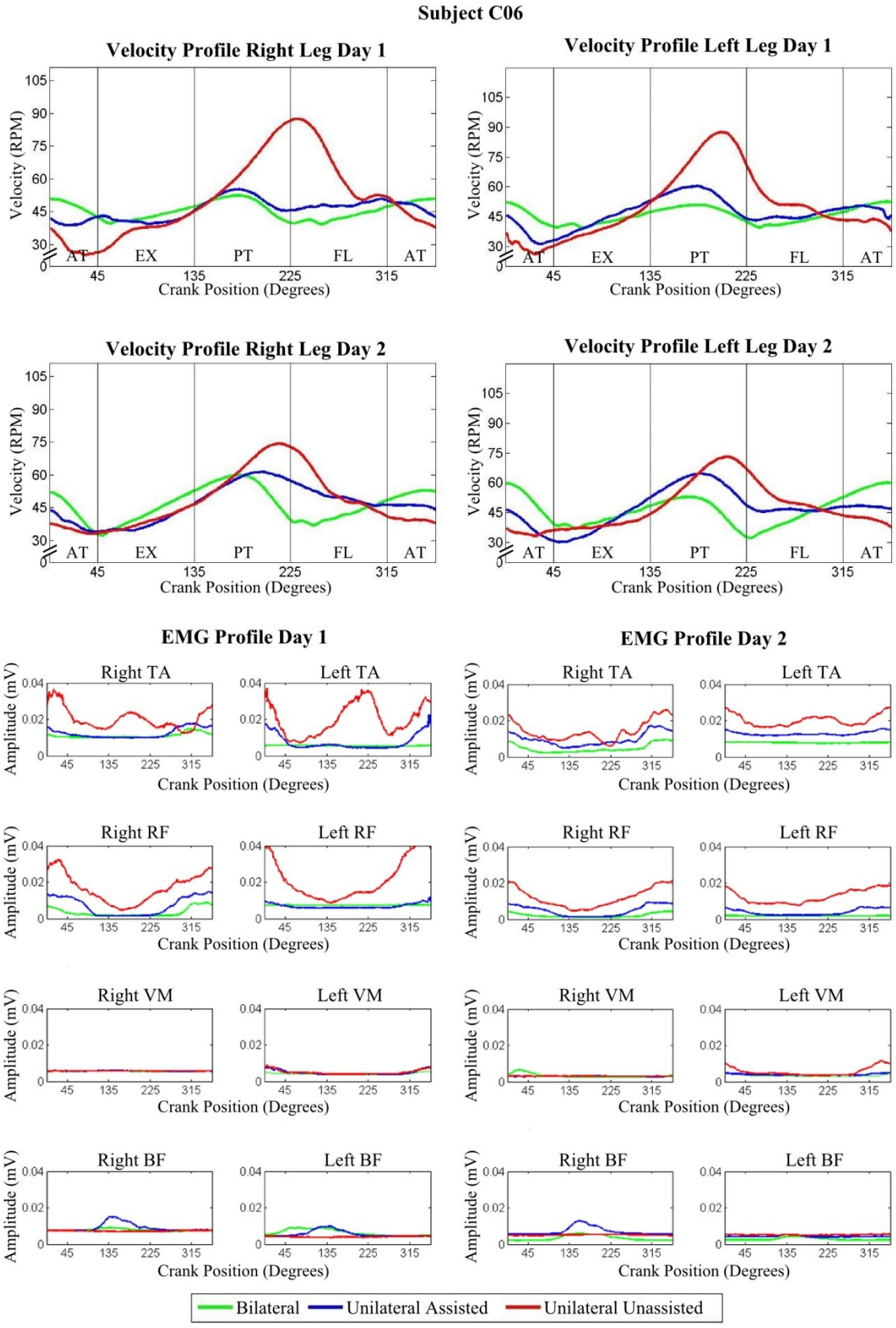
Subject C06
Velocity Profile Right Leg Day 1
Velocity Profile Left Leg Day 1
Velocity Profile Right Leg Day 2
Velocity Profile Left Leg Day 2
Velocity (RPM)
AT
EX
PT
FL
AT
Crank Position (Degrees)
EMG Profile Day 1
EMG Profile Day 2
Right TA
Left TA
Right RF
Left RF
Right VM
Left VM
Right BF
Left BF
Amplitude (mV)
Bilateral
Unilateral Assisted
Unilateral Unassisted

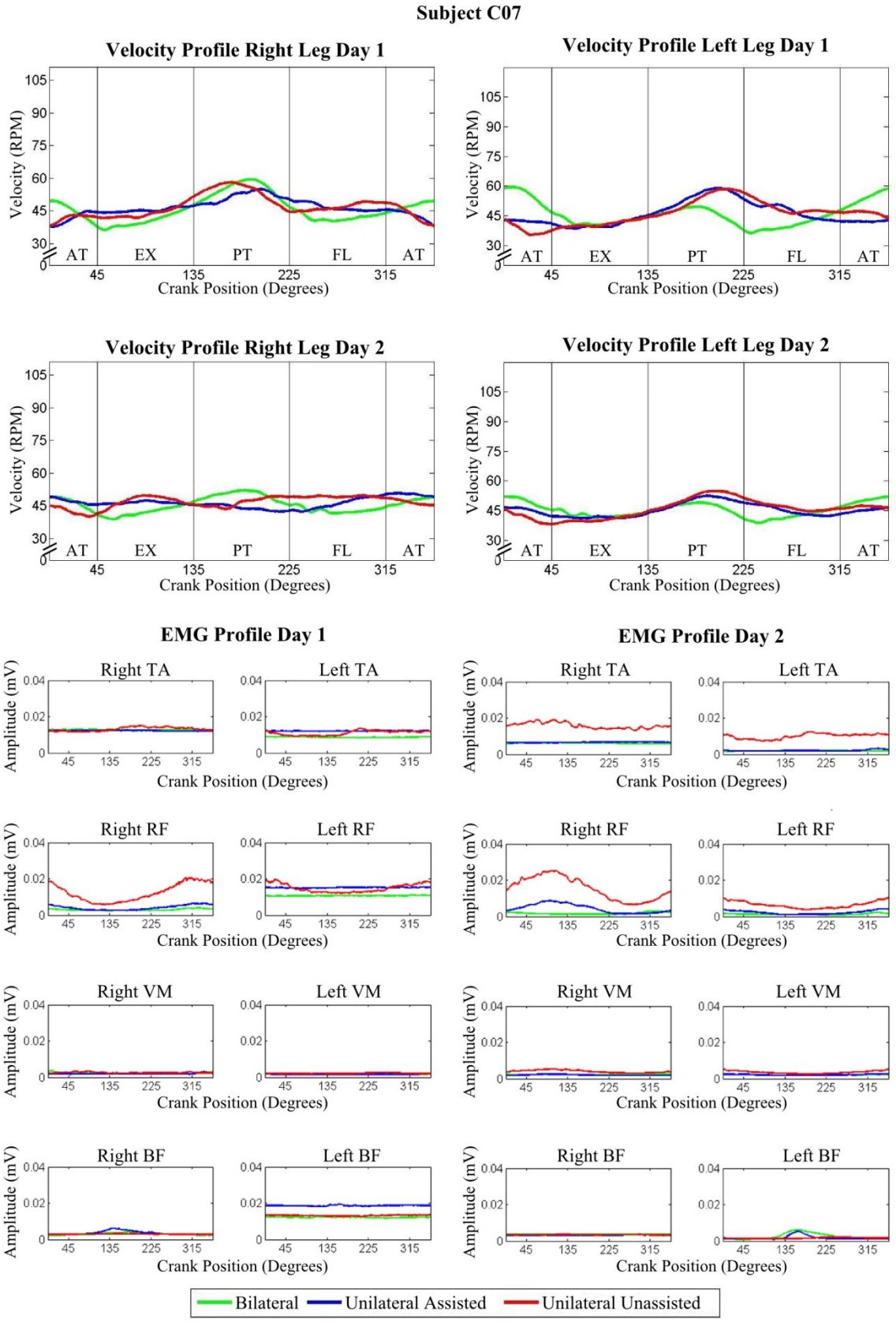
Subject C07
Velocity Profile Right Leg Day 1
Velocity Profile Left Leg Day 1
Velocity Profile Right Leg Day 2
Velocity Profile Left Leg Day 2
Velocity (RPM)
AT
EX
PT
FL
AT
Crank Position (Degrees)
EMG Profile Day 1
EMG Profile Day 2
Right TA
Left TA
Right RF
Left RF
Right VM
Left VM
Right BF
Left BF
Amplitude (mV)
Bilateral
Unilateral Assisted
Unilateral Unassisted

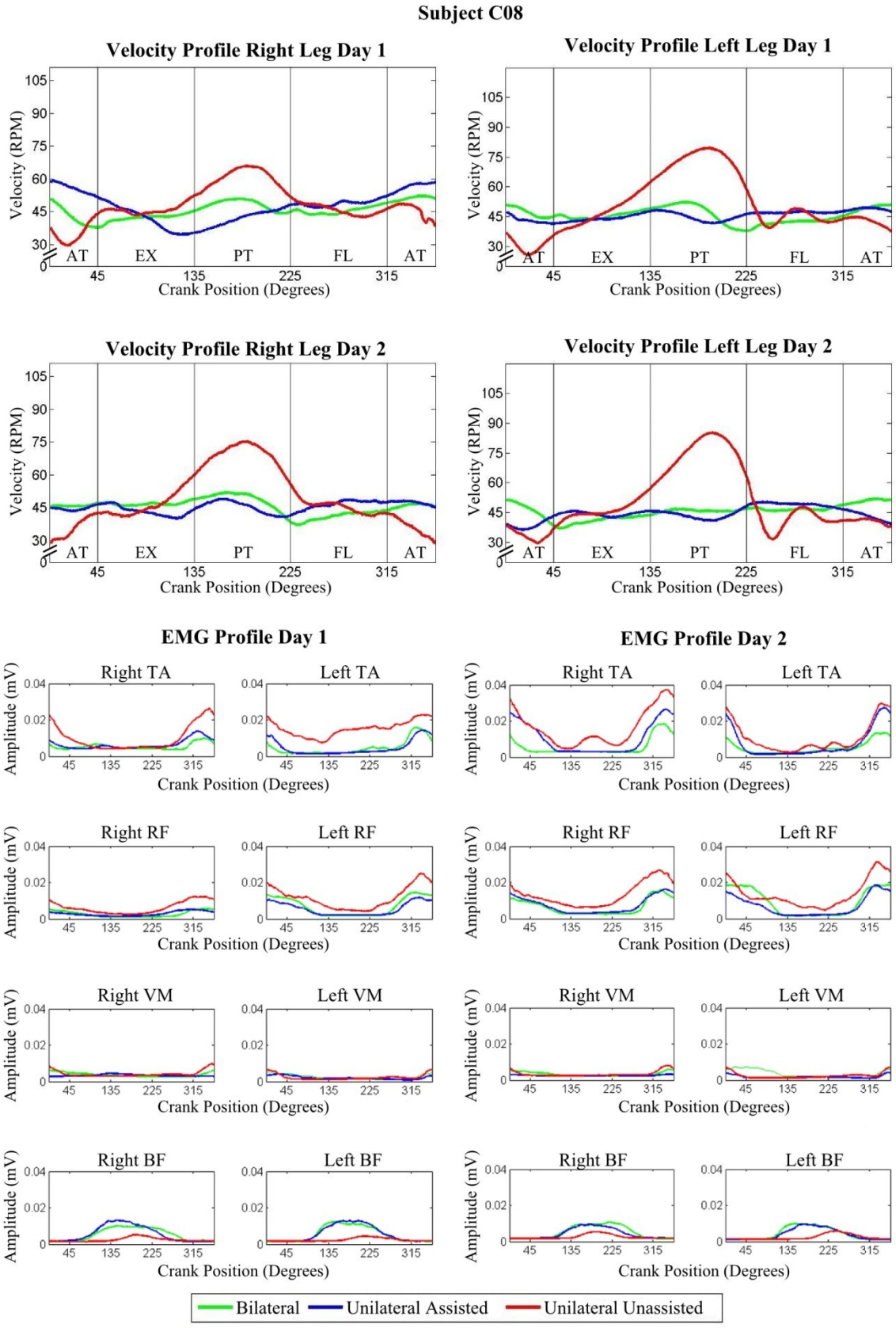
Subject C08
Velocity Profile Right Leg Day 1
Velocity Profile Left Leg Day 1
Velocity Profile Right Leg Day 2
Velocity Profile Left Leg Day 2
Velocity (RPM)
105
90
75
60
45
30
0
AT
EX
PT
FL
AT
45
135
225
315
Crank Position (Degrees)
EMG Profile Day 1
EMG Profile Day 2
Right TA
Left TA
Right RF
Left RF
Right VM
Left VM
Right BF
Left BF
Amplitude (mV)
0.04
0.02
0
Bilateral
Unilateral Assisted
Unilateral Unassisted

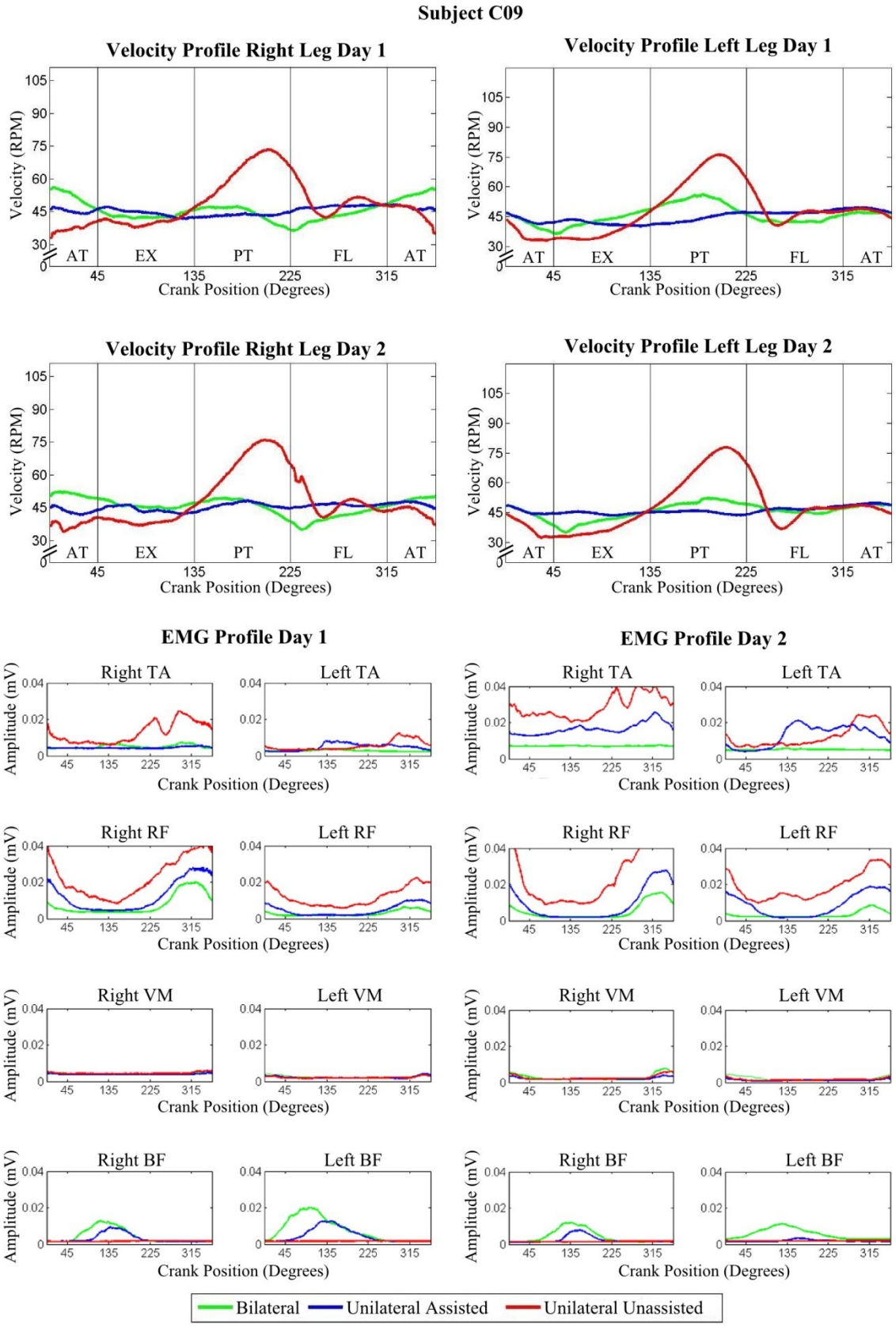
Subject C09
Velocity Profile Right Leg Day 1
Velocity Profile Left Leg Day 1
Velocity Profile Right Leg Day 2
Velocity Profile Left Leg Day 2
Velocity (RPM)
105
90
75
60
45
30
0
AT
EX
PT
FL
AT
45
135
225
315
Crank Position (Degrees)
EMG Profile Day 1
EMG Profile Day 2
Right TA
Left TA
Right RF
Left RF
Right VM
Left VM
Right BF
Left BF
Amplitude (mV)
0.04
0.02
0
Bilateral
Unilateral Assisted
Unilateral Unassisted

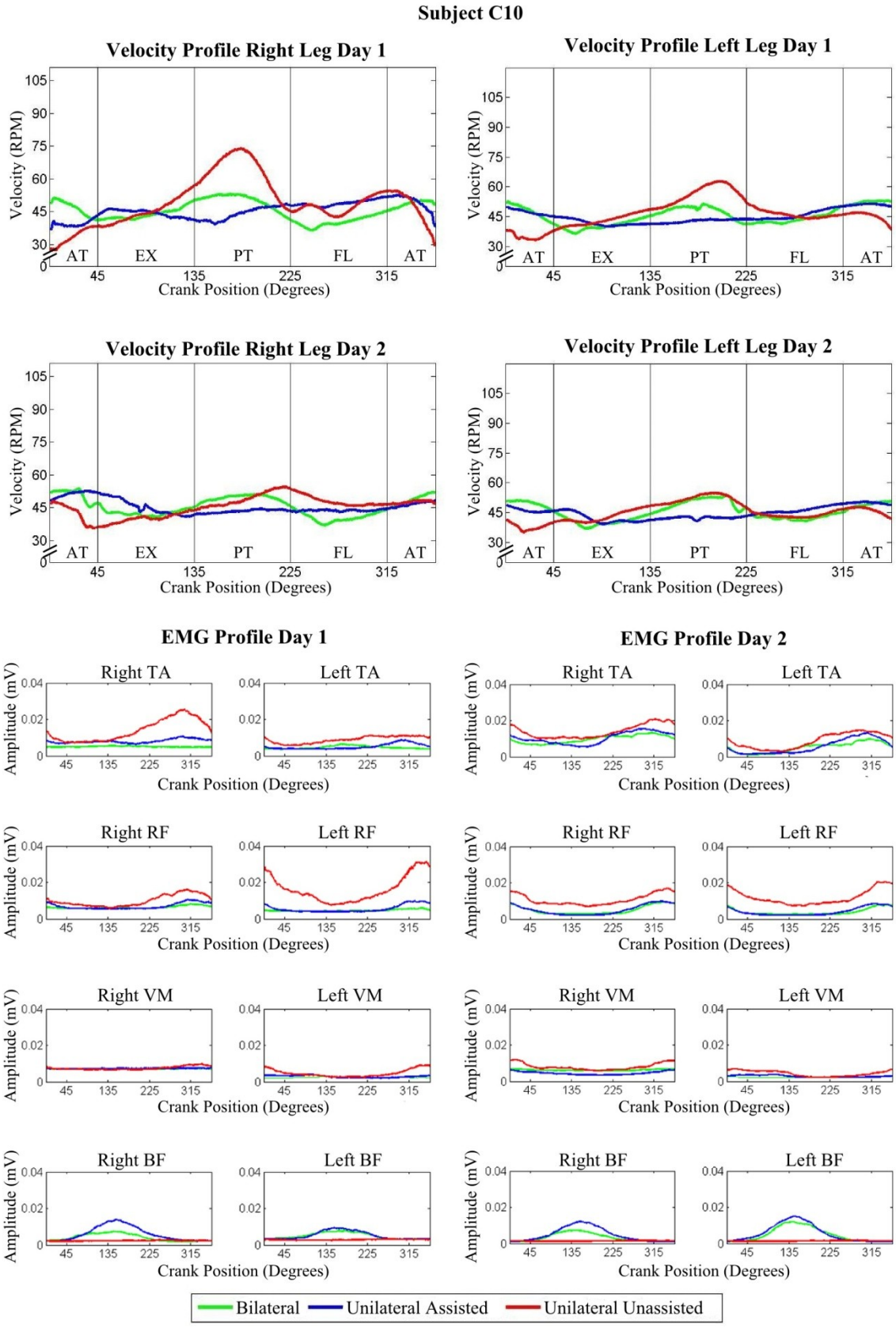
Subject C10
Velocity Profile Right Leg Day 1
Velocity Profile Left Leg Day 1
Velocity Profile Right Leg Day 2
Velocity Profile Left Leg Day 2
Velocity (RPM)
105
90
75
60
45
30
0
AT
EX
PT
FL
AT
45
135
225
315
Crank Position (Degrees)
EMG Profile Day 1
EMG Profile Day 2
Right TA
Left TA
Right RF
Left RF
Right VM
Left VM
Right BF
Left BF
Amplitude (mV)
0.04
0.02
0
Bilateral
Unilateral Assisted
Unilateral Unassisted

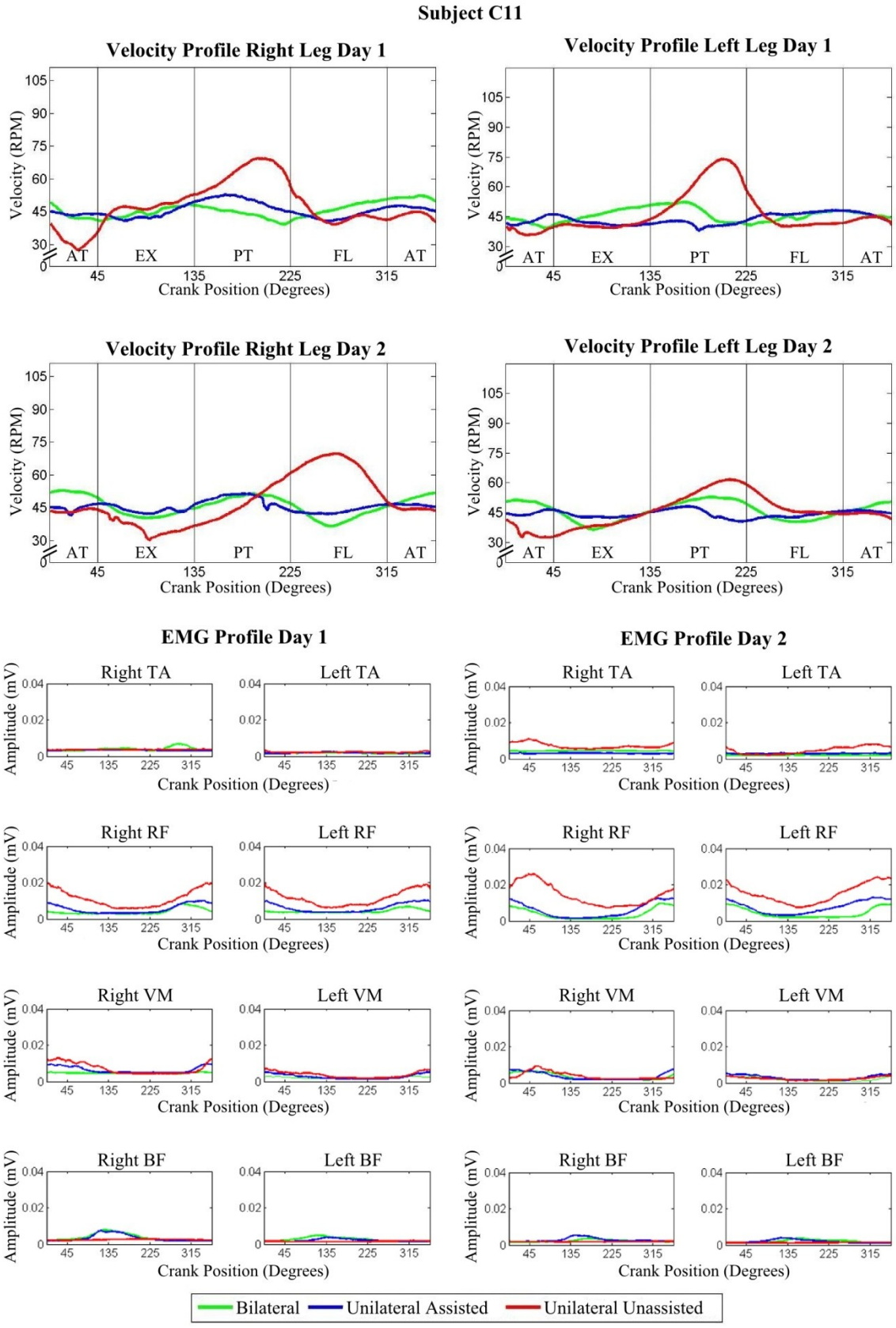
Subject C11
Velocity Profile Right Leg Day 1
Velocity Profile Left Leg Day 1
Velocity Profile Right Leg Day 2
Velocity Profile Left Leg Day 2
Velocity (RPM)
105
90
75
60
45
30
0
AT
EX
PT
FL
AT
45
135
225
315
Crank Position (Degrees)
EMG Profile Day 1
EMG Profile Day 2
Right TA
Left TA
Right RF
Left RF
Right VM
Left VM
Right BF
Left BF
Amplitude (mV)
0.04
0.02
0
Bilateral
Unilateral Assisted
Unilateral Unassisted

APPENDIX D: INDIVIDUAL RESULTS FOR FMRI EXPERIMENT

Subject C01

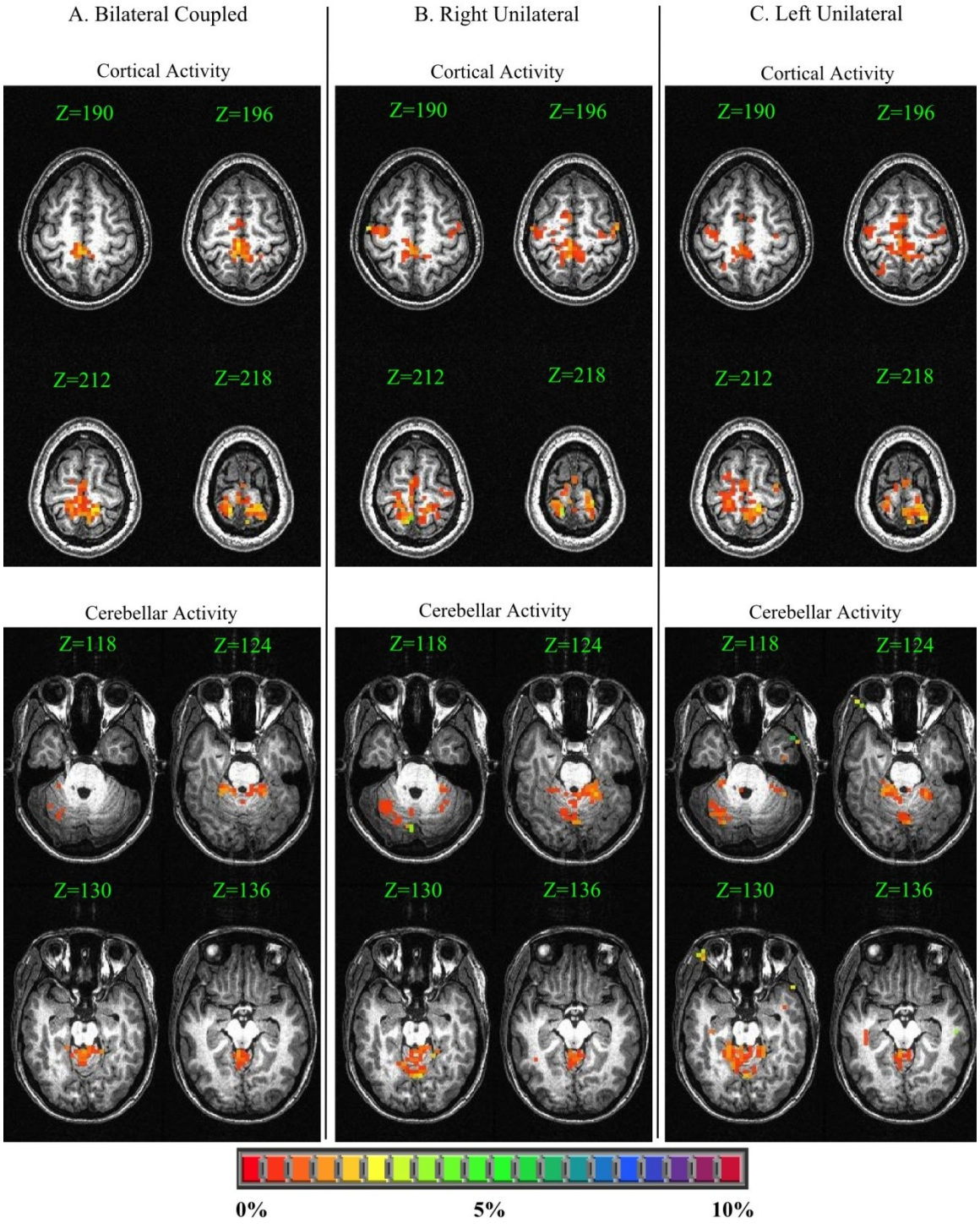

Subject C03

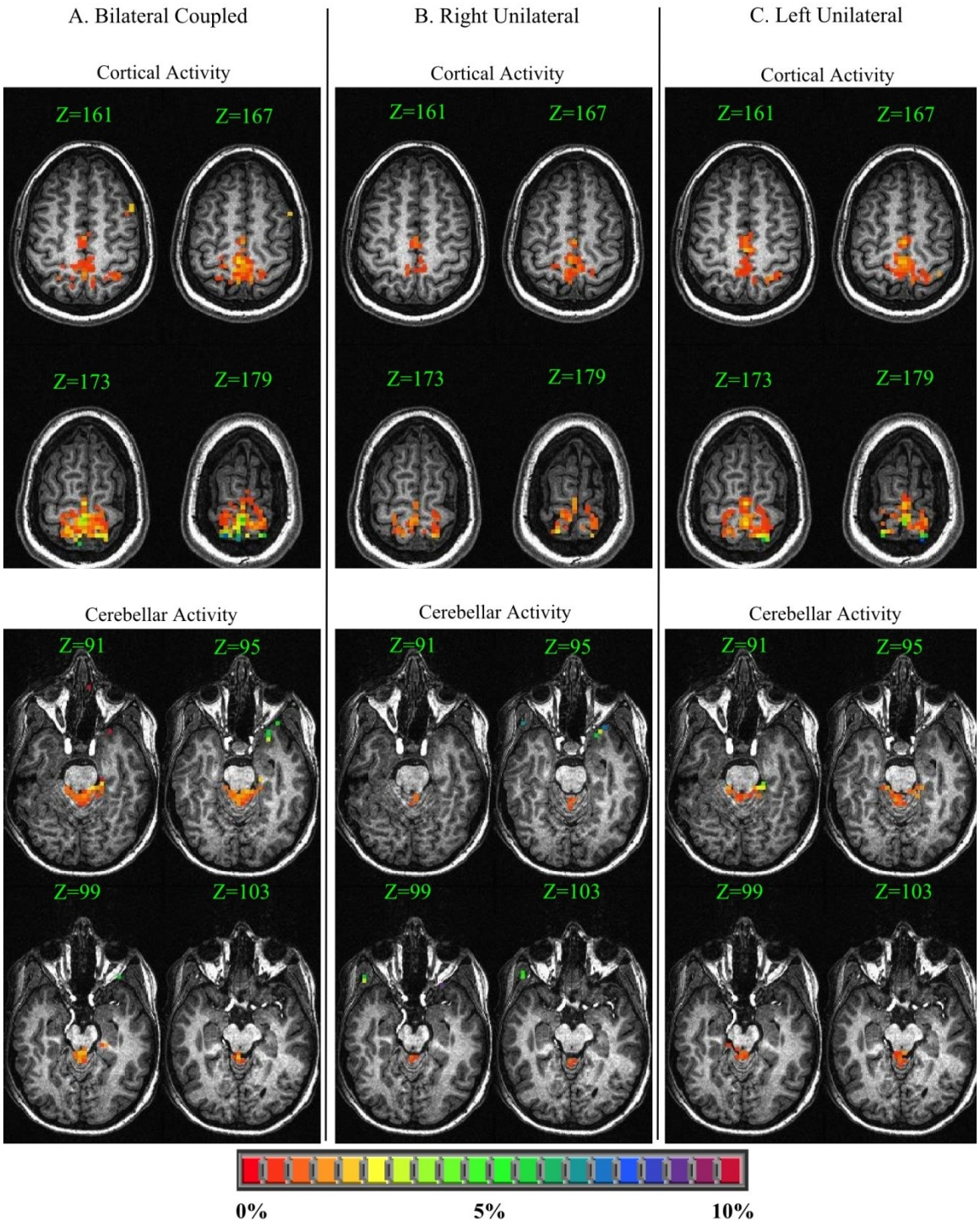
A. Bilateral Coupled
B. Right Unilateral
C. Left Unilateral
Cortical Activity
Cortical Activity
Cortical Activity
Z=161
Z=167
Z=173
Z=179
Z=161
Z=167
Z=173
Z=179
Z=161
Z=167
Z=173
Z=179
Cerebellar Activity
Cerebellar Activity
Cerebellar Activity
Z=91
Z=95
Z=99
Z=103
Z=91
Z=95
Z=99
Z=103
Z=91
Z=95
Z=99
Z=103
0%
5%
10%

Subject C04

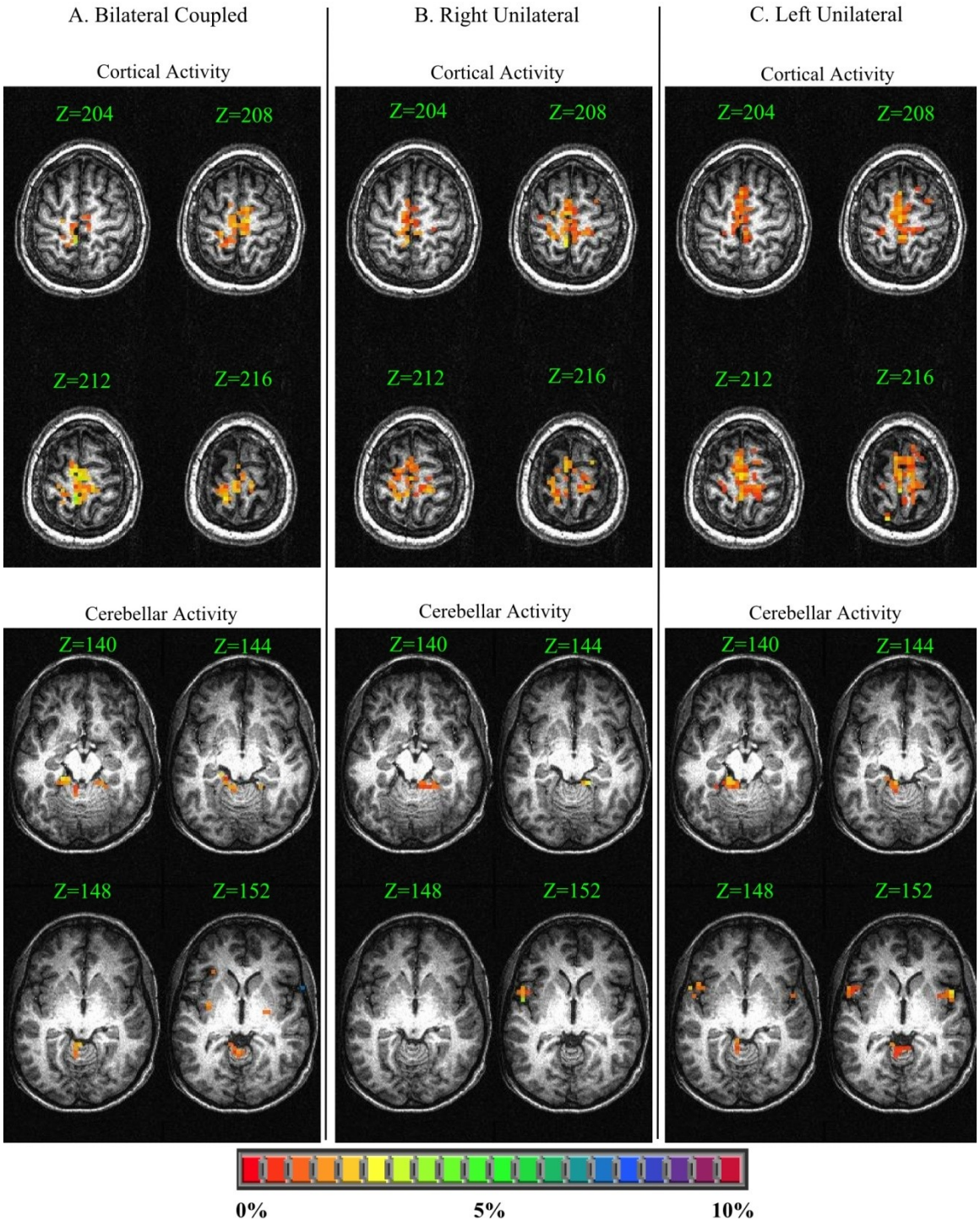
A. Bilateral Coupled
B. Right Unilateral
C. Left Unilateral
Cortical Activity
Cortical Activity
Cortical Activity
Z=204
Z=208
Z=212
Z=216
Z=204
Z=208
Z=212
Z=216
Z=204
Z=208
Z=212
Z=216
Cerebellar Activity
Cerebellar Activity
Cerebellar Activity
Z=140
Z=144
Z=148
Z=152
Z=140
Z=144
Z=148
Z=152
Z=140
Z=144
Z=148
Z=152
0%
5%
10%

Subject C05

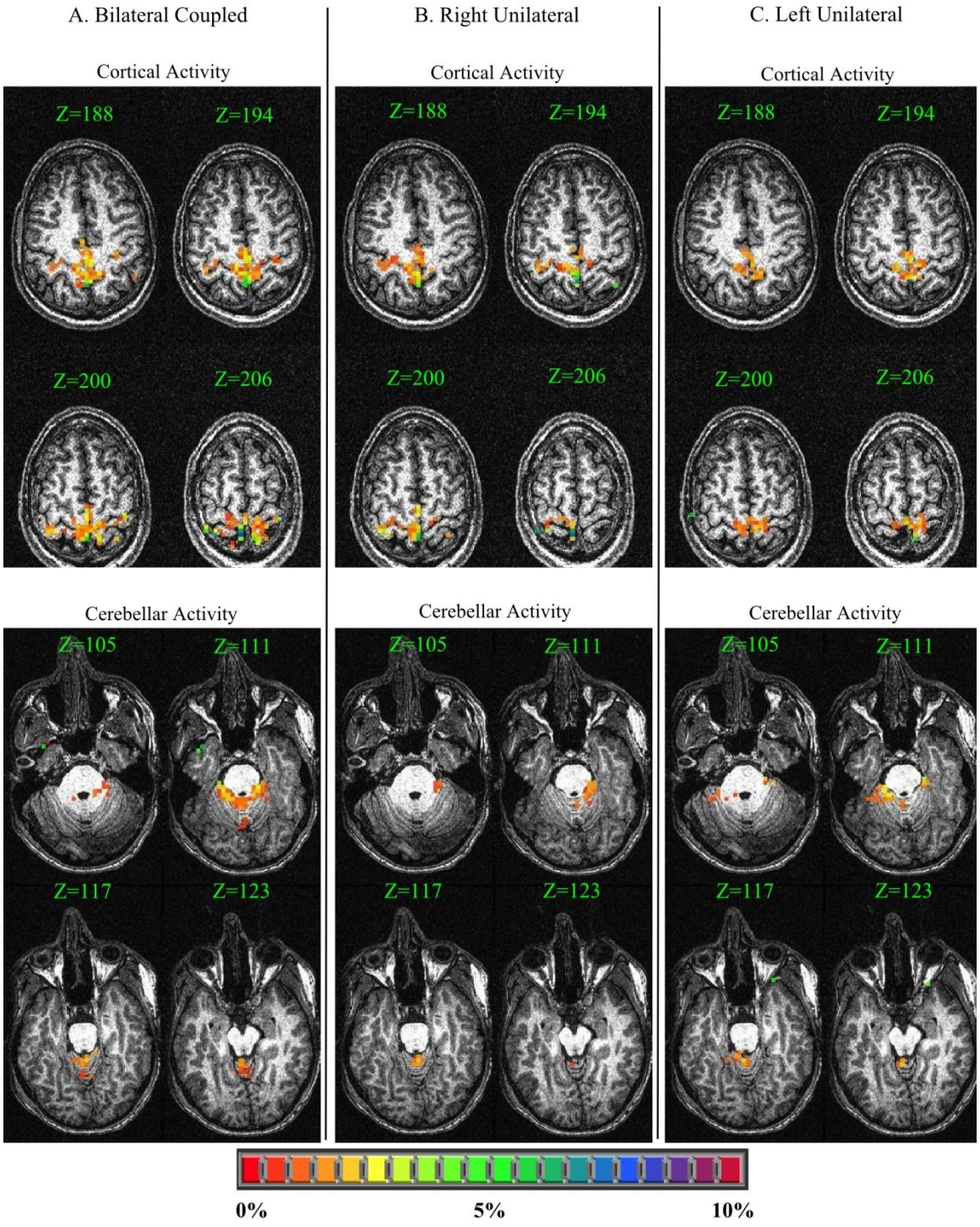
A. Bilateral Coupled
B. Right Unilateral
C. Left Unilateral
Cortical Activity
Cortical Activity
Cortical Activity
Z=188
Z=194
Z=188
Z=194
Z=188
Z=194
Z=200
Z=206
Z=200
Z=206
Z=200
Z=206
Cerebellar Activity
Cerebellar Activity
Cerebellar Activity
Z=105
Z=111
Z=105
Z=111
Z=105
Z=111
Z=117
Z=123
Z=117
Z=123
Z=117
Z=123
0%
5%
10%

Subject C06

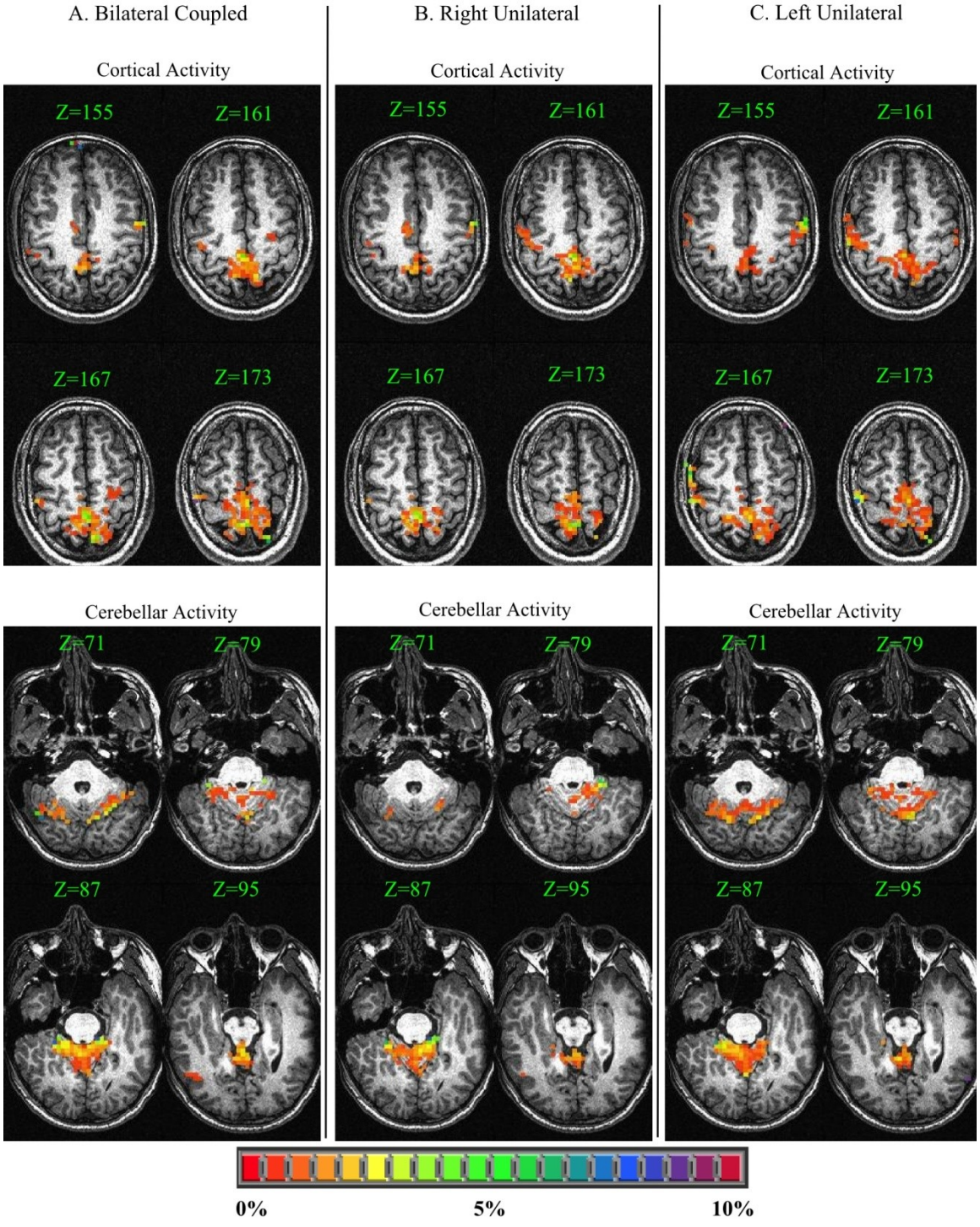
A. Bilateral Coupled
B. Right Unilateral
C. Left Unilateral
Cortical Activity
Cortical Activity
Cortical Activity
Z=155
Z=161
Z=167
Z=173
Z=155
Z=161
Z=167
Z=173
Z=155
Z=161
Z=167
Z=173
Cerebellar Activity
Cerebellar Activity
Cerebellar Activity
Z=71
Z=79
Z=87
Z=95
Z=71
Z=79
Z=87
Z=95
Z=71
Z=79
Z=87
Z=95
0%
5%
10%

Subject C07

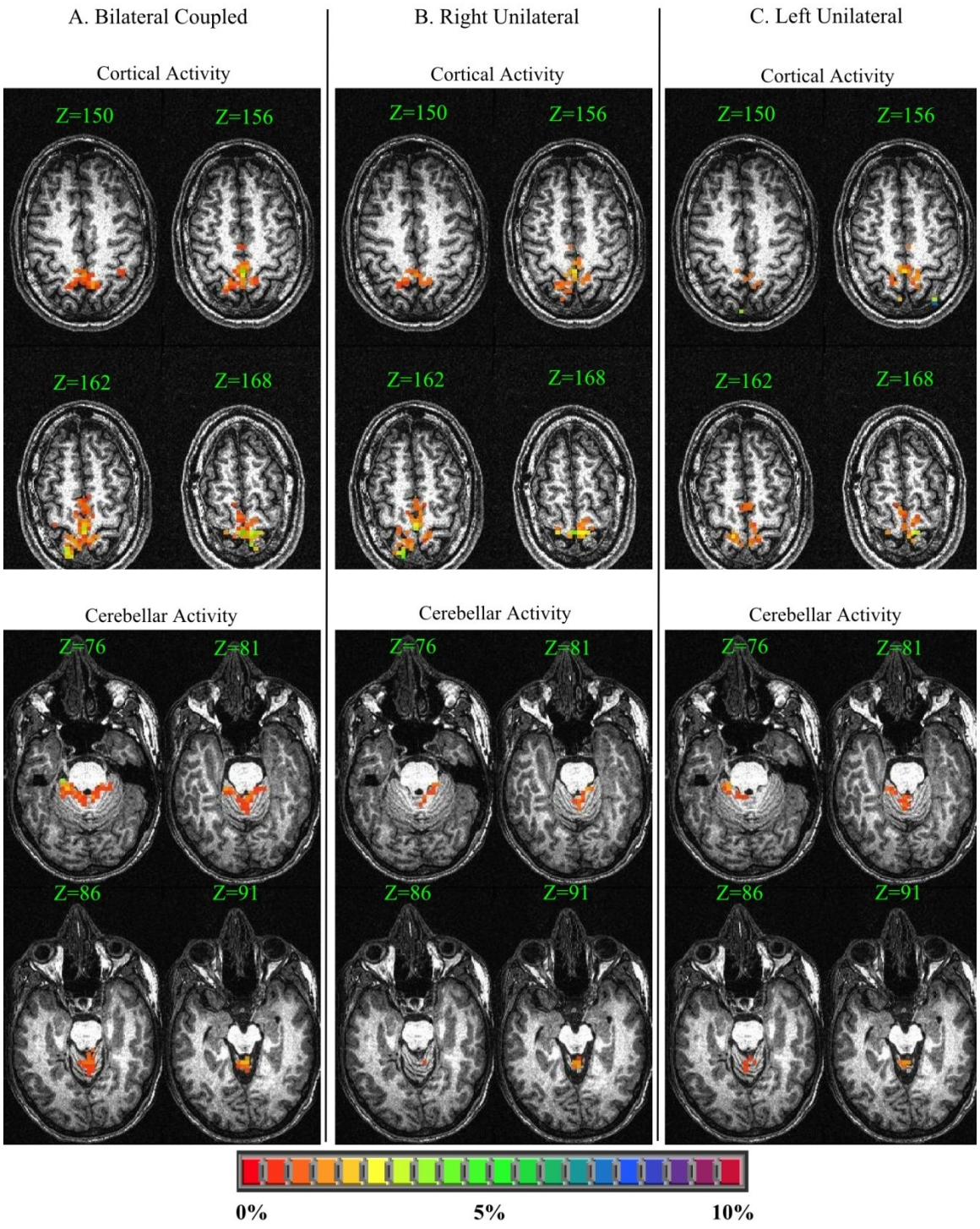
A. Bilateral Coupled
B. Right Unilateral
C. Left Unilateral
Cortical Activity
Cortical Activity
Cortical Activity
Z=150
Z=156
Z=162
Z=168
Cerebellar Activity
Cerebellar Activity
Cerebellar Activity
Z=76
Z=81
Z=86
Z=91
0%
5%
10%

Subject C08

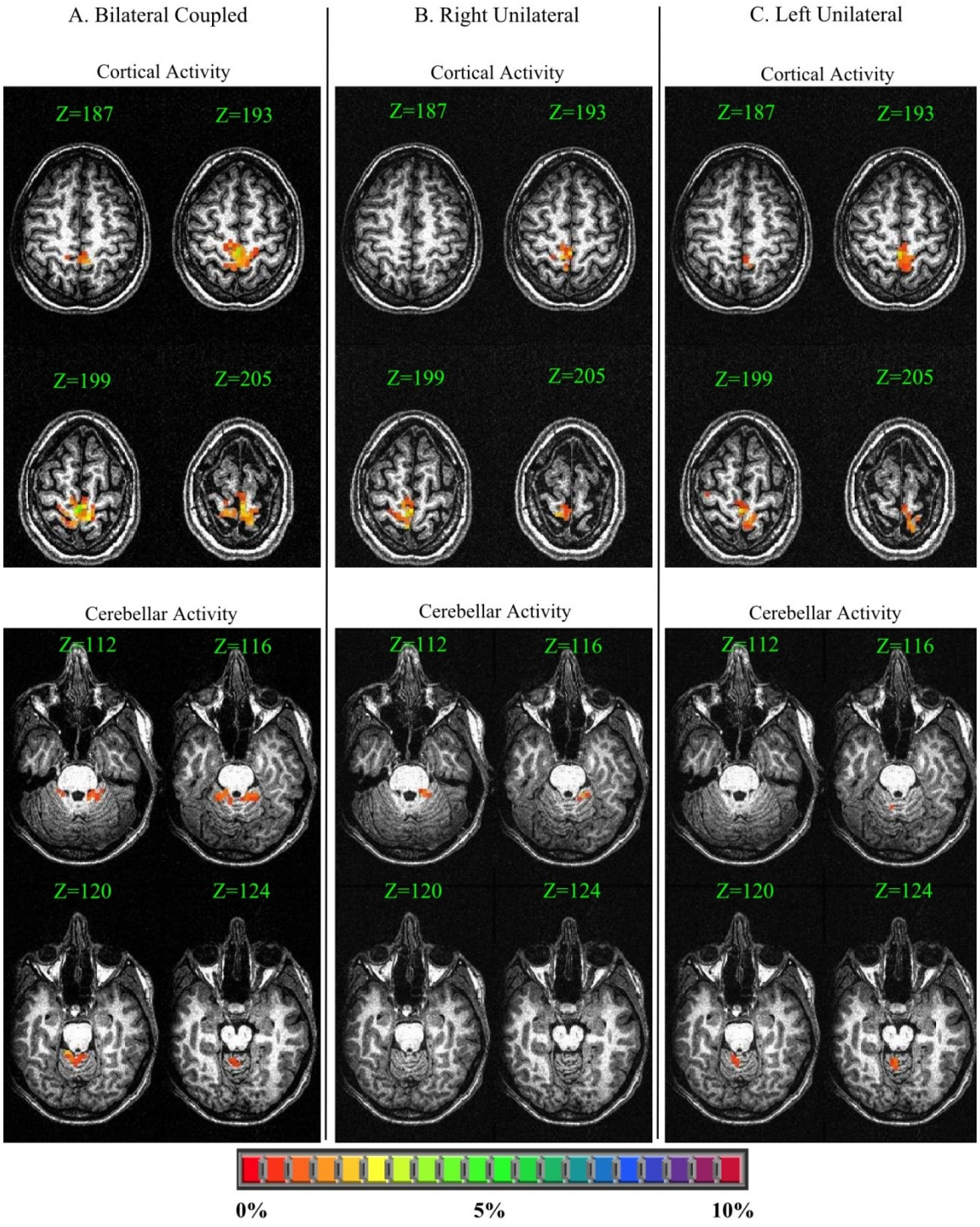
A. Bilateral Coupled
B. Right Unilateral
C. Left Unilateral
Cortical Activity
Cortical Activity
Cortical Activity
Z=187
Z=193
Z=199
Z=205
Z=187
Z=193
Z=199
Z=205
Z=187
Z=193
Z=199
Z=205
Cerebellar Activity
Cerebellar Activity
Cerebellar Activity
Z=112
Z=116
Z=120
Z=124
Z=112
Z=116
Z=120
Z=124
Z=112
Z=116
Z=120
Z=124
0%
5%
10%

Subject C10

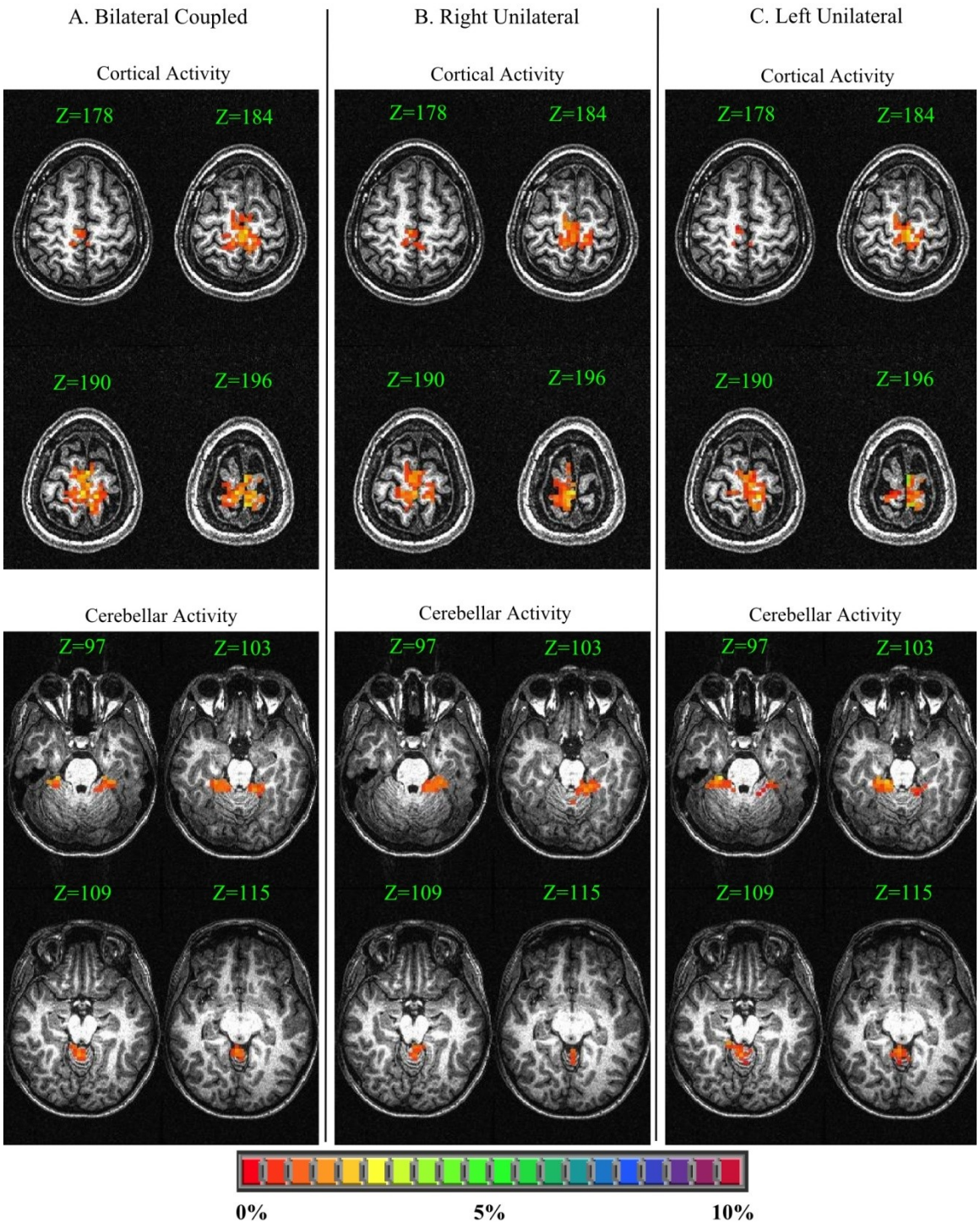
A. Bilateral Coupled
B. Right Unilateral
C. Left Unilateral
Cortical Activity
Cortical Activity
Cortical Activity
Z=178
Z=184
Z=190
Z=196
Cerebellar Activity
Cerebellar Activity
Cerebellar Activity
Z=97
Z=103
Z=109
Z=115
0%
5%
10%

Subject C11

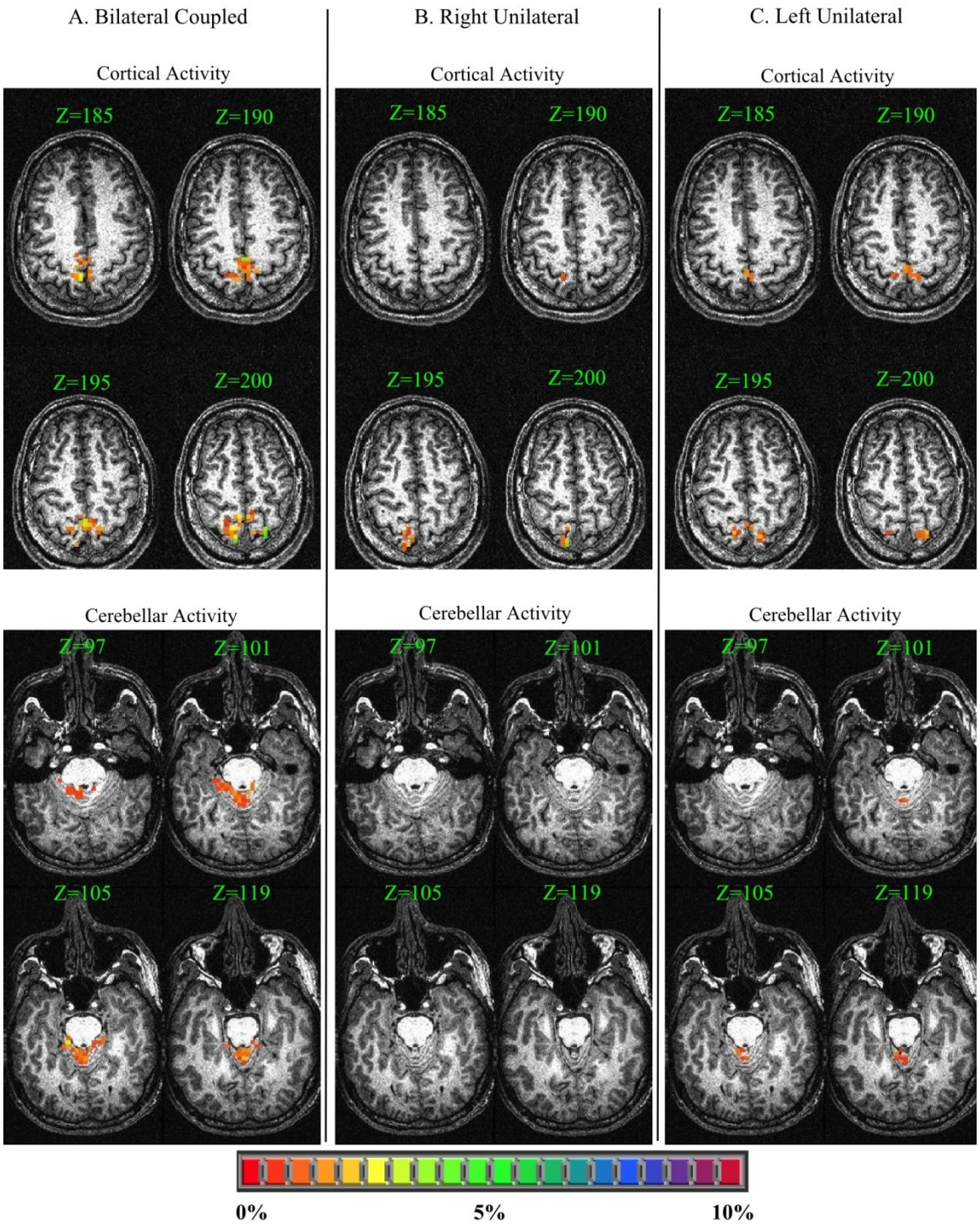
A. Bilateral Coupled
B. Right Unilateral
C. Left Unilateral
Cortical Activity
Cortical Activity
Cortical Activity
Z=185
Z=190
Z=195
Z=200
Cerebellar Activity
Cerebellar Activity
Cerebellar Activity
Z=97
Z=101
Z=105
Z=119
0%
5%
10%

APPENDIX E: PROGRAM CODE

MATLAB Code for Validation Results

Program	Function
ArandB_PedalRate.m	Calculates the pedaling rate after each experimental run
velbinnerA.m	Creates velocity profiles by binning the data – right encoder
velbinnerAl.m	Creates velocity profiles by binning the data – left encoder
velsmoother.m	Data smoothing function
PedalRate	Calculate pedal rate for velocity conversion
meanVolt.m	Calculate voltage for velocity conversion
ArandB_quadrants.m	Calculates quadrant data for velocity
EMGbinnerA.m	Creates EMG profiles by binning the data – right encoder
EMGbinnerAl.m	Creates EMG profiles by binning the data – left encoder
function_EMG.m	Processes the EMG data
EMGmeasures.m	Calculate peak and sum EMG measures

ArandB_PedalRate.m

```
[file,path_file] = uigetfile('*.txt');
input=importdata([path_file file],'\t');

figure
set(gcf,'position',[100 100 1800 900]);

% For oringal txt data
wave = input.data(:,[1 2]);

CPS = [];

%Bad point elimination
len = length(wave(:,2));
diffs = abs(wave(2:len,2)-wave(1:len-1,2));
mwave = diffs>.05 & diffs<9.5;    %np
%mwave = diffs>.05 & diffs<2;    %sc
locs = find(mwave);
locs2 = locs(2:2:end);
wave(locs,2) = 0;

% Determine when new wave revolutions occur. Find minimums to identify...
% individual cycles.
newcycle=[];
    for i=1:size(wave(:,2),1)-1
        if (abs(wave(i,2)-wave(i+1,2)))>.1
            newcycle=[newcycle;i+1];
        end
    end
```

```
num_revs=(length(newcycle)-1);

% Plot wave angle with cycle identification - just a check
set(gcf,'position',[100 150 1800 900]);
title ('wave Angle with Cycle Identification');
hold on;
plot (wave(:,2));
plot(newcycle,wave(newcycle,2),'ro');

% Do these data points accurately represent cycles.
qstring = 'Are the chosen points acceptable?';
reply = questdlg(qstring,'Verify points','yes','no','no');

if strcmp(reply,'no')==1;
   error('Fix the problem, try again')
else
   close all
end

CPStemp = [];
CPStemp(:,1) = 1./(wave(newcycle(2:num_revs+1),1)-wave(newcycle(1:num_revs)));

CPS = [CPS ;CPStemp];

for i = 2:length(newcycle)
   rates(i-1) = wave(newcycle(i),1) - wave(newcycle(i-1),1);
end

rates = 1./rates.*60;

rates(rates<20) = [];
rates(rates>100) = [];

mean_rate = mean(rates)
std_rate = std(rates)
```

velbinnerA.m

```
function vel_bins = velbinnerA(path_file, file)

%Set EMG degree bin size
bin_size = 1;

% Load data file.
%[file,path_file] = uigetfile('*.txt');
input=importdata([path_file file],'\t');

% For oringal txt data
wave = input.data(:,[1 2]);

%Bad point elimination
len = length(wave(:,2));
```

```
diffs = abs(wave(2:len,2)-wave(1:len-1,2));
mwave = diffs>.02 & diffs<9.5;    %np
%mwave = diffs>.05 & diffs<2;    %sc
locs = find(mwave);
locs2 = locs(2:2:end);
wave(locs,2) = 0;

% Determine when new wave revolutions occur. Find minimums to identify...
% individual cycles.
nc=[];
      for i=1:size(wave(:,2),1)-1
          if (abs(wave(i,2)-wave(i+1,2)))>.1
             nc=[nc;i+1];
          end
      end

%if recorded on left, adjust
lcheck = wave(nc(1)+50,2) - wave(nc(1)+100,2);
if lcheck > 0
   wave(:,2) = abs(wave(:,2)-max(wave(:,2)));
else
end

%%
%binning

deg = wave(:,2);
deg = deg+min(deg);
deg = deg/max(deg)*360;

tempvel = input.data(:,3);

data_length=length(tempvel);
r = 10;
n=1;
for i = r+1:data_length-r
   vel_temp(n) = mean(tempvel(i-r:i+r));
   n=n+1;
end
tempvel = vel_temp';
deg(1:r-1) = [];
deg(length(deg)-r:length(deg)) =[];

deg = round(deg);

n = 1;
for d = 1:bin_size:360
   velmask = deg==d;
   bin = tempvel.*velmask;
   vel_bins(n) = sum(bin)/(length(find(bin)));
   n=n+1;
end

if lcheck > 0
```

```
   vel_bins = circshift(vel_bins,[1 180]);
else
end

end
```

velbinnerAl.m

```
function vel_bins = velbinnerA(path_file, file)

%Set EMG degree bin size
bin_size = 1;

% Load data file.
input=importdata([path_file file],'\t');

% For oringal txt data
wave = input.data(:,[1 2]);

%Bad point elimination
len = length(wave(:,2));
diffs = abs(wave(2:len,2)-wave(1:len-1,2));
mwave = diffs>.02 & diffs<9.5;    %np
%mwave = diffs>.05 & diffs<2;    %sc
locs = find(mwave);
locs2 = locs(2:2:end);
wave(locs,2) = 0;

% Determine when new wave revolutions occur. Find minimums to identify...
% individual cycles.
nc=[];
      for i=1:size(wave(:,2),1)-1
          if (abs(wave(i,2)-wave(i+1,2)))>.1
             nc=[nc;i+1];
          end
      end

%if recorded on left, adjust
lcheck = wave(nc(1)+50,2) - wave(nc(1)+100,2);
if lcheck > 0
   wave(:,2) = abs(wave(:,2)-max(wave(:,2)));
else
end

%%
%createfigure_SplitCrank_val(wave,newcycle,file)
%binning

deg = wave(:,2);
deg = deg+min(deg);
deg = deg/max(deg)*360;

tempvel = input.data(:,3);
```

```
data_length=length(tempvel);
r = 10;
n=1;
for i = r+1:data_length-r
   vel_temp(n) = mean(tempvel(i-r:i+r));
   n=n+1;
end
tempvel = vel_temp';
deg(1:r-1) = [];
deg(length(deg)-r:length(deg)) =[];

deg = round(deg);

n = 1;
for d = 1:bin_size:360
   velmask = deg==d;
   bin = tempvel.*velmask;
   vel_bins(n) = sum(bin)/(length(find(bin)));
   n=n+1;
end

if lcheck > 0
   vel_bins = circshift(vel_bins,[1 180]);
else
end

end
```

velsmoother.m

```
function vel_bins_smooth = velsmoother(vel_bins)

r = 2;
for i = 1:360
   l = i-r;
   u = i+r;
   if l<=0
      l=l+360;
      vel_bins_smooth(i) = mean([vel_bins(1:u) vel_bins(l:360)]);

   elseif u>360
      u=u-360;
      vel_bins_smooth(i) = mean([vel_bins(1:u) vel_bins(l:360)]);
   else
      vel_bins_smooth(i) = mean(vel_bins(l:u));
   end

end

end
```

PedalRate.m

```
function mean_rate = PedalRate(path_file, file)

input=importdata([path_file file],'\t');

wave = input.data(:,[1 2]);

%Bad point elimination

len = length(wave(:,2));
diffs = abs(wave(2:len,2)-wave(1:len-1,2));
mwave = diffs>.05 & diffs<9.5;
locs = find(mwave);
locs2 = locs(2:2:end);
wave(locs,2) = 0;

% Determine when new wave revolutions occur. Find minimums to identify...
% individual cycles.

newcycle=[];
      for i=1:size(wave(:,2),1)-1
          if (abs(wave(i,2)-wave(i+1,2)))>.1
             newcycle=[newcycle;i+1];
          end
      end

 num_revs=(length(newcycle)-1);

 % Plot wave angle with cycle identification - just a check

for i = 2:length(newcycle)
   rates(i-1) = wave(newcycle(i),1) - wave(newcycle(i-1),1);
end

rates = 1./rates.*60;

rates(rates<20) = [];
rates(rates>100) = [];

mean_rate = mean(rates);
%std_rate = std(rates)
End
```

meanVolt.m

```
function meanvolt = meanVolt(path_file, file)

%Set EMG degree bin size
bin_size = 1;

% Load data file.
%[file,path_file] = uigetfile('*.txt');
```

```
input=importdata([path_file file],'\t');

% For oringal txt data
wave = input.data(:,[1 2]);

%Bad point elimination
len = length(wave(:,2));
diffs = abs(wave(2:len,2)-wave(1:len-1,2));
mwave = diffs>.02 & diffs<9.5;    %np
%mwave = diffs>.05 & diffs<2;    %sc
locs = find(mwave);
locs2 = locs(2:2:end);
wave(locs,2) = 0;

% Determine when new wave revolutions occur. Find minimums to identify...
% individual cycles.
nc=[];
      for i=1:size(wave(:,2),1)-1
          if (abs(wave(i,2)-wave(i+1,2)))>.1
              nc=[nc;i+1];
          end
      end

%if recorded on left, adjust
lcheck = wave(nc(1)+50,2) - wave(nc(1)+100,2);
if lcheck > 0
   wave(:,2) = abs(wave(:,2)-max(wave(:,2)));
else
end

%%
%Mean voltage from first to last new-cycle points
vel = input.data(:,3);
vel = vel(nc(1):nc(length(nc)),:);
meanvolt = mean(vel);

end
```

ArandB_quadrants.m

```
%%
%Sum/mean/max of quadrants Velocity
clear

s = 'max'; %Change to sum/mean/max

for k = 1:9
load(sprintf('C0%d_vel_adj_day2.mat', k));
end
load('C10_vel_adj_day2.mat');
load('C11_vel_adj_day2.mat');
```

```
%Bilat
for k = 1:9
    eval(sprintf('Q_b(k,1) = %s(C0%d_b([315:360 1:45]))',s,k));
    eval(sprintf('Q_b(k,2) = %s(C0%d_b(45:135))',s,k));
    eval(sprintf('Q_b(k,3) = %s(C0%d_b(135:225))',s,k));
    eval(sprintf('Q_b(k,4) = %s(C0%d_b(225:315))',s,k));
end
for k=10:11;
    eval(sprintf('Q_b(k,1) = %s(C%d_b([315:360 1:45]))',s,k));
    eval(sprintf('Q_b(k,2) = %s(C%d_b(45:135))',s,k));
    eval(sprintf('Q_b(k,3) = %s(C%d_b(135:225))',s,k));
    eval(sprintf('Q_b(k,4) = %s(C%d_b(225:315))',s,k));
end

%Right
for k = 1:9
    eval(sprintf('Q_r(k,1) = %s(C0%d_r([315:360 1:45]))',s,k));
    eval(sprintf('Q_r(k,2) = %s(C0%d_r(45:135))',s,k));
    eval(sprintf('Q_r(k,3) = %s(C0%d_r(135:225))',s,k));
    eval(sprintf('Q_r(k,4) = %s(C0%d_r(225:315))',s,k));
end
for k=10:11;
    eval(sprintf('Q_r(k,1) = %s(C%d_r([315:360 1:45]))',s,k));
    eval(sprintf('Q_r(k,2) = %s(C%d_r(45:135))',s,k));
    eval(sprintf('Q_r(k,3) = %s(C%d_r(135:225))',s,k));
    eval(sprintf('Q_r(k,4) = %s(C%d_r(225:315))',s,k));
end

%Left
for k = 1:9
    eval(sprintf('Q_l(k,1) = %s(C0%d_l([315:360 1:45]))',s,k));
    eval(sprintf('Q_l(k,2) = %s(C0%d_l(45:135))',s,k));
    eval(sprintf('Q_l(k,3) = %s(C0%d_l(135:225))',s,k));
    eval(sprintf('Q_l(k,4) = %s(C0%d_l(225:315))',s,k));
end
for k=10:11;
    eval(sprintf('Q_l(k,1) = %s(C%d_l([315:360 1:45]))',s,k));
    eval(sprintf('Q_l(k,2) = %s(C%d_l(45:135))',s,k));
    eval(sprintf('Q_l(k,3) = %s(C%d_l(135:225))',s,k));
    eval(sprintf('Q_l(k,4) = %s(C%d_l(225:315))',s,k));
end

%Right Unassisted
for k = 1:9
    eval(sprintf('Q_ru(k,1) = %s(C0%d_ru([315:360 1:45]))',s,k));
    eval(sprintf('Q_ru(k,2) = %s(C0%d_ru(45:135))',s,k));
    eval(sprintf('Q_ru(k,3) = %s(C0%d_ru(135:225))',s,k));
    eval(sprintf('Q_ru(k,4) = %s(C0%d_ru(225:315))',s,k));
end
for k=10:11;
    eval(sprintf('Q_ru(k,1) = %s(C%d_ru([315:360 1:45]))',s,k));
    eval(sprintf('Q_ru(k,2) = %s(C%d_ru(45:135))',s,k));
    eval(sprintf('Q_ru(k,3) = %s(C%d_ru(135:225))',s,k));
    eval(sprintf('Q_ru(k,4) = %s(C%d_ru(225:315))',s,k));
end
```

```
%Left Unassisted
for k = 1:9
   eval(sprintf('Q_lu(k,1) = %s(C0%d_lu([315:360 1:45]))',s,k));
   eval(sprintf('Q_lu(k,2) = %s(C0%d_lu(45:135))',s,k));
   eval(sprintf('Q_lu(k,3) = %s(C0%d_lu(135:225))',s,k));
   eval(sprintf('Q_lu(k,4) = %s(C0%d_lu(225:315))',s,k));
end
for k=10:11;
   eval(sprintf('Q_lu(k,1) = %s(C%d_lu([315:360 1:45]))',s,k));
   eval(sprintf('Q_lu(k,2) = %s(C%d_lu(45:135))',s,k));
   eval(sprintf('Q_lu(k,3) = %s(C%d_lu(135:225))',s,k));
   eval(sprintf('Q_lu(k,4) = %s(C%d_lu(225:315))',s,k));
end

%Bilat Left
for k = 1:9
   eval(sprintf('Q_bl(k,3) = %s(C0%d_b([315:360 1:45]))',s,k));
   eval(sprintf('Q_bl(k,4) = %s(C0%d_b(45:135))',s,k));
   eval(sprintf('Q_bl(k,1) = %s(C0%d_b(135:225))',s,k));
   eval(sprintf('Q_bl(k,2) = %s(C0%d_b(225:315))',s,k));
end
for k=10:11;
   eval(sprintf('Q_bl(k,3) = %s(C%d_b([315:360 1:45]))',s,k));
   eval(sprintf('Q_bl(k,4) = %s(C%d_b(45:135))',s,k));
   eval(sprintf('Q_bl(k,1) = %s(C%d_b(135:225))',s,k));
   eval(sprintf('Q_bl(k,2) = %s(C%d_b(225:315))',s,k));
end

Q1 = [Q_b(:,1),Q_r(:,1),Q_ru(:,1),Q_bl(:,1),Q_l(:,1),Q_lu(:,1)];
Q2 = [Q_b(:,2),Q_r(:,2),Q_ru(:,2),Q_bl(:,2),Q_l(:,2),Q_lu(:,2)];
Q3 = [Q_b(:,3),Q_r(:,3),Q_ru(:,3),Q_bl(:,3),Q_l(:,3),Q_lu(:,3)];
Q4 = [Q_b(:,4),Q_r(:,4),Q_ru(:,4),Q_bl(:,4),Q_l(:,4),Q_lu(:,4)];
```

EMGbinnerA.m

```
function emg_bins = EMGbinnerA(path_file, file)
%Set EMG degree bin size
bin_size = 1;

% Load data file.

%[file,path_file] = uigetfile('*.txt');
input=importdata([path_file file],'\t');

% For oringal txt data
wave = input.data(:,[1 2]);

%Bad point elimination

len = length(wave(:,2));
diffs = abs(wave(2:len,2)-wave(1:len-1,2));
mwave = diffs>.02 & diffs<9;
```

```
locs = find(mwave);
locs2 = locs(2:2:end);
wave(locs,2) = 0;

% Determine when new wave revolutions occur. Find minimums to identify...
% individual cycles.

nc=[];
      for i=1:size(wave(:,2),1)-1
          if (abs(wave(i,2)-wave(i+1,2)))>.1
             nc=[nc;i+1];
          end
      end

 num_revs=(length(nc)-1);

%if recorded on left, adjust
lcheck = wave(nc(1)+50,2) - wave(nc(1)+100,2);
if lcheck > 0
   wave(:,2) = abs(wave(:,2)-max(wave(:,2)));
else
end

%%
% Function to process EMG data

emg_channel_names = ['R_ta', 'R_vm', 'R_rf', 'R_bf', 'L_ta', 'L_vm', 'L_rf', 'L_bf'];

R_ta = input.data(:,4);
R_vm = input.data(:,5);
R_rf = input.data(:,6);
R_bf = input.data(:,7);
L_ta = input.data(:,8);
L_vm = input.data(:,9);
L_rf = input.data(:,10);
L_bf = input.data(:,11);

EMG_mat = [R_ta, R_vm, R_rf, R_bf, L_ta, L_vm, L_rf, L_bf];
Gain_mat = ones(1,8).*10000;
NoEMGch=size(EMG_mat);
NoEMGch=NoEMGch(2);


for i = 1:NoEMGch;
   [EMG_LE] = function_EMG(EMG_mat(:,i), Gain_mat(:,i));
   emg_norm_mat(:,:,i)=EMG_LE;
end

%Group EMG data into bins based on variable range of degrees

deg = wave(:,2);
deg = deg+min(deg);
deg = deg/max(deg)*360;
```

```
deg = round(deg);

for i = 1:8
   tempemg = emg_norm_mat(:,:,i);
   n = 1;
   for d = 1:bin_size:360
      emgmask = deg==d;
      bin = tempemg.*emgmask;
      emg_bins(n,i) = sum(bin)/(length(find(bin)));
      n=n+1;
   end
end

%shift for left
if lcheck > 0
   emg_bins = circshift(emg_bins,[180 8]);
else
end
end
```

EMGbinnerAl.m

```
function emg_bins = EMGbinnerAl(path_file, file)
%Set EMG degree bin size
bin_size = 1;


% Load data file.

%[file,path_file] = uigetfile('*.txt');
input=importdata([path_file file],'\t');

% For oringal txt data
wave = input.data(:,[1 2]);

%Bad point elimination

len = length(wave(:,2));
diffs = abs(wave(2:len,2)-wave(1:len-1,2));
mwave = diffs>.02 & diffs<9;
locs = find(mwave);
locs2 = locs(2:2:end);
wave(locs,2) = 0;

% Determine when new wave revolutions occur. Find minimums to identify...
% individual cycles.

nc=[];
      for i=1:size(wave(:,2),1)-1
         if (abs(wave(i,2)-wave(i+1,2)))>.1
            nc=[nc;i+1];
         end
      end
```

```
 num_revs=(length(nc)-1);

%if recorded on left, adjust
lcheck = wave(nc(1)+50,2) - wave(nc(1)+100,2);
if lcheck > 0
   wave(:,2) = abs(wave(:,2)-max(wave(:,2)));
else
end

%%
% Function to process EMG data

emg_channel_names = ['R_ta', 'R_vm', 'R_rf', 'R_bf', 'L_ta', 'L_vm', 'L_rf', 'L_bf'];

R_ta = input.data(:,4);
R_vm = input.data(:,5);
R_rf = input.data(:,6);
R_bf = input.data(:,7);
L_ta = input.data(:,8);
L_vm = input.data(:,9);
L_rf = input.data(:,10);
L_bf = input.data(:,11);

EMG_mat = [R_ta, R_vm, R_rf, R_bf, L_ta, L_vm, L_rf, L_bf];
Gain_mat = ones(1,8).*10000;
NoEMGch=size(EMG_mat);
NoEMGch=NoEMGch(2);

for i = 1:NoEMGch;
   [EMG_LE] = function_EMG(EMG_mat(:,i), Gain_mat(:,i));
   emg_norm_mat(:,:,i)=EMG_LE;
end

%Group EMG data into bins based on variable range of degrees

deg = wave(:,2);
deg = deg+min(deg);
deg = deg/max(deg)*360;
deg = round(deg);

for i = 1:8
   tempemg = emg_norm_mat(:,:,i);
   n = 1;
   for d = 1:bin_size:360
      emgmask = deg==d;
      bin = tempemg.*emgmask;
      emg_bins(n,i) = sum(bin)/(length(find(bin)));
      n=n+1;
   end
end
end
```

function_EMG.m

```
% Function to process EMG channels (function_EMG)

function [le]= function_EMG(emg_ch, emg_gain, emg_channel_name, num_revs,emg_channel)

% Convert from Volts to mV

emg_ch=emg_ch*1000/emg_gain;

% Remove bias/offset.

raw2 = emg_ch - mean (emg_ch);

% Process raw signal by rectifying and low pass filtering at 40 Hz

rect = abs(raw2);
[b,a] = butter(4,40/500,'low');
le = filtfilt(b,a,rect);

%Change negative values to zero.
%Find values in EMG signal that are less than Zero and Change them to Zero.

i=find(le<=0) ;
le(i)=0;
```

EMGmeasures.m

```
load newEMGbyday0.mat

%BilatLeft peak locs must shift 180

%Day 1

%Peak (max)
for n = 1:8
for k = 1:11
   eval(sprintf('Peak_EMG1(k,1,n) = max(C%d_b_EMG1(:,n));',k));
   eval(sprintf('Peak_EMG1(k,2,n) = max(C%d_r_EMG1(:,n));',k));
   eval(sprintf('Peak_EMG1(k,3,n) = max(C%d_l_EMG1(:,n));',k));
   eval(sprintf('Peak_EMG1(k,4,n) = max(C%d_ru_EMG1(:,n));',k));
   eval(sprintf('Peak_EMG1(k,5,n) = max(C%d_lu_EMG1(:,n));',k));
end
end

%Min
for n = 1:8
for k = 1:11
   eval(sprintf('Min_EMG1(k,1,n) = min(C%d_b_EMG1(:,n));',k));
   eval(sprintf('Min_EMG1(k,2,n) = min(C%d_r_EMG1(:,n));',k));
   eval(sprintf('Min_EMG1(k,3,n) = min(C%d_l_EMG1(:,n));',k));
   eval(sprintf('Min_EMG1(k,4,n) = min(C%d_ru_EMG1(:,n));',k));
   eval(sprintf('Min_EMG1(k,5,n) = min(C%d_lu_EMG1(:,n));',k));
```

```
end
end

%Area under curve (sum because each point*1 degree)
for n = 1:8
for k = 1:11
   eval(sprintf('Sum_EMG1(k,1,n) = sum(C%d_b_EMG1(:,n));',k));
   eval(sprintf('Sum_EMG1(k,2,n) = sum(C%d_r_EMG1(:,n));',k));
   eval(sprintf('Sum_EMG1(k,3,n) = sum(C%d_l_EMG1(:,n));',k));
   eval(sprintf('Sum_EMG1(k,4,n) = sum(C%d_ru_EMG1(:,n));',k));
   eval(sprintf('Sum_EMG1(k,5,n) = sum(C%d_lu_EMG1(:,n));',k));
end
end

%Day 2

%Peak (max)
for n = 1:8
for k = 1:11
   eval(sprintf('Peak_EMG2(k,1,n) = max(C%d_b_EMG2(:,n));',k));
   eval(sprintf('Peak_EMG2(k,2,n) = max(C%d_r_EMG2(:,n));',k));
   eval(sprintf('Peak_EMG2(k,3,n) = max(C%d_l_EMG2(:,n));',k));
   eval(sprintf('Peak_EMG2(k,4,n) = max(C%d_ru_EMG2(:,n));',k));
   eval(sprintf('Peak_EMG2(k,5,n) = max(C%d_lu_EMG2(:,n));',k));
end
end

%Min
for n = 1:8
for k = 1:11
   eval(sprintf('Min_EMG2(k,1,n) = min(C%d_b_EMG2(:,n));',k));
   eval(sprintf('Min_EMG2(k,2,n) = min(C%d_r_EMG2(:,n));',k));
   eval(sprintf('Min_EMG2(k,3,n) = min(C%d_l_EMG2(:,n));',k));
   eval(sprintf('Min_EMG2(k,4,n) = min(C%d_ru_EMG2(:,n));',k));
   eval(sprintf('Min_EMG2(k,5,n) = min(C%d_lu_EMG2(:,n));',k));
end
end

%Area under curve (sum because each point*1 degree)
for n = 1:8
for k = 1:11
   eval(sprintf('Sum_EMG2(k,1,n) = sum(C%d_b_EMG2(:,n));',k));
   eval(sprintf('Sum_EMG2(k,2,n) = sum(C%d_r_EMG2(:,n));',k));
   eval(sprintf('Sum_EMG2(k,3,n) = sum(C%d_l_EMG2(:,n));',k));
   eval(sprintf('Sum_EMG2(k,4,n) = sum(C%d_ru_EMG2(:,n));',k));
   eval(sprintf('Sum_EMG2(k,5,n) = sum(C%d_lu_EMG2(:,n));',k));
end
end

%Location of Peak
for n = 1:8
for k = 1:11
   eval(sprintf('[p,PeakLoc_EMG2(k,1,n)] = max(C%d_b_EMG2(:,n));',k));
   eval(sprintf('[p,PeakLoc_EMG2(k,2,n)] = max(C%d_r_EMG2(:,n));',k));
   eval(sprintf('[p,PeakLoc_EMG2(k,3,n)] = max(C%d_l_EMG2(:,n));',k));
```

```
    eval(sprintf('[p,PeakLoc_EMG2(k,4,n)] = max(C%d_ru_EMG2(:,n));',k));
    eval(sprintf('[p,PeakLoc_EMG2(k,5,n)] = max(C%d_lu_EMG2(:,n));',k));
    eval(sprintf('[p,PeakLoc_EMG2(k,6,n)] = max(circshift(C%d_b_EMG2(:,n),[180 1]));',k));
end
end

%STD
for n = 1:8
for k = 1:11
    eval(sprintf('STD_EMG2(k,1,n) = std(C%d_b_EMG2(:,n));',k));
    eval(sprintf('STD_EMG2(k,2,n) = std(C%d_r_EMG2(:,n));',k));
    eval(sprintf('STD_EMG2(k,3,n) = std(C%d_l_EMG2(:,n));',k));
    eval(sprintf('STD_EMG2(k,4,n) = std(C%d_ru_EMG2(:,n));',k));
    eval(sprintf('STD_EMG2(k,5,n) = std(C%d_lu_EMG2(:,n));',k));
end
end


%Percent EMG signal change - to check for valid signal
PSC_EMG1 = (Peak_EMG1-Min_EMG1)./(Min_EMG1).*100;
PSC_EMG2 = (Peak_EMG2-Min_EMG2)./(Min_EMG2).*100;
```

Presentation Code for fMRI Experiments

Controls audio cues during scanning

```
#scenario_type = fMRI_emulation;
scenario_type = fMRI;
pulses_per_scan = 1;
pulse_code = 1;
#scan_period = 2000; #Comment out when using fMRI mode
default_font_size = 150;


begin;
text { caption = "Set By PCL"; font_size = 150; preload = false; } awake;
wavefile { filename = "PedalTone_45RPM_start.wav";} pedalstart;
wavefile { filename = "PedalTone_45RPM.wav";} pedaltone;
wavefile { filename = "PedalTone_45RPM_stop.wav";} pedalstop;
wavefile { filename = "The next session is coming soon.wav";} programcomplete;

trial {
        picture {
                background_color = 0,0,0;
                text { caption = "Waiting for scanner...";font_size = 80; font_color = 255,0,0; };
                x=0;y=0;
        };
        time = 0;
        code = "waiting";
} waiting;


trial {
        picture {
                background_color = 0,0,0;
                text { caption = "+"; font_size = 150;};
                x=0;y=0;
        };
        time = 0;
        mri_pulse = 1;
        code = "trigger";
} trigger;


trial {
        trial_duration =18000;
        picture {
                background_color = 0,0,0;
                text { caption = "Resting before 1st pedal"; font_size = 80; font_color = 255,215,0; };
                x=0;y=0;
        };
        time = 0;
  sound { wavefile pedaltone; pan=1;} prestart1;
  code="prestart";
} prestart;


trial {
```

```
            trial_duration =20000;
            picture {
                        background_color = 0,0,0;
                        text { caption = "Pedal"; font_color = 124,252,0; };
                        x=0;y=0;
            };
            time = 0;
  sound { wavefile pedalstart; pan=1;} start1;
  code="pedal";
} pedal;


trial {
            trial_duration =20000;
            picture {
                        background_color = 0,0,0;
                        text { caption = "Stop... "; font_color = 255,0,0; };
                        x=0;y=0;
            };
            time = 0;
  sound { wavefile pedalstop; pan=1;} stop1;
  code="stop";
} stop;


trial {
            trial_duration =3000;
            picture {
                        background_color = 0,0,0;
                        text { caption = "Program complete..."; font_size = 80; };
                        x=0;y=0;
            };
            time = 0;
  sound { wavefile programcomplete; } programcomplete1;
  code="programcomplete";
} done;

#*****************************************************************************************
*******#

begin_pcl;

output_file out;
int current_mri_pulse;
int next_mri_pulse;
int time = 0;
int count = 1;
string message;


# This section creates a subdirectory named Subjects
string directory = "C:\\Pedal";

if ( !directory_exists(directory) ) then
   create_directory(directory)
end;
```

```
string filename = "Pedal.txt";

delete_file(directory + "\\" + filename);

waiting.present();

# obtain the current MRI pulse count
current_mri_pulse = pulse_manager.main_pulse_count();

# set up to wait for the next MRI pulse count
next_mri_pulse = current_mri_pulse + 1       ;

# poll the Presentation Pulse Manager until the next MRI pulse
# arrives
loop until (pulse_manager.main_pulse_count() == next_mri_pulse)
  begin
  end;

out = new output_file;

out.open_append(directory + "\\" + filename);
out.print(date_time("yyyymmddhhnnsszzz") + "\n");

prestart.set_start_time(time);
prestart.present();

loop int j=1; until j>5 begin #-----------------------------------------------

        if j==1 then;
        trigger.set_mri_pulse(9);
        trigger.present();
        time = pulse_manager.main_pulse_time(pulse_manager.main_pulse_count());
        end;

        if j==2 then;
        trigger.set_mri_pulse(11);
        trigger.present();
        time = pulse_manager.main_pulse_time(pulse_manager.main_pulse_count());
        end;

        if j==3 then;
        trigger.set_mri_pulse(13);
        trigger.present();
        time = pulse_manager.main_pulse_time(pulse_manager.main_pulse_count());
        end;

        if j==4 then;
        trigger.set_mri_pulse(15);
        trigger.present();
        time = pulse_manager.main_pulse_time(pulse_manager.main_pulse_count());
        end;

        if j==5 then;
        trigger.set_mri_pulse(15);
        trigger.present();
```

```
        time = pulse_manager.main_pulse_time(pulse_manager.main_pulse_count());
        end;

        loop int i=1; until i > 1 begin
                pedal.set_start_time(time);
                pedal.present();
                i=i+1
        end;

        loop int i=2; until i > 2 begin
                stop.set_start_time(time);
                stop.present();
                i=i+1
        end;

        j=j+1
end;

done.present();
```

Spike2 Code for fMRI Experiments

Synchronizes Spike2 to start data collection when scanning begins

```
var flg,ret;
var daten$,timen$,secondsn%;

FileDelete("c:\\Pedal\\Pedal.txt");

'PrintLog("Spike waiting for c:\\Pedal\\Pedal.txt > C:\\Pedal\\spike.log");

flg := FileOpen("c:\\Pedal\\Pedal.txt",8,0);
'PrintLog("%f\n",flg);

while flg < 0  do
   flg := FileOpen("c:\\Pedal\\Pedal.txt",8,0);
   'PrintLog("%f\n",flg);
   wend


'ret :=FileNew(1);
'FileSaveAs("spike.log");
Seconds(0);
timen$ := Time$();
daten$ := Date$();
'Print("%f\n",secondsn%);
'Print("%s\n",timen$);
'Print("%s\n",daten$);
'FileSave();
'FileClose();

PrintLog("c:\Pedal\Pedal.txt exists at %s %s%s, beginning acquisition", daten$, timen$);
'FileOpen("C:\Pedal\spike.log");

'FileDelete("Pedal.txt");

SampleStart();
```

AFNI Code

Program Name	Function
csh.to3d	Converts DICOM formatted MRI data to 3D image datasets
csh.3dTshift.pedal	Aligns time series of each voxel to the same temporal origin
csh.3dToutcount.pedal	Checks data for outliers
csh.3dTcat.pedal	Concatenates the runs from each condition together
csh.3dvolreg.pedal	Registers functional data to anatomical scan
csh.3dDeconvolve.standard.pedal	Performs multiple linear regression to determine which voxels have task related activity
csh.3dFWHMx.Alphasim.pedal	Calculates which voxels are statistically active
csh.psc.pedal	Calculates the percent signal change for active voxels
csh.3dSkullStrip	Determines where the skull is in the anatomical data to ignore any signals outside of it
csh.3dmerge.maskout.pedal3	Applies statistics and skull mask to data, removes any signals greater than 10%
csh.masksize	Changes ROI masks created on the anatomical data into the functional data's resolution
csh.ROImeasures	Calculates volume and mean intensity in the ROI's
csh.3dmerge.maskout.pedalTLRC	Blurs data and creates group average
csh.pedal.logic	Finds common region of activation across condition for each individual subject
csh.group.blur.logic	Blurs data and creates group average of common region

csh.to3d

```
#!/bin/tcsh

#if (0) then
cd anat

to3d \
-prefix anat \
*MRDC*

mv *anat* ../
#endif
#**********************************************************************************************
********************#
#if (0) then

cd biped

set conditions = (pedal1 pedal2 pedal3 pedal4)

foreach condition ( $conditions )

        echo $condition
        cd $condition

        to3d \
        -prefix $condition \
        -time:zt 36 89 2000 alt+z \
        *MRDC*

        mv *orig* ../
        cd ..

end
#endif

cd ..

cd leped

set conditions = (pedal1 pedal2 pedal3 pedal4)

foreach condition ( $conditions )

        echo $condition
        cd $condition

        to3d \
        -prefix $condition \
        -time:zt 36 89 2000 alt+z \
        *MRDC*

        mv *orig* ../
        cd ..
end
```

```
#endif

cd ..
cd riped

set conditions = (pedal1 pedal2 pedal3 pedal4)

foreach condition ( $conditions )
	echo $condition
	cd $condition

	to3d \
	-prefix $condition \
	-time:zt 36 89 2000 alt+z \
	*MRDC*
	mv *orig* ../
	cd ..
end

#endif
cd ..
```

csh.3dTshift.pedal

```
#!/bin/csh

set conditions = (pedal1 pedal2 pedal3)

foreach condition ( $conditions )

	echo $condition

	3dTshift \
	-verb \
	-tzero 0 \
	-prefix $condition.tshift \
	-ignore 4 \
	-heptic \
	$condition+orig

end
```

csh.3dToutcount.pedal

```
#!/bin/csh

set runs = (pedal1.tshift pedal2.tshift pedal3.tshift)
foreach run ( $runs )

        3dToutcount \
        -automask \
        $run+orig \
        > $run.outcount

End
```

csh.3dTcat.pedal

```
#!/bin/csh

#if (0) then

#rm *tshift.cat*


#***************************************************************************************
**********************************************************#

# three runs
3dTcat \
pedal1.tshift+orig'[4..108]' \
pedal2.tshift+orig'[4..108]' \
pedal3.tshift+orig'[4..108]' \
-prefix pedal.tshift.cat


#endif
```

csh.3dvolreg.pedal

```
#!/bin/csh

set runs = (pedal.tshift.cat)


#***************************************************************************************
****************************************#
```

```
#Run by using 1 ref-point. The zero point of the run that closest to the anat, line 16 and 31

#if (0) then
foreach run ($runs)

        3dvolreg \
        -heptic \
        -prefix $run.volreg \
        -base 'pedal.reg+orig[0]' \
        -dfile $run.volreg.dfile \
        -1Dfile $run.volreg.1Dfile \
        $run+orig

end
#endif

#if (0) then
# Rerun volreg to see the effect of volreg from the data with 1 ref-point
foreach run ($runs)

        3dvolreg \
        -heptic \
        -prefix $run.volreg.twice \
        -base 'pedal.reg+orig[0]' \
        -dfile $run.volreg.twice.dfile \
        -1Dfile $run.volreg.twice.1Dfile \
        $run.volreg+orig

end
#endif
```

csh.3dDeconvolve.standard.pedal

```
#!/bin/csh

#*********************************************************#
# With censor file


3dDeconvolve \
-float \
-input pedal.tshift.cat.volreg+orig \
-concat concat.pedal.315 \
-polort A \
-num_stimts 7 \
\
-censor Mcensor315.1D \
```

```
\
-stim_file 1 Mcanonical315.1D \
\
\
-stim_minlag 1 0 \
-stim_maxlag 1 0 \
\
-stim_label 1 pedal \
\
-stim_file 2 pedal.tshift.cat.volreg.1Dfile'[0]' -stim_base 2 -stim_label 2 roll \
-stim_file 3 pedal.tshift.cat.volreg.1Dfile'[1]' -stim_base 3 -stim_label 3 pitch \
-stim_file 4 pedal.tshift.cat.volreg.1Dfile'[2]' -stim_base 4 -stim_label 4 yaw \
-stim_file 5 pedal.tshift.cat.volreg.1Dfile'[3]' -stim_base 5 -stim_label 5 dS \
-stim_file 6 pedal.tshift.cat.volreg.1Dfile'[4]' -stim_base 6 -stim_label 6 dL \
-stim_file 7 pedal.tshift.cat.volreg.1Dfile'[5]' -stim_base 7 -stim_label 7 dP \
\
-fitts pedal.tshift.cat.decon.fitts_censor.modify \
-errts pedal.tshift.cat.decon.errts_censor.modify \
\
-fout \
-tout \
-bout \
-full_first \
-bucket pedal.tshift.cat.decon.bucket_censor.modify
csh pedal.REML_cmd
```

csh.3dFWHMx.Alphasim.pedal

```
#!/bin/csh

#***********************************************************************************
***********************************************************#
# Calculate the amount of blur in your data (needed for Alphasim)
# Note: The results will be approx the same regardless the #maxlags, so we can run only 1 #maxlags
#***********************************************************************************
***********************************************************#

set maxlags = (15)

#if (0) then

        3dFWHMx \
        -dset pedal.tshift.cat.decon.errts_censor.modify+orig \
        -mask anat_pedal_strip_1500_PTE_mesh_bigvoxels.mask+orig \
        -out pedal.FWHMx.

#endif
```

```
#***************************************************************************#
# Specify characteristics of your data and individual voxel p, find the cluster size that gives you an alpha of
0.05
#***************************************************************************#

if (0) then

        AlphaSim \
        -quiet \
        -mask anat_pedal_strip_1500_PTE_mesh_bigvoxels.mask+orig \
        -fwhmx 4.32  -fwhmy 4.33  -fwhmz 3.2 \
        -rmm 6.6 \
        -pthr 0.005 \
        -iter 1000 \
        -out alphasim_0.005.txt

#Alpha = 0.05   #of Cl = 7  x56.25 = 393.8

Endif
```

csh.psc.pedal

```
#!/bin/csh

#***************************************************************************#
# Computing %signal change
# Note: we have to use 3dDecon w/o REML b/c REML doesn't have baseline
#***************************************************************************#
set runs = (pedal.tshift.cat)
foreach run ($runs)

3dcalc \
-fscale \
-a $run.decon.bucket_censor.modify+orig'[1]' \
-b $run.decon.bucket_censor.modify+orig'[7]' \
-c $run.decon.bucket_censor.modify+orig'[13]' \
\
-d pedal.tshift.cat.decon.bucket_censor.modify+orig'[19]' \
\
-expr "100 * (d/((a+b+c)/3)) * step( 1 - abs( (d/((a+b+c)/3)) ) )" \
\
-prefix $run.decon.bucket_censor.modify.PSC
end

#***************************************************************************#
# Putting coef and stat data together
```

```
# Note: It is an optinal. We don't need it afterward. It is good for visually checking
#***********************************************************************#

foreach run ($runs)
        3dbuc2fim \
        -prefix $run.decon.bucket_censor.modify.PSC.stat \
        $run.decon.bucket_censor.modify.PSC+orig'[0]'\
        $run.decon.bucket_censor.modify_REML+orig'[2]'
End
```

csh.3dSkullStrip

```
#!/bin/csh

#if (0) then
# Making a skull strip from anatomical image
3dSkullStrip \
-input anat+orig \
-push_to_edge \
-blur_fwhm 4 \
-ld 50 \
-prefix anat_pedal_strip_PTE_mesh
#endif

#if (0) then
# Making a mask using the skull-strip
3dcalc \
-a anat_pedal_strip_PTE_mesh+orig \
-expr "step(a-1500)" \
-prefix anat_pedal_strip_1500_PTE_mesh
#endif

#if (0) then
# Changing the sample size of anat to functional scan size (b/c the resolution of anat is diff from functional
scan)
3dfractionize \
-template pedal.tshift.cat+orig \
-input anat_pedal_strip_1500_PTE_mesh+orig \
-prefix anat_pedal_strip_1500_PTE_mesh_bigvoxels
#endif

#if (0) then
# Making the fractionized file to be a mask for Alphasim
3dcalc \
-a anat_pedal_strip_1500_PTE_mesh_bigvoxels+orig \
-expr "step(a)" \
-prefix anat_pedal_strip_1500_PTE_mesh_bigvoxels.mask
```

```
#endif
```

csh.3dmerge.maskout.pedal3

```
#!/bin/csh

set runs = (pedal.tshift.cat)

# From csh.3dmerge.noneg.maskout.pedal
rm *AUC*
foreach run ($runs)
3dmerge \
        -1thresh 2.85 \
        -1clust 6.6 393.8 \
        -1dindex 0 \
        -1tindex 1 \
        -prefix $run.decon.bucket_censor.modify.PSC_AUC_thresh.stat \
        $run.decon.bucket_censor.modify.PSC.stat+orig
end

foreach run ($runs)

3dcalc \
        -a $run.decon.bucket_censor.modify.PSC_AUC_thresh.stat+orig \
        -b anat_pedal_strip_1500_PTE_mesh_bigvoxels.mask+orig \
        -expr "step(b)*a" \
        -prefix $run.decon.bucket_censor.modify.PSC.STAT.MASK
end

#**************************

foreach run ($runs)
3dcalc \
        -a $run.decon.bucket_censor.modify.PSC.STAT.MASK+orig'[0]' \
        -expr "a*within(a,-10,10) " \
        -prefix $run.decon.bucket_censor.modify.PSC.STAT.MASK_outlier
End
```

csh.masksize

```
#!/bin/csh


# Changing the resolution of the anat masks to the functional scan
```

```
set areas = (M1R M1L S1R S1L A6R A6L CbR CbL M1a S1a A6a Cba M1S1R M1S1L M1S1a
M1S1A6R M1S1A6L M1S1A6a)
foreach area ($areas)
   3dfractionize \
   -template pedal.reg+orig \
   -input "$area"+orig \
   -prefix "$area"_low+orig
end
```

csh.ROImeasures

```
#!/bin/csh


# draw the activation maps in each ROI

set areas = (A6R A6L CbR CbL M1a S1a A6a Cba M1S1R M1S1L M1S1a)
foreach area ($areas)

3dcalc \
-a pedal.tshift.cat.decon.bucket_censor.modify.PSC.STAT.MASK_outlier+orig \
-b "$area"_low+orig \
-expr "step(b)*a" \
-prefix "$area"_PSMO+orig


3dBrickStat \
        -volume \
        -max \
        -mean \
        -positive \
        "$area"_PSMO+orig \
        >"$area"_PSMOmeasures.txt

End
```

csh.3dmerge.maskout.pedalTLRC

```
#!/bin/csh

set runs = (pedal.tshift.cat)

# From csh.3dmerge.noneg.maskout.pedal
rm *AUC*
foreach run ($runs)
3dmerge \
```

```
        -1thresh 2.85 \
        -1clust 6.6 393.8 \
        -1dindex 0 \
        -1tindex 1 \
        -prefix $run.decon.PSC_AUC_thresh.REML_stat \
        $run.decon.bucket_censor.modify.PSC.stat+orig

3dmerge \
        -1thresh 2.85 \
        -1clust_order 6.6 393.8  \
        -1dindex 0 \
        -1tindex 1 \
        -prefix $run.decon.PSC_AUC_order.thresh.REML_stat \
        $run.decon.bucket_censor.modify.PSC.stat+orig
end

foreach run ($runs)

        3dcalc \
        -a $run.decon.PSC_AUC_thresh.REML_stat+orig \
        -b anat_pedal_strip_1500_PTE_mesh_bigvoxels.mask+orig \
        -expr "step(b)*a" \
        -prefix $run.decon.PSC_AUC_thresh.REML_stat.mask

        3dcalc \
        -a $run.decon.PSC_AUC_order.thresh.REML_stat+orig \
        -b anat_pedal_strip_1500_PTE_mesh_bigvoxels.mask+orig \
        -expr "step(b)*a" \
        -prefix $run.decon.PSC_AUC_order.thresh.REML_stat.mask
end

foreach run ($runs)
        3dmerge \
        -1clust_order 6.6 393.8\
        -1erode 25 \
        -1dilate \
        -prefix $run.decon.PSC_AUC_order.thresh.REML_stat.mask.ERODE \
        $run.decon.PSC_AUC_order.thresh.REML_stat.mask+orig
end

foreach run ($runs)
3dmerge \
        -1clust_order 6.6 393.8\
        -prefix $run.decon.PSC_AUC_order.thresh.REML_stat.mask.ERODE.CLUST \
        $run.decon.PSC_AUC_order.thresh.REML_stat.mask.ERODE+orig
end


foreach run ($runs)
```

```
        adwarp\
        -apar anat+tlrc \
        -dpar $run.decon.PSC_AUC_order.thresh.REML_stat.mask.ERODE.CLUST+orig \
        -resam NN
end

rm *PSC.STAT.MASK*
foreach run ($runs)
3dcalc \
        -a $run.decon.PSC_AUC_order.thresh.REML_stat.mask.ERODE.CLUST+orig \
        -b $run.decon.bucket_censor.modify.PSC.stat+orig \
        -expr "step(a)*b" \
        -prefix $run.decon.bucket_censor.modify.PSC.STAT.MASK
end

foreach run ($runs)
        adwarp\
        -apar anat+tlrc \
        -dpar $run.decon.bucket_censor.modify.PSC.STAT.MASK+orig \
        -resam NN
end

rm *WithNeg.txt
foreach run ($runs)
3dmaskave \
        -mask $run.decon.PSC_AUC_order.thresh.REML_stat.mask.ERODE.CLUST+orig \
        -quiet \
        -dump \
        'pedal.tshift.cat.decon.bucket_censor.modify.PSC.STAT.MASK+orig' \
        >pedal_Overall_WithNeg.txt
end

foreach run ($runs)
3dcalc \
        -a $run.decon.bucket_censor.modify.PSC.STAT.MASK+orig'[0]' \
        -expr "a*within(a,-10,10) " \
        -prefix $run.decon.bucket_censor.modify.PSC.STAT.MASK_outlier

3dmaskave \
        -mask $run.decon.PSC_AUC_order.thresh.REML_stat.mask.ERODE.CLUST+orig \
        -quiet \
        -dump \
        'pedal.tshift.cat.decon.bucket_censor.modify.PSC.STAT.MASK_outlier+orig' \
        >pedal_Overall_outlier_WithNeg.txt
end

foreach run ($runs)
adwarp\
        -apar anat+tlrc \
```

```
        -dpar $run.decon.bucket_censor.modify.PSC.STAT.MASK_outlier+orig \
        -resam NN
end
```

csh.pedal.logic

```
#!/bin/csh
#if(0) then

3dcalc \
        -a pedal.PSMO.bilat+orig \
        -b pedal.PSMO.right+orig \
        -c pedal.PSMO.left+orig \
        -expr "and(step(a),step(b),step(c))" \
        -prefix pedal.BRL.mask \
#endif

# draw the activation maps in each ROI

set areas = (A6R A6L CbR CbL A6a Cba M1S1R M1S1L M1S1a)
set conds = (bilat right left)
foreach area ($areas)
foreach cond ($conds)

3dcalc \
        -a pedal.PSMO."$cond"+orig \
        -b pedal.BRL.mask+orig \
        -c "$area"_low+orig \
        -expr "step(c)*step(b)*a" \
        -prefix "$area"."$cond".BRL+orig


3dBrickStat \
        -volume \
        -max \
        -mean \
        -positive \
        "$area"."$cond".BRL+orig \
        >"$area"."$cond".BRL.measures.txt
end
end
```

csh.group.blur.logic

```
#!/bin/csh
#if (0) then

3dcalc \
        -a pedal.bilat.group.4mmblur.thresh+tlrc \
        -b pedal.right.group.4mmblur.thresh+tlrc \
        -c pedal.left.group.4mmblur.thresh+tlrc \
        -expr "and(step(a),step(b),step(c))" \
        -prefix pedal.group.BRL.mask \

set conditions = (bilat right left)

foreach condition ( $conditions )

3dcalc \
        -a pedal."$condition".group.4mmblur.thresh+tlrc \
        -b pedal.group.BRL.mask+tlrc \
        -expr "step(b)*a" \
        -prefix pedal."$condition".group.4mmblur.BRL+tlrc

end
#endif
```